Investigating the Cytotoxicity of Ebolavirus Proteins

Diego Cantoni

A thesis submitted to the University of Kent for the degree of PhD in Microbiology in the Faculty of Sciences

School of Biosciences

2019

I Declaration

No part of this thesis has been submitted in support of an application for any degree or qualification of the University of Kent or any other University or institute of learning.

Diego Cantoni
July 2019

II Acknowledgements

First and foremost, I'd like to extend my sincerest gratitude to my family for their unconditional support that permitted me to undertake my PhD with the utmost of enthusiasm. Secondly, I will be forever grateful to Dr Jeremy Rossman not only for the possibility to undertake my PhD program under his supervision, but as the large source of motivation during this time, always enabling me to explore obscure avenues where questions remain unanswered regarding a virus that is so deadly and mysterious.

I would also like to thank all the members past and present of the laboratory for your unfaltering support, thrilling scientific discussions and everlasting patience. Matthew, Fred, Basma, and Nafisa I will forever cherish the lessons and memories formed during this time.

I would like to thank the Tsaousis and Fenton laboratory for their input during group meetings, support and guidance in experimental protocols, and permitting me to engage in collaborative work that made me appreciate a different fields of biology.

I would like to thank the Ortega-Roldan laboratory for engaging in a structural project presented in this thesis. Their infectious happiness in the lab made my enthusiasm to learn unique techniques, with particular emphasis on how fruitful Nuclear Magnetic Resonance can be in the pursuit for data.

Finally I would like to thank the department for creating a warm and stimulating environment to work in. I would like to particularly thank the managers of various research facilities; Ian Brown (Microscopy Suite), Gary Thompson (NMR Facility) and Kevin Howland (Biomolecular Science Facility) for their support and patience.

Throughout these informative years I was able to personally develop, appreciating the importance of certain life values which were often put to the test; patience, resilience and self-awareness. For this reason, I will always look back at my time as a PhD student to be one of the most developmental parts of my life.

III Achievements

Publications

This thesis contains two reviews published as first author in unedited form:

Cantoni, Diego, Arran Hamlet, Martin Michaelis, Mark N. Wass, and Jeremy S. Rossman. "Risks posed by Reston, the forgotten Ebolavirus." mSphere 1, no. 6 (2016): e00322-16.

Cantoni, Diego, and Jeremy S. Rossman. "Ebolaviruses: New roles for old proteins." PLoS neglected tropical diseases 12, no. 5 (2018): e0006349.

Publications as co-author regarding Ebolaviruses

Pappalardo, Morena, Ian G. Reddin, Diego Cantoni, Jeremy S. Rossman, Martin Michaelis, and Mark N. Wass. "Changes associated with Ebola virus adaptation to novel species." Bioinformatics 33, no. 13 (2017): 1911-1915.

Conference Attendances

Attended Microbiology Society Annual Conference, Liverpool, 2016
Presented Poster at Negative Strand Virus Meeting, Verona, 2018

Grant Awards

Royal Society of Tropical Medicine and Hygiene:
Structure and function of the Ebolavirus delta-peptide on lipid membranes. £4,750

IV Abstract

Viral proteins have a multitude of roles during pathogenesis and replication, in order to maximise likelihood of virus survival during infection. However, in many cases viral proteins are cytotoxic, resulting in the decimation of immune cells, imbalanced antiviral responses and, in the case of deadly haemorrhagic viruses, organ failure, often leading to death of the host. This is largely the effect of ebolaviruses during infections in humans, as the increased understanding of this virus has allowed us to recognize how its proteins are involved in pathogenesis. However, there is still a substantial amount of knowledge to be discovered about this deadly virus. Here, we attempt to increase our knowledge on cytotoxicity of several Ebola virus proteins, namely VP24 and delta-peptide. Our journey in the past three years has uncovered a novel effect of VP24 in mammalian cells. Largely known for its interferon antagonism, prolonged incubation of VP24 appears to upregulate markers of cell cycle arrest, such as p21. Furthermore, we report increased expression of γH2AX, a marker for DNA damage. In the case of delta-peptide, we attempted several techniques for gathering structure-function data, such as nuclear magnetic resonance imaging to lipidic cubic phase crystallography. We have managed to generate peptide crystals in a lipid environment, with the intention of carrying out x-ray scatter to generate a structure. By increasing our knowledge on viral proteins, every small piece of research forms a chain of information with the hopes to generating a successful form of treatment against this deadly disease.

V Contents

VI List of Figures

VII List of Tables

VIII Abbreviations

∆-peptide – Delta peptide

AH – Amphipathic helix

ATP – Adenosine Triphosphate

BDBV – Bundibugyo virus

BSA – Bovine Serum Albumen

CD – Circular Dichroism

CV – Column Volume

DAPI – 4’,6-diamino-2-phenylindole

DMEM – Dulbecco’s Modified Eagle Medium

DNA – Deoxyribonucleic Acid

EBOV – Ebola virus

EDTA – Ethylenediaminetetraacetic acid

EVD – Ebola virus Disease

FBS – Foetal Bovine Serum

GP – Glycoprotein

GP1 – Glycoprotein Subunit 1

GP1,2 – Glycoprotein Subunit 1 and 2

GP2 – Glycoprotein Subunit 2

HA - haemagglutinin

HEK 293t – Human Embryonic Kidney cell line expressing a t antigen

HeLa – Henrietta Lacks Cervical Epithelial Adenocarcinoma cell line

HEPES – 4-(2-Hydroxyethyl) Piperazine-1-ethanosulfonic acid

Huh-7 – human hepatocellular carcinoma cell line

IAP – Inhibitor of apoptosis

IFN – Interferon

IPTG - Isopropyl β-D-1-thiogalactopyranoside

IRF-3 – Interferon Regulatory Transcription Factor 3

IRF-7 – Interferon Regulatory Transcription Factor 7

KPNA 1-5 – Karyopherin subunit alpha

L – L Polymerase Protein

LIR – LC3-interacting Region

LB – Lysogeny Broth

LUV – Large Unilamellar Vesicle

MLKL – Mixed Lineage Kinase Domain-like Protein

MTS - 3-(4,5-dimethylthiazol-2-yl)-5-(3-carboxymethoxyphenyl)-2-(4-sulfophenyl)-2H-tetrazolium

NHP – Non Human Primate

NMR – Nuclear Magnetic Resonance

NOESY – Nuclear Overhauser Effect Spectroscopy

NP – Nucleoprotein

PEI – Polyethylenimine

POPC - 1-palmitoyl-2-oleoyl-sn-glycero-3-phosphocholine

P/S – Penicillin/Streptomycin

PVDF – Polyvinylidene fluoride

RESTV – Reston virus

RIPK1 – Receptor-Interacting Kinase 1

RIPK3 – Receptor-Interacting Kinase 3

RNA – Ribonucleic Acid

ROS – Reactive oxygen species

sGP – Small glycoprotein

ssGP – small secreted glycoprotein

SOC – Super optimal broth

STAT1 – Signal transducer and activator of transcription protein 1

SUDV – Sudan virus

TACE – Tumor Necrosis Factor-alpha-converting Enzyme

TAE – Tris-acetate-EDTA

TAFV – Taï Forest virus

TBS – Tris-buffered Saline

TBS-T – Tris-buffered Saline with Tween

TLR4 – Toll-like Receptor 4

TNF-α – Tumour Necrosis Factor Alpha

VLP – virus-like particle

VP24 – viral protein 24

VP30 – viral protein 30

VP35 – viral protein 35

VP40 – viral protein 40

WT – Wild Type

1 Introduction

1.1 Overview of Ebolavirus

1.1.1 History of Ebolavirus

On the 26th of August 1976, a 44 year-old teacher visited the mission hospital of his local village called Yambuku, Zaire (now known as Democratic Republic of Congo). With the intent of seeking medical attention for an illness he acquired resembling malaria, he was given an injection of chloroquine. However, syringe needles were often reused on several patients at the hospital, and without knowing that the index case was infected with a very deadly unknown pathogen, the disease swiftly spread to other patients. The destruction that ensued was rapid; within a little more than a month, 280 out of the 318 people that were infected succumbed to the virus (Commission, 1978). Blood samples from one of the Belgian nurses present at the Mission Hospital were sent in a Thermos flask to Antwerp for further analysis, as no one knew what virus was responsible for this outbreak. At the time, researchers were aware of a deadly filovirus circulating in Africa called Marburg virus, which also causes haemorrhagic fever. All the more coincidentally, another deadly haemorrhagic virus was causing an outbreak in Sudan with similar mortality as seen in Yambuku (Team, 1978). The research team in Antwerp collaborated with several other established research centres including Porton Down in the UK and the CDC Atlanta, Georgia, where cultures of the virus were observed under electron microscopy. It was at this point where the newly discovered virus was given its name: Ebola virus, after the Ebola river near Yambuku (Pattyn *et al.*, 1977). Interestingly, the pathogen responsible for the 1976 outbreak in Sudan was revealed to be Sudan virus, one of the 5 members of the *Ebolavirus* genus.

1.1.2 Phylogeny and Genome

Ebolaviruses are single-sense negative-strand RNA viruses. They belong to the family of filoviridae, which is comprised of three genera: Ebolavirus, Cuevavirus and Marburgvirus. There are currently five members pertaining to the Ebolavirus genus; Ebola virus (EBOV), Sudan virus (SUDV), Taï Forest virus (TAFV) Bundibugyo virus (BDBV) and Reston virus (RESTV) (Maes *et al.*, 2019). A new filovirus has been recently discovered in Africa named Bombali virus (BOMV), retaining 55-59% similarity at nucleotide level and 64-72% similarity at amino acid level [Figure 1] (Goldstein *et al.*, 2018). There is no evidence of BOMV infecting humans to date. Due to its discovery in August 2018, it has yet to be assigned taxonomically by the International Committee on Taxonomy of Viruses.

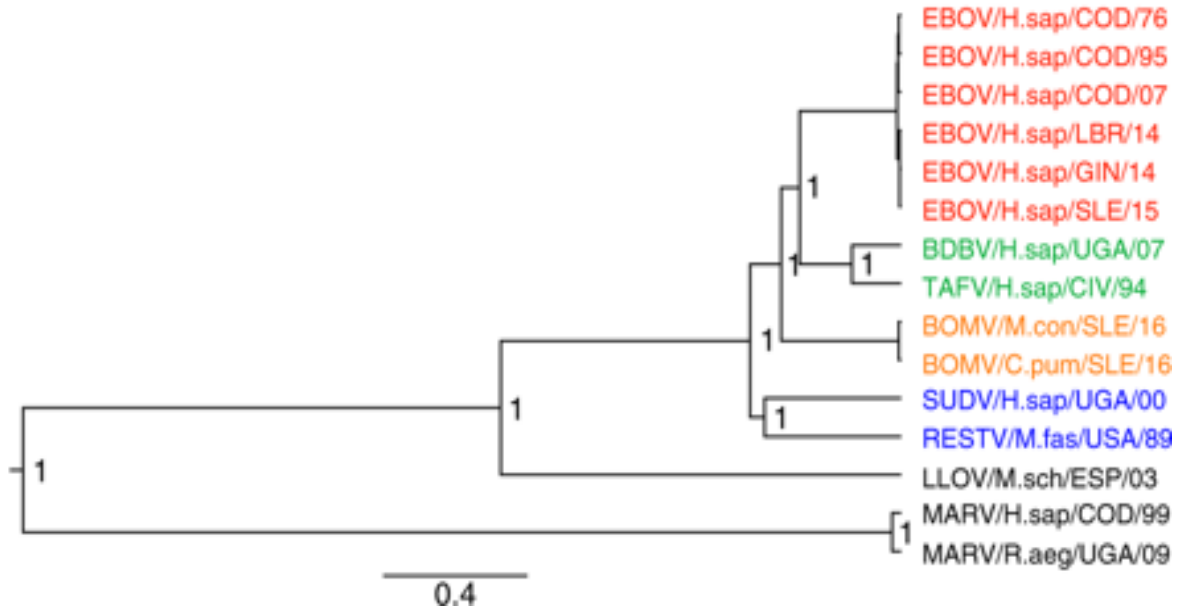

Figure 1. Phylogenetic Analysis of filoviruses based on full genome sequences.
This phylogenetic tree represents how closely related the different members of the filoviridae are. BOMV has also been included. Adapted from *The discovery of Bombali virus adds further support for bats as hosts of Ebolaviruses.* Goldstein *et al.,* 2018.

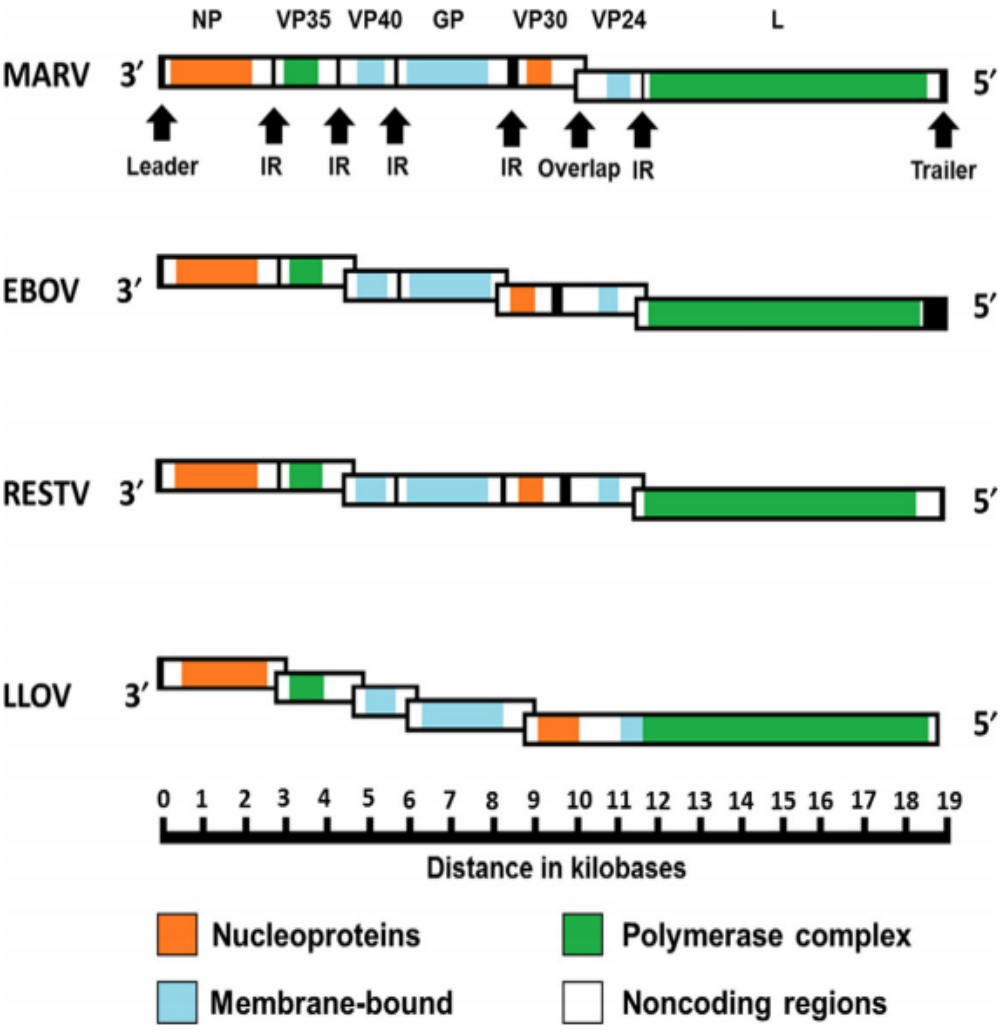

Figure 2. Filovirus genome organisation.

The schematics depict how the genes are arranged, highlighting the intergenic regions and gene overlaps between the species. The schematic representing EBOV may also represent BDBV, TAFV and SUDV as they are arranged in similar fashion. Figure adapted from *Filoviruses: Ecology, Molecular Biology, and Evolution.* Emanuel, Marzi, Feldmann, 2018

The genome length across *Ebolaviruses* is approximately 19 kilobases in length, comprising of 7 genes; nucleoprotein (NP), viral protein (VP)35, VP40, glycoprotein (GP), VP30, VP24 and the L polymerase protein (L), separated by intergenic regions and overlaps [Figure 2] (Emanuel, Marzi and Feldmann, 2018). However, the genome organisation differs between EBOV and RESTV. EBOV contains several

gene overlaps between VP35 and VP40, GP and VP30, and VP24 and L (Ikegami *et al.*, 2001). RESTV however does not retain an overlap between GP and VP30.

Each gene of *Ebolaviruses* contains a single open reading frame (ORF), with the exception of GP, containing 3 overlapping ORFs, each leading to production of different variants of GP products [Figure 3] (Volchkov *et al.*, 1995; Sanchez *et al.*, 1996). This is due to site-specific transcriptional editing by L polymerase, resulting in secreted (s)GP being produced from undedited RNA, whereas the full length GP is produced when an additional adenosine is inserted into the transcript. Lastly, when two aditional adenosine residues are added, a third GP gene product is produced called small soluble (ss)GP (Mehedi *et al.*, 2011).

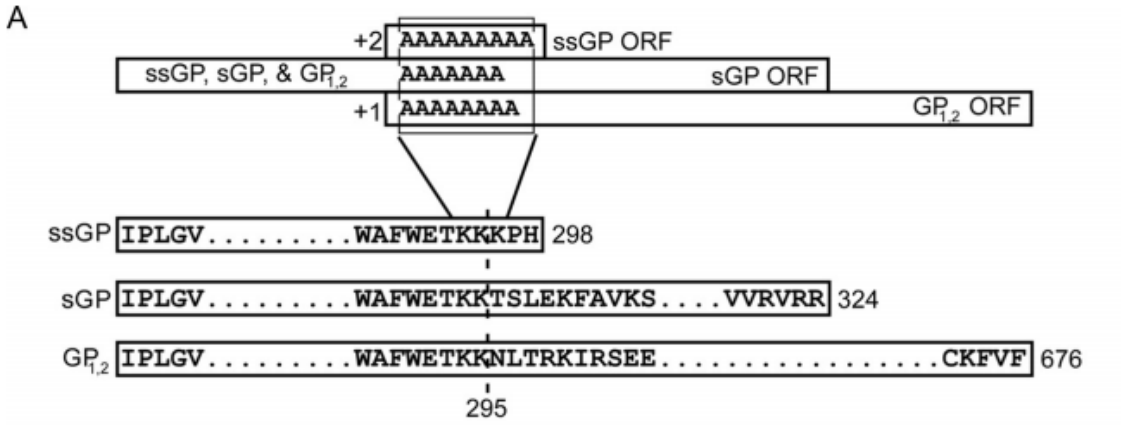

Figure 3. Open Reading Frames in the GP gene.

The first 295 amino acids of all GP gene products are the same but differ towards the C-terminal end. The most expressed product from the GP gene is sGP, followed by GP and lastly ssGP. Figure taken from Mehedi *et al.,* 2011.

1.1.3 Ecology and Epidemiology

Almost all *Ebolaviruses*, with the exception of Reston virus, are found in Africa. The reservoir for this deadly virus has yet to be conclusively determined, though it is highly suspected that fruit bats are the reservoir, as experimental inoculation of the virus did not result in illness despite viral replication (Swanepoel *et al.*, 1996). A survey conducted in Gabon during Ebola virus outbreaks between 2001 and 2003 also found viral RNA in liver and spleen samples of 3 different species of fruit bats (Leroy *et al.*, 2005). The hypothesis of fruit bats being the reservoir also stems from

the fact that every outbreak appears to have resulted from environments shared by humans or susceptible hosts, and fruit bats (Groseth, Feldmann and Strong, 2007). Interestingly, fruit bats outside of Africa have been reported to host filoviruses such as Lloviu Cuevavirus in Spain, Hungary and China, strongly suggesting that bats are reservoirs of filoviruses and that these viruses are globally distributed, despite not being pathogenic in humans compared to the filoviruses found in Africa (Hayman, 2016). Another question that is often pondered is whether seasonal changes affect transmission as this may affect the distribution of bats, for example; food scarcity, weather patterns or pregnancy, as these factors may affect bat migrations resulting in closer contact between humans or other hosts, making the spillovers of virus between bats and humans much more likely (Leroy *et al.*, 2005). Risk factors have been identified for potential outbreaks, as many index patients have lifestyles that brings them into close proximity with bats such as hunters or workers entering forests, caves or abandoned mines (Groseth, Feldmann and Strong, 2007). Human to human transmission of the virus is very efficient for a virus only transmitted through infected fluids. This was seen during the 2014-2016 Ebola virus outbreak as the index patient was an 18 month old boy from a village in Guinea's Guéckédou prefecture called Meliandou in December 2013 (Baize *et al.*, 2014; Timothy *et al.*, 2019). By February-March 2014 patients were tested positive for Ebola virus infection in Macenta and Kissidougu. By the end of March the virus has reached the capital city of Conakry, due to an infected individual related to the index case's extended family, which initiated multiple chains of transmission (Kaner and Schaack, 2016). This is testament to how rapid Ebola virus can be transmitted by human to human contact especially in areas where humans live in close contact and often travel.

Year	Country	Ebolavirus species	Cases	Deaths	Case fatality
2018-2019	DRC	EBOV	Ongoing		
2018	DRC	EBOV	54	33	61%
2017	DRC	EBOV	8	4	50%
2015	Italy	EBOV	1	0	0%
2014	DRC	EBOV	66	49	74%
2014	Spain	EBOV	1	0	0%
2014	UK	EBOV	1	0	0%
2014	USA	EBOV	4	1	25%
2014	Senegal	EBOV	1	0	0%
2014	Mali	EBOV	8	6	75%
2014	Nigeria	EBOV	20	8	40%
2014-2016	Sierra Leone	EBOV	14124*	3956*	28%
2014-2016	Liberia	EBOV	10675*	4809*	45%
2014-2016	Guinea	EBOV	3811*	2543*	67%
2012	DRC	BDBV	57	29	51%
2012	Uganda	SUDV	7	4	57%
2012	Uganda	SUDV	24	17	71%
2011	Uganda	SUDV	1	1	100%
2008	DRC	EBOV	32	14	44%
2007	Uganda	BDBV	149	37	25%
2007	DRC	EBOV	264	187	71%
2005	Congo	EBOV	12	10	83%
2004	Sudan	SUDV	17	7	41%
2003	Congo	EBOV	35	29	83%
2003	Congo	EBOV	143	128	90%
2001-2002	Congo	EBOV	59	44	75%
2001-2002	Gabon	EBOV	65	53	82%
2000	Uganda	SUDV	425	224	53%
1996	South Africa (ex-Gabon)	EBOV	1	1	100%
1996	Gabon	EBOV	60	45	75%
1996	Gabon	EBOV	31	21	68%
1995	DRC	EBOV	315	254	81%
1994	Côte d'Ivoire	TAFV	1	0	0%
1994	Gabon	EBOV	52	31	60%
1979	Sudan	SUDV	34	22	65%
1977	DRC	EBOV	1	1	100%
1976	Sudan	SUDV	284	151	53%
1976	DRC	EBOV	318	280	88%

Table 1. Chronology of previous Ebola Virus disease outbreaks
This table was adapted from the World Health Organisation fact sheet on Ebola Virus Disease page. Accessed on 15th of April, 2019. * Includes suspect, probable and confirmed EVD cases. DRC: Democratic Republic of Congo
https://www.who.int/en/news-room/fact-sheets/detail/ebola-virus-disease

1.1.4 Ebola Virus Disease

Ebola virus enters the human body through mucosal surfaces and sites of skin injury. At early stages of infection, an asymptomatic incubation period exists whereby an individual would continue with their daily routine. However, as viral load increases during incubation, initial non-specific symptoms of Ebola virus disease (EVD) become apparent such as fatigue, muscle weakness and malaise, followed by onset of fever (Bwaka *et al.*, 1999). At around 1 week of illness, further symptoms include vomiting, watery diarrhoea and nausea, at which this point the infected individual is considered to be most infectious (Baseler *et al.*, 2017). A diffuse maculopapular rash becomes visible. Week 2 is when EVD peaks as organ damage occurs such as renal failure and hepatic injury [Figure 4]. It is at this point where haemorrhaging occurs.

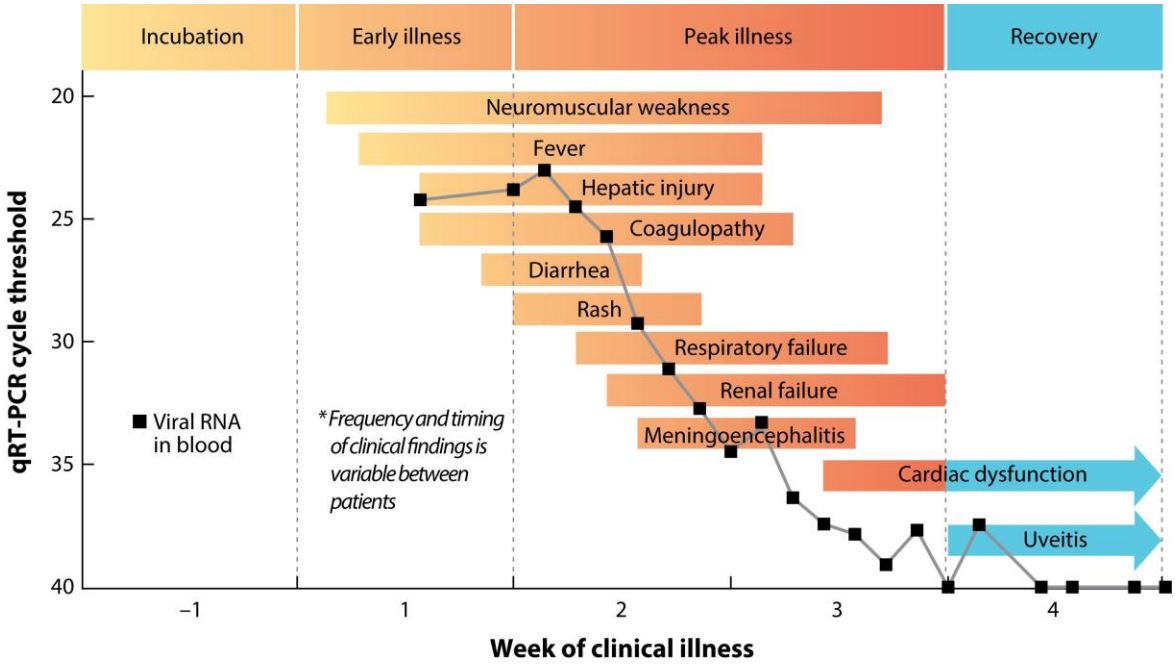

Baseler L, et al. 2017.
Annu. Rev. Pathol. Mech. Dis. 12:387–418

Figure 4. Timeline of the typical case of Ebola Virus Disease in humans. The timeline of EVD shows that peak illness is associated with peak viremia, as detected by qRT-PCR, a measurement used to detect viral RNA in the blood of patients.

Furthermore, EVD causes central nervous system dysfunction resulting in neuromuscular impairment and meningoencephalitis befalls the infected individual at this stage of infection (Chertow *et al.*, 2016). Other organs affected include eyes, as ocular disturbances resulting in blurred vision and onset of uveitis occur in late stages of infection, and the heart, as myocardial disfunction has been detected in infected individual. During week 2 and week 3 of infection viral load begins to decrease. Week 4 is considered to be the recovery phase for survivors of EVD as tissue damage repair occurs. However, sites of immunological privilege allow for persistence of the virus such as eyes, central nervous system and testis (Baseler *et al.*, 2017). Symptoms often reported by survivors include uveitis, blurred vision, muscular pain and fatigue.

Current literature has suggested that factors present in acute phase of EVD may determine chances of survival. Factors present in the early stages of infection include viral load and activation of various host pathways in response to the infection. With regards to viral load, ct (cycle threshold) values by quantitative real-time PCR have been fairly useful to determine outcome. CT values are defined as the number of cycles during PCR that are required for florescent signal to exceed background fluorescence, thus giving you a positive result. Therefore, a low ct value indicates high amounts of viral load. During infection, low ct values ~12 suggest fatal outcome whereas ~30 suggest survival (Fitzpatrick *et al.*, 2015). However, the issue lies when ct values fall in the middle of these two extremes, by which point it may be considered that an individual would have an equal chance of fatal or survival chance. By looking at gene pathways one could further predict the severity of EVD and tailor the treatment required for the patient. Some of the biggest differences between fatal and survivor outcome was the activation of interferon signalling pathways, as a high amount of activation was correlated with fatal outcome (X. Liu *et al.*, 2017). Furthermore, differences in types of immune cell abundance was also associated with patient outcome, as fatal cases often had less circulating CD14+ monocytes and lower NK cells in peripheral blood (X. Liu *et al.*, 2017). These indicators suggest that a robust immune response to the virus may be a key factor in fatal outcomes.

Therefore, understanding determinants for outcome of EVD may be of great use for diagnostic and treatment approaches.

1.2 Ebolavirus Proteins

**The following sections on Ebolavirus proteins and their roles were taken from our published review:* Ebolaviruses: New roles for old proteins (Cantoni and Rossman, 2018). *The figure legends have been renumbered for the purpose of this thesis.*

1.2.1 VP24*

VP24 is one of the most studied filovirus proteins, with the majority of studies focusing on its primary role in inhibiting the host IFN response. VP24 is known to inhibit IFN-α/β and IFN-γ activation by binding to key host proteins from the karyopherin α family: karyopherin α1, α5 and α6, preventing their binding to and the subsequent nuclear import of signal transducer and activator of transcription 1 (STAT1) (Reid *et al.*, 2006). In addition, VP24 blocks IFN signalling by directly binding to STAT1, preventing its phosphorylation, nuclear import and transcription of interferon stimulated genes (ISG) (Reid *et al.*, 2006; Zhang, Bornholdt, *et al.*, 2012; Xu *et al.*, 2014). Recent data suggests VP24 is also able to block IFN induction by supressing nuclear factor-kappa B (NF-kB) activation following tumour necrosis factor alpha (TNF- α) stimulation (Guito *et al.*, 2017) and by supressing retinoic acid-inducible gene I (RIG-I) dependent activation of IFN-γ1 gene expression (F. He *et al.*, 2017). Furthermore, the innate response antagonist domains (IRAD) in EBOV VP24 and VP35 have been implicated in preventing the maturation of EBOV-infected dendritic cells by modulating global gene expression (Lubaki *et al.*, 2013; Ilinykh *et al.*, 2015). This effect required both VP24 and VP35 IRAD domains, though the VP24 IRAD domain alone was sufficient to down-regulate cytokine signalling pathways (Ilinykh *et al.*, 2015). These results highlight the importance of cooperative action of multiple viral proteins for evasion of the host immune response.

VP24 has also recently been seen to function in capsid assembly (Huang *et al.*, 2002). NP and VP35 are known to be the major components of the viral nucleocapsid, though VP24 is weakly associated and may act as a catalyst for particle formation (Huang *et al.*, 2002). Further evidence for a structural role of VP24 comes from the observation that N- or C-terminal deletions in VP24 inhibited the formation of nucleocapsid-like structures mediated by VP24, VP35 and NP co-expression (Han *et al.*, 2003). It was suggested that the N-terminal domain of VP24 facilitates capsid formation by mediating protein-protein interactions. This is supported by the observation that mutation of the VP24 N-terminal domain results in protein aggregation (Han *et al.*, 2003). A recent study confirmed the interaction between VP24 and NP, showing that VP24 residues V170 and N171 are located on a highly-conserved exposed loop that interacts with NP during nucleocapsid assembly (Banadyga *et al.*, 2017). Co-expression of VP24 and VP40 results in a greater production of virus-like particles (VLPs) than when VP40 is expressed alone (Licata *et al.*, 2004). Similarly, in live EBOV infection, VP24 small interfering RNA (siRNA) knockdown decreases viral budding and increases the retention of viral proteins within the cell (Mateo *et al.*, 2011). Further evidence suggests that VP24 binds to VP35 on the outer surface of the nucleocapsid where it organizes the adjacent NP layer, promoting nucleocapsid stability and explaining the observed interactions between NP, VP24 and VP35 during nucleocapsid formation (Beniac *et al.*, 2012).

In addition to its role in nucleocapsid stability, VP24 may be necessary for incorporation of the viral RNA genome into the nucleocapsid. Several studies have shown that VP24, together with VP35, induce conformational changes in NP that are necessary for vRNA encapsidation (Huang *et al.*, 2002; Noda *et al.*, 2005; Watanabe, Noda and Kawaoka, 2006). It was shown that VP24 may be directly involved in length-dependent RNA interactions and packaging (Watt *et al.*, 2014). In the study, transcription and replication-competent virus-like particles (trVLPs) were analysed for RNA content and a significant reduction of packaged RNA was observed when VP24 was knocked-down with an interfering micro-RNAs (miRNA). The trVLPs that were produced showed a twofold reduction in RNA content and a tenfold reduction of infectivity, suggesting that VP24 may play an essential role in

RNA packaging. Furthermore, disruption of the VP24-NP interaction reduced RNA packaging and resulted in a significant reduction in reporter activity, highlighting the importance of VP24 in RNA packaging (Banadyga *et al.*, 2017). In addition, trVLP reporter gene activity was significantly affected by the presence of VP24 in a genome-length dependent manner. Using the trVLP tetra-cistronic genome system, the presence of VP24 during VLP production resulted in a 25-fold increase in reporter gene activity upon subsequent infection, whereas the presence of VP24 had no effect when mono-cistronic mini-genome systems were used in the trVLP, suggesting a genome length-dependent role for VP24 in RNA packaging and VLP/virion infectivity. Surprisingly, VP24 may also have a length-dependent role in transcriptional regulation. It was observed that VP24 moderately inhibited the expression of reported genes from mono-cistronic mini-genome plasmids (Watanabe *et al.*, 2007). However, VP24 expression had no effect on protein expression from the trVLP tetra-cistronic genomes (Watt *et al.*, 2014). Whilst the impact of VP24 on protein expression is not clear, VP24 itself may be subject to length-dependent transcriptional regulation. Recent work has implicated the length of the intergenic region (IR) between VP30-VP24 as having a significant impact on VP24 expression by regulating transcription initiation frequency (Neumann, Watanabe and Kawaoka, 2009; Brauburger *et al.*, 2014). The importance of the broad range of VP24 functions during virus replication are highlighted by the fact that it has not been possible to create a VP24-deficient recombinant EBOV, even when VP24 is supplied in trans (Mateo *et al.*, 2011).

1.2.2 VP35*

As with VP24, VP35 is primarily known for its multifaceted ability to suppress the host cell immune response. VP35 is a type-I interferon antagonist, inhibiting the activation of interferon regulatory factor (IRF)-3 via double-stranded RNA binding and reducing IFN-α/β production by inhibiting RIG-I signalling (Basler *et al.*, 2000; Cárdenas *et al.*, 2006; Luthra *et al.*, 2013). VP35 also blocks IFN production by increasing protein inhibitor of activated STAT 1 (PIAS1)-mediated SUMOylation of IRF-7, thus inhibiting IFN production following toll-like receptor (TLR) and RIG-I activation (Chang *et al.*, 2009). Lastly, VP35 is a suppressor of RNA silencing,

functionally equivalent to the human immunodeficiency virus (HIV-1) trans-activator of transcription (Tat) protein and important for viral evasion of the innate immune response (Haasnoot *et al.*, 2007). Together, there is significant evidence demonstrating VP35's intricate ability to inhibit innate immune signalling and the host antiviral response [Figure 5].

Recent work suggests that VP35 may have more diverse functions during virus replication, as VP35 was shown to interact with L and facilitate genome transcription through the formation of the RdRp complex and genome packaging through association with NP (Groseth *et al.*, 2009; Prins *et al.*, 2010; Kirchdoerfer *et al.*, 2016). The first 450 residues of VP35 appear to be essential for binding to L and thus RdRp function, whereas the C-terminus associates with NP, thus linking NP-L during nucleocapsid assembly (Prins *et al.*, 2010; Trunschke *et al.*, 2013). N-terminal deletions in VP35 block these interactions and were sufficient to inhibit the replication and transcription of a EBOV mini-genome system (Trunschke *et al.*, 2013). The role of the VP35 C-terminus in capsid assembly is perhaps surprising, as this region contains the interferon inhibitory domain responsible for its main role in immune

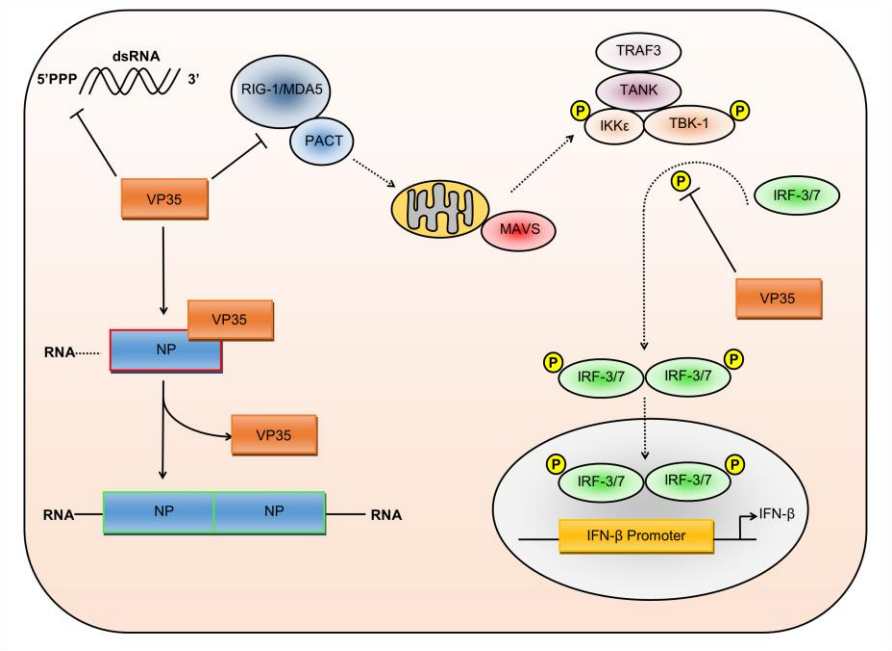

Figure 5. Multiple roles of VP35 during virus replication
VP35 inhibits the type-I IFN response through several different mechanisms. VP35 can bind to dsRNA, preventing the activation of RIG-I signalling. In addition, VP35 blockade of IRF3 and IRF7 phosphorylation inhibits the production of IFN-β. Recent studies have also highlighted the importance of VP35 in regulating NP–RNA association. During viral genome replication, the VP35 N-terminal peptide binds to NP, enabling the vRNA to associate with the RdRp complex for replication. During virus assembly, VP35 disassociates, enabling NP to oligomerise, bind RNA, and form the nucleocapsid. 5'PPP, 5' triphosphate; dsRNA, double-stranded RNA; IFN, interferon; IKK, inhibitor of nuclear factor kappa B kinase subunit epsilon; IRF, interferon regulatory factor; MAVS, mitochondrial antiviral-signalling protein; MDA5, melanoma differentiation-associated protein 5; NP, nucleoprotein; PACT, protein activator of the interferon-induced protein kinase; RdRp, RNA-dependent RNA polymerase; RIG-I, retinoic acid-inducible gene I; TANK, tumour necrosis factor–receptor-associated factor family member–associated nuclear factor kappa B activator; TBK1, tumour necrosis factor–receptor-associated factor family member–associated nuclear factor kappa B activator binding kinase 1; TRAF3, tumour necrosis factor–receptor-associated factor 3; VP, viral protein; vRNA, viral RNA.

evasion. However, this domain contains several conserved stretches of basic residues, the central region is involved in dsRNA binding and IFN inhibition whereas a preceding stretch mediates interaction with NP (Prins *et al.*, 2010). Further research found the VP35-NP interaction controls the switch between RNA-bound NP and free NP, thus switching between genome replication and genome packaging in the nucleocapsid (Leung *et al.*, 2015). A N-terminal peptide derived from the VP35 NP-binding protein region (NPBP) binds NP with high affinity causing the release of

RNA from NP and resulting in the activation of genome transcription and the inhibition of NP oligomerization [Figure 5] (Leung *et al.*, 2015). Additional investigation of VP35-NP binding showed two further interaction sites. Hydrophobic VP35-NP binding at these sites inhibited NP oligomerisation and prevented NP-RNA binding by blocking access to the RNA binding domain (Kirchdoerfer *et al.*, 2015). Work by Leung et al. suggest that during nucleocapsid formation the NPBP peptide first disassociates from NP, then RNA binds to NP followed by NP oligomerization. In contrast, Kirchdoerfer et al. show that monomeric NP has no significant affinity for RNA, suggesting that the NPBP peptide would be displaced by an additional NP molecule, causing NP oligomerization which would then allow for RNA binding. However, in either process, VP35-NP interactions are crucial for virus replication and are being explored as targets for future therapeutics (Ren *et al.*, 2016; G. Liu *et al.*, 2017).

VP35 also undergoes further protein-protein interactions that may affect viral genome transcription through the interaction with the cytoplasmic dynein light chain (LC8) (Kubota *et al.*, 2009). LC8 is a highly conserved 8kDa subunit of the cytoplasmic dynein motor complex but can also exist as a dimer in soluble form, where it can affect viral transcription and assembly (Tan *et al.*, 2007; Kirkham *et al.*, 2016). LC8 was seen to stabilize VP35 N-terminal oligomerisation in a dose-dependent manner and enhance viral genome synthesis (Luthra *et al.*, 2015). It was noted that LC8 functions mostly in the early stages of infection, enhancing early viral gene expression before the host cells are able to establish the antiviral state. Thus, VP35 modulation of viral RNA transcription can facilitate virus replication while simultaneously enhancing immune evasion.

1.2.3 VP30*

The minor nucleoprotein VP30 has the primary role of initiating EBOV transcription (Weik *et al.*, 2002). It is dynamically phosphorylated, whereby upon phosphorylation, transcription is negatively regulated, enabling binding to NP (Modrof *et al.*, 2002; Biedenkopf, Lier and Becker, 2016). In turn this permits interactions that regulate viral RNA synthesis (Kirchdoerfer *et al.*, 2016). VP30 binds zinc ions due to the

presence of an unconventional zinc-binding motif, facilitating RNA binding and increasing viral genome transcription (Modrof, Becker and Mühlberger, 2003; John *et al.*, 2007; Biedenkopf *et al.*, 2016; Schlereth *et al.*, 2016).

In addition to its RNA binding role in transcription, VP30 also interferes with cellular RNA silencing (Fabozzi *et al.*, 2011). In the presence of siRNA, VP30 was seen to interact with the essential RNA interference (RNAi) protein Dicer, though the VP35 N-terminus RNA binding domain was not required for the interaction or for the suppression of RNAi [Figure 6]. As with the RNA silencing suppressor activity of VP35, the exact role of RNAi in antiviral immunity is not clear, nor is the consequence on EBOV replication of blocking miRNA/siRNA processing as mediated by VP30 (Li *et al.*, 2013). However, despite the fact that RNA binding is not required for RNA silencing suppression, VP30 was seen to bind to a variety of non-viral RNAs. VP30-RNA binding required specific base composition and structure of the target RNA molecule (Schlereth *et al.*, 2016), though it is not clear if there is a function of VP30 binding to non-viral RNA or if this is a consequence of its necessary binding to viral RNA during transcription.

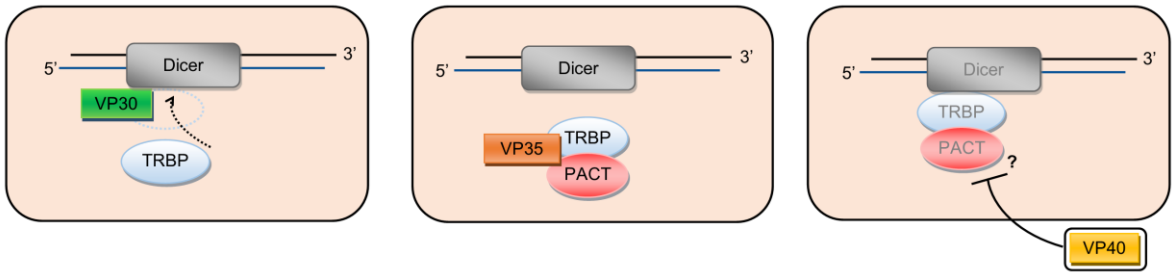

Figure 6. Ebolavirus proteins VP30, VP35, and VP40 are suppressors of RNA silencing

Cellular RNA interference requires the assembly of the Dicer:TRBP:PACT complex. VP30 inhibits RNAi by interacting with Dicer, preventing TRBP binding and complex activity. VP35 also inhibits complex assembly by binding TRBP and PACT, preventing their association with Dicer. VP40 suppresses RNAi during infection or when transferred to bystander immune cells through exosomes, though the mechanism by which VP40 inhibits the Dicer machinery is currently unknown. PACT, protein activator of the interferon-induced protein kinase; RNAi, RNA interference; TRBP, Trans-activation response RNA binding protein; VP, viral protein.

1.2.4 VP40*

The matrix protein VP40 has roles predominantly in virus assembly and budding (Ruigrok *et al.*, 2000; Pleet *et al.*, 2017). VP40 can assemble either as a hexamer, which appears to be involved in budding, or as an octamer that functions in genome replication and RNA binding (Timmins, Schoehn, Kohlhaas, *et al.*, 2003; Bornholdt *et al.*, 2013). Most research has focused on the role of VP40 in assembly and budding, however, recent studies have begun to elucidate novel roles.

VP40 is known to be sufficient to mediate the formation and budding of VLPs; however, recent results have demonstrated that VP40 induces the formation for exosomes that are capable of inducing bystander cell death (Harty *et al.*, 2000; Pleet *et al.*, 2016). Exosome release has been seen in virally-infected cells and VP40 expression was seen to increase the expression of several endosomal sorting complex required for trafficking (ESCRT) proteins involved in exosome biogenesis, including: tumor susceptibility gene 101 (TSG101), vacuolar protein-sorting-associated protein 25 (VPS25), and VPS36 (Wauquier *et al.*, 2010; Pleet *et al.*, 2016). This is consistent with previous reports showing VP40 utilizing ESCRT proteins to aid viral budding, though how VP40 switches between budding and exosome release is not clear (Licata *et al.*, 2003; Timmins, Schoehn, Ricard-Blum, *et al.*, 2003; Han *et al.*, 2015).

Transfer of VP40-induced exosomes to naïve T-lymphocytes and monocytes induced apoptosis and significantly reduced cell viability similarly to that seen when exosomes from virally infected cells were used (Wauquier *et al.*, 2010; Pleet *et al.*, 2016). However, Pleet et al. noted that the presence of VP40 in the exosomes caused a downregulation of miRNA machinery in both the donor and recipient cells, including a reduction in the expression of Dicer, argonaute-1, and Drosha [Figure 6]. It was previously noted that VP35, VP30 and VP40 are capable of interacting with the miRNA/RNAi pathway (Fabozzi *et al.*, 2011), however, this was the first demonstration that the suppression of RNA silencing can be transferred to naïve cells in the absence of virus. Currently, the precise mechanism in which VP40 interacts with miRNA machinery has yet to be characterised and it is not yet known if the action of VP40 on the miRNA machinery directly causes apoptosis or if the exosomes contain other proteins or RNA's that may be responsible for causing the

induction of apoptosis. However, the repression of key proteins in the miRNA pathway has been previously linked to the induction of apoptosis, thus the suppression of RNA silencing may serve both to directly counteract the innate cellular immune response and to induce apoptosis of bystander immune cells, blocking the activation of adaptive immunity (Han *et al.*, 2013; Pleet *et al.*, 2016, 2017).

Due to the essential role of VP40 in viral assembly and budding, several studies have looked at inhibiting VP40 for the creation of new antiviral therapeutics (R. V Stahelin, 2014; Biedenkopf *et al.*, 2017). As VP40 also plays a role in immune evasion (via RNAi suppression and exosome-bystander cell death), there is increased motivation for developing therapeutics that target one or multiple of the functions of VP40. It is known that viral replication requires VP40 phosphorylation at tyrosine 13 by the cellular tyrosine kinase Abelson murine leukemia viral oncogene homolog 1 (c-Abl1) (García *et al.*, 2012). In addition, recent results showed that cyclin-dependent kinase 2 (Cdk2) in complex with Cyclin A or Cyclin E phosphorylated exosomal VP40 at serine-233 (Pleet *et al.*, 2016). Thus, the inhibition or modulation of VP40 phosphorylation may be a target for new therapeutics. Lastly, Pleet et al. showed that treatment with the FDA-approved drug Oxytetracycline reduced VP40-exosome release and significantly increased donor cell viability upon treatment with VP40-exosomes, further suggesting that targeting the secondary functions of VP40 may be a new approach for developing antivirals for EVD.

1.2.5 Glycoprotein*

The GP gene has been shown to encode for three different products due to transcriptional editing by L polymerase: full length GP which consist of GP1 (receptor binding) and GP2 (viral fusion) subunits, soluble GP (sGP) which lacks the transmembrane domain, and small soluble GP (ssGP) (Volchkova *et al.*, 1998; Mehedi *et al.*, 2011). Due to furin cleavage of sGP, a smaller cleaved fragment is also produced, called Δ-peptide (V.A., H.-D. and V.E., 1999). GP is the only viral protein located on the surface of the virion and has a critical role in attachment and

fusion (Shimojima *et al.*, 2006; Lee and Saphire, 2009; Moller-Tank *et al.*, 2015). Ebolaviruses are thought to predominantly enter cells via GP-dependent macropinocytosis though other mechanisms have been reported, depending on factors such as host cell type (Nanbo *et al.*, 2010; Aleksandrowicz *et al.*, 2011). After entry, GP directs fusion between the viral membrane and endo-lysosomes that contain the viral receptor Niemann-Pick C1 (NPC1) and two pore segment channel 2 (TPC2), enabling release of the viral genome (Mingo *et al.*, 2015; Simmons *et al.*, 2016). During the 2014-2016 outbreak, a mutation in GP at A82V was detected with high frequency (Diehl *et al.*, 2016; Urbanowicz *et al.*, 2016; Dietzel *et al.*, 2017). It is worth mentioning that Urbanowicz *et al* reported an increase in infectivity using pseudotyped virus as opposed to live virus, however, this mutation increased GP membrane fusion activity and increased infectivity in a variety of cell types, including: Chimpanzee fibroblasts (S008842), Rhesus epithelial (FRhK4), African green monkey epithelial (Vero) and human dendritic cells. The authors propose that this mutation is likely a result of EBOV adaptation to the human host, as several viral variants have been seen to increase human cell infectivity while decreasing virus entry in nonhuman primates (Hoffmann *et al.*, 2017; Ruedas *et al.*, 2017; Wang *et al.*, 2017). Thus, the specific nature of protein function needs to be considered in the context of the given host.

GP has been shown to have a multitude of secondary roles beyond attachment and fusion that affect both virus replication and pathogenicity. Several studies have shown that GP contributes to EBOV virulence; however, it is not sufficient on its own to be defined as a virulence marker, despite having marked effects beyond entry and fusion (Groseth *et al.*, 2012). EBOV GP expression has been well established as having a cytotoxic effect on host cells (Yang *et al.*, 2000; Ray *et al.*, 2004; Sullivan *et al.*, 2005). GP cytotoxicity is mediated through the mucin-like domain and its effect on the extracellular signal–regulated kinase (ERK) mitogen-activated protein kinase (MAPK) pathway (Zampieri *et al.*, 2007). EBOV GP reduces the phosphorylation and catalytic activity of ERK2 resulting in the loss of cell adherence, cell rounding and the induction of non-apoptotic cell death. The decrease in ERK2 activity was also necessary for GP-induced downregulation of αV integrin expression; further impairing cell adherence and tight junction formation. In addition, the sGP cleavage

product, Δ-peptide, may play a role in EBOV pathogenicity by acting as a viroporin (Gallaher and Garry, 2015). Δ-peptide is able to form pores in the plasma membrane of mammalian cells, increasing ion permeability and causing cytotoxicity (J. He *et al.*, 2017). However, it is not known if the Δ-peptide can be released from cells or if its induction of cytoxicity is limited to within the infected cell. In order to regulate the toxicity caused by GP and its cleavage products at early stages of infection, GP expression is dynamically regulated (Alazard-Dany *et al.*, 2006). The balance and timing of EBOV GP/sGP/ssGP/shed-GP/ Δ-peptide expression has been found to be pivotal in virus replication, affecting not only cell death but viral assembly and budding (Mohan *et al.*, 2015).

Whilst VP40 expression is sufficient to produce VLPs, GP expression enhances VLP generation, suggesting a possible secondary role for GP in viral egress (Licata *et al.*, 2004). Recent work suggests that GP does not directly affect viral assembly or budding, but rather counteracts the cellular budding restriction factor tetherin (Kaletsky *et al.*, 2009). In the absence of GP, VLPs assemble and bud but are retained on the cell surface through the anti-viral tethering actions of the tetherin protein. GP expression enabled VLP release but did not affect tetherin cell-surface localization nor was a specific GP-tetherin interaction found (Lopez *et al.*, 2010). It was shown that the GP glycosylation and its receptor-binding domain (RBD) were critical for anti-tetherin activity, though mutation of the RBD did not affect interactions with tetherin and inhibition of GP-NPC1 binding did not affect the anti-tetherin activity (Brinkmann *et al.*, 2016). Instead, it is thought that GP is specifically able to block the association between VP40 and tetherin, though the nature of tetherin-VP40 interaction and the mechanism of GP inhibition is not known (Gustin *et al.*, 2015).

EBOV infection causes significant impairment of the endothelial barrier function. GP repression of ERK2 activity reduces integrin expression and cell adherence; however, GP also induces endothelial cell activation, further decreasing endothelial barrier functions (Wahl-Jensen *et al.*, 2005). During EBOV infection of endothelial cells, cell adhesion molecules (CAM) ICAM-1 and VCAM-1 were found to be transcriptionally upregulated, with increased cell surface expression of CAMs. The activity occurs with cellular GP expression as well as following the transfer of GP-containing VLPs, viral replication does not appear to be required. Endothelial

activation was not observed in the absence of GP, nor with the GP transcriptional variant sGP or the GP cleavage product Δ-peptide (Wahl-Jensen *et al.*, 2005). GP-induced endothelial cell activation may facilitate decreased barrier function whilst the upregulation of CAMs may facilitate adhesion and subsequent infection of immune cells, such as macrophages. A model was proposed whereby activated endothelial cells results in increased leukocyte recruitment, resulting in thrombomodulin release resulting in an activated, leukocyte rich endothelium in a procoagulant state (McElroy *et al.*, 2014). Whether this is an unintended consequence of GP or has a role in increased viral spread and infectivity is yet to be investigated.

EBOV GP has also been implicated in modulation of the host immune system. GP on the cell plasma membrane has been shown to be cleaved by tumour necrosis factor α-converting enzyme (TACE), resulting in the release of a soluble cleaved product called shed GP that is missing the transmembrane domain (Dolnik *et al.*, 2004). Shed GP was seen to activate uninfected macrophages and dendritic cells, resulting in the production of multiple pro- and anti-inflammatory cytokines, including TNF-α with subsequent effects on vascular permeability (Escudero-Pérez *et al.*, 2014). It is thought that shed GP activates macrophages by binding to and activating TLR4 in a manner requiring GP glycosylation. Recently it was also shown that full-length GP on VLPs can also trigger the activation of TLR4 in macrophages, resulting in a similar activation phenotype (Olejnik *et al.*, 2017). In contrast, GP binding to TLR4 on T lymphocytes directly triggers cell death through an upregulation of caspase 9, even in the absence of infection (Iampietro *et al.*, 2017). In dendritic cells, GP was found to interact with the liver and lymph node sinusoidal endothelial cell C-type lectin (LSECtin), a C-type lectin, which contains two amino acids residues Asn256 and Asn274 that bind GP in a Ca^{2+} dependant manner, triggering the activation of spleen tyrosine kinase (Syk) signalling and the production of inflammatory cytokines TNF-α and Interleukin-6 (IL-6) (Zhao *et al.*, 2016). As shed GP retains most of the structure of full-length GP, this soluble molecule is capable of binding to and neutralizing circulating anti-GP antibodies, facilitating viral immune evasion (Dolnik *et al.*, 2004).

Similarly, sGP has been implicated in evading the immune system via antigenic subversion (Mohan *et al.*, 2012). It was found that boosting GP-immunised mice with

sGP biased B-cell response toward epitopes that were shared between sGP and GP, reducing GP-specific antibody production and possibly impeding the immune-mediated clearance of EBOV infection. The structure of sGP in complex with antibodies was recently solved and highlights differences in antibody reactivity between GP and sGP (Pallesen *et al.*, 2016). Whilst GP is trimeric, sGP oligomerises into a parallel homodimer. Cross-reactive c13C6 antibody epitopes are presented similarly on GP and sGP, though the authors report that one c13C6 antibody binds to one GP trimer whereas multiple different immune-complexes were formed with sGP, ranging from rectangular complexes with a 2:2 ratio of c13C6 antibody to sGP dimer up to pentagonal 5:5 antibody:sGP complexes (Pallesen *et al.*, 2016). This further supports the hypothesis that sGP enhances viral immune evasion by biasing the antibody response toward sGP binding.

Whilst the multitude of GP secondary effects have a significant impact on EBOV infection, pathogenesis and immune evasion, GP remains the immunodominant protein on the EBOV virion and vaccination with the GP protein on pseudotyped viruses, rVSV-ZEBOV, has been highly effective in preventing EVD (Henao-Restrepo *et al.*, 2016).

1.2.6 Nucleoprotein and L-polymerase*

NP has a distinct function in the replication cycle in such that it is a key component of the viral ribonucleoprotein complex and has critical roles in protecting viral RNA from degradation and in mediating genome encapsidation during virus assembly (Baseler *et al.*, 2017). At present, all research has focused on these primary activities of NP and any secondary roles remain to be determined (Huang *et al.*, 2002; Watanabe, Noda and Kawaoka, 2006; Kirchdoerfer *et al.*, 2015). Similarly, the RNA dependent L-polymerase is an essential component of the (RdRp) complex and required for viral genome transcription and replication (Baseler *et al.*, 2017). It has been observed that L can also edit mRNA, as seen with the GP gene, where L-editing results in the production of the GP transcript instead of sGP (Volchkov *et al.*, 1995). L-editing may also regulate the different expression levels of GP, sGP and ssGP. During serial passage in tissue culture cells, L was found to add a single

uridine (U) residue to a site consisting of 7 U's in the GP gene, changing the expression ratio of GP:sGP to 80:20. A single passage in guinea pigs caused reversion of the genome back to 7 U's and changed the GP:sGP expression ratio back to 20:80, which may facilitate immune evasion during *in vivo* replication (Volchkova *et al.*, 2011). In contrast, during viral replication in the human hepatocarcinoma cell line (Huh7) a 9U variant was seen that retained the high level expression of sGP but had enhanced expression of ssGP (Mehedi *et al.*, 2011). It is speculated that these rapid alterations in the GP gene may act as a regulatory mechanism, enabling efficient virus replication in different host environments. At present, no other roles for the L protein have been postulated.

1.3 Viral Entry, Replication and Egress

1.3.1 Attachment and Entry

Attachment to cellular membranes largely revolves around interactions with EBOV GP, exposed on the virion membrane, and virion lipid binding to phosphatidylserine receptors. GP contains O- and N-linked glycans which allows binding to several carbohydrate-binding receptors on the cell surface such as C-type lectins DC-SIGN, L-SIGN, LSECTin, and hMGL (Alvarez *et al.*, 2002; Takada *et al.*, 2004; Gramberg *et al.*, 2005). These C-type lectin receptors are present on various cells, resulting in broad cell tropism for the virus. Furthermore, GP has been shown to bind to glycosaminoglycans exposed on the cell membrane surface, further facilitating virion attachment to the cell membrane (O'Hearn *et al.*, 2015). The presence of these receptors interacting with GP are known for viral attachment, however cells lacking expression of glycan receptors are still susceptible to viral infection, therefore implicating that other receptors are crucial for viral attachment and internalisation (Davey *et al.*, 2017). The virion leaflet contains phosphatidylserine residues which interact with TIM receptors as they possess an immunoglobulin variable-like domain that contains a phosphatidylserine binding pocket (Moller-Tank *et al.*, 2013). In addition, TAM receptors complexed with Gas6 and Protein S allow binding to phosphatidylserine residues, enhancing EBOV attachment.

The mechanism regarding EBOV internalisation has been heavily researched. Current data has implicated macropinocytosis as the main mechanism for virion entry in a GP dependent manner. Upon GP binding to receptors, activation of cellular actin modulators such as PI3K, small GTPase, PKC and Pak1 occur, resulting in actin rearrangement, a positive marker for macropinocytosis (Nanbo *et al.*, 2010). This leads to cellular membrane ruffling on the periphery of where the virion is bound, which ultimately results in a wave-like mechanism engulfing the particle in a macropinosome [Figure 7]. EBOV virions were found to co-localise with SNX5, a family of membrane proteins associated with macropinosomes (Nanbo *et al.*, 2010). Further evidence to support macropinocytosis mediated entry is that inhibitors of PI3K and Akt significantly reduced infection of EBOV (Saeed *et al.*, 2008).

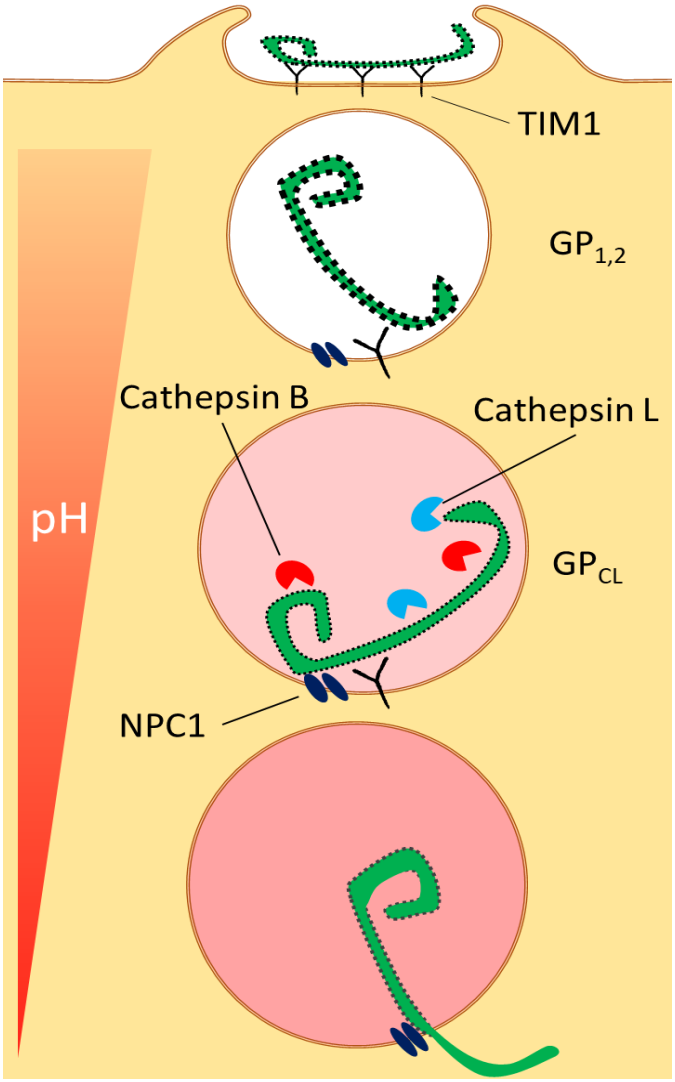

Figure 7. Schematic representation of EBOV entry and trafficking.

EBOV GP binds to various C-type lectins and glycosaminoglycans whereas phosphatidylserine exposed on the virion membrane binds to TIM receptors, anchoring it to the membrane. Activation of actin modulators result in macropinocytosis. As pH drops, cysteine proteases cleave GP, exposing binding pockets to NPC1. It is hypothesised that further modification of GP exposes a membrane fusion loop in GP2, resulting in fusion to the endosomal membrane and spillage of viral contents into the cytoplasm.

Upon internalisation, EBOV is trafficked via the endosomal pathway, leading to acidified $Rab7^{+}$ compartments (Saeed *et al.*, 2010). A drop in pH activates proteolytic activity of cathepsin B and cathepsin L, resulting in cleavage of the GP1,2 protein, yielding a cleaved GP (GPcl) containing a 18kD subunit of GP1 with exposed residues increasing receptor binding capability and ultimately enhancing infectivity

(Chandran *et al.*, 2005) (Kaletsky, Simmons and Bates, 2007). The GP1 subunit then binds to NPC-1 receptors which is required for viral membrane fusion in endosomes (Carette *et al.*, 2011; Spence *et al.*, 2016). How membrane fusion occurs remains poorly understood. It is hypothesised that cleavage of the GP1 from GPcl induces further conformational changes that may expose an internal fusion loop in GP2 required for membrane fusion (Davey *et al.*, 2017). Furthermore, it appears that the fusion event is independent of low pH (Markosyan *et al.*, 2016).The mechanisms by which GP2 interacts with the lipid membrane of the endosomes revolves around rearrangement of three N-terminal heptad repeats, allowing protrusion of a hydrophobic coiled-coil that fuses to the membrane (Gregory *et al.*, 2011). After fusion, the virus delivers its contents through the pore in the endosome.

1.3.2 Replication and Assembly

Replication and transcription occurs at the ribonucleoprotein (RNP) complex, which is believed to comprise of NP, VP30, VP35 and L (Groseth *et al.*, 2009). The RNP is released from the virion and acts as a template for the synthesis of its complementary positive-sense RNA, called the antigenome. The antigenome then acts as a template in order to generate new viral genomes. The minimal EBOV proteins in the RNP required for this are NP, the polymerase cofactor VP35 and L (Mühlberger, 2007). Viral replication occurs inside inclusion bodies and as infection progresses, these structures move from perinuclear regions towards the cell membrane, diminishing in size, suggesting nucleocapsids are on route to sites of viral budding (Hoenen *et al.*, 2012).

Transcription of the EBOV genome starts from the ‘3 end and is terminated and reinitiated at each transcription stop and start signals between the genes (Mühlberger, 2007). Transcription is regulated by VP30 at a very early stage and is regulated by a RNA stem loop structure in the first gene (Weik *et al.*, 2002). The L polymerase binds to the polymerase binding site at the ‘3 end of the genome, reads the sequence, stops and reinitiates at each gene junction (Whelan, Barr and Wertz, 2004). Due to disassociation of the polymerase complex from the RNA strand

between reads, upstream genes are highly expressed (NP) whereas downstream genes are lowly expressed.

It is hypothesised that regulation between replication and transcription is owed to dynamic phosphorylation of VP30. Since VP30 is known to stabilise the VP35-L RNA binding, phosphorylation states modulate the conformation of the RNP, resulting in either a transcriptase or replicase complex (Biedenkopf *et al.*, 2013).

Assembly occurs after the production of viral proteins from monocistronic mRNA by host ribosomes. As the viral proteins are generated in the cytosol they get trafficked to the cell membrane to assemble into virions. This trafficking occurs by VP40 hijacking the ESCRT pathway, For full length GP synthesis, the correct mRNA transcripts have to be generated by by transcriptional editing into the 8A transcript (Sanchez *et al.*, 1996). GP is synthesised and undergoes heavy modifications beginning in the endoplasmic reticulum. The precursor GP (GP0) is cleaved in the

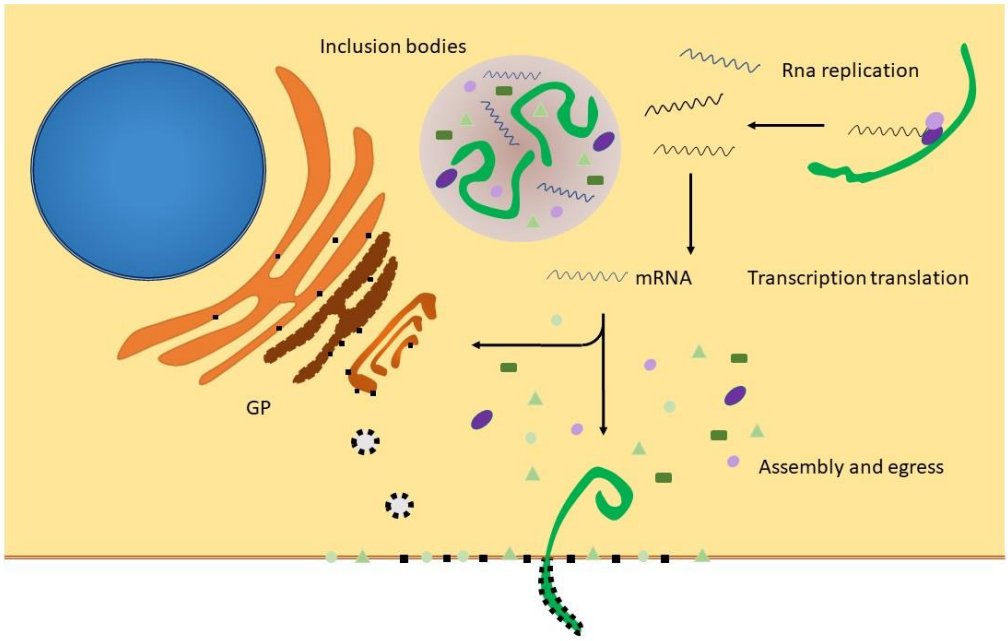

Figure 8. Replication, Assembly and Egress
As the viral contents are delivered into the cytoplasm, transcription of viral mRNA by the ribonucleoprotein complex occurs inside inclusion bodies. The glycoprotein undergoes a series of post translational modifications as it travels through the endoplasmic reticulum and golgi body, culminating in its' transport to the plasma membrane, where VP40 is also present. When the nucleocapsids are transported to the membrane containing GP and VP40, egress occurs into the extracellular environment.

endoplasmic reticulum and heavily glycosylated. At the *trans* golgi GP is cleaved by protease furin yielding a GP1 and GP2 subunit (Volchkov *et al.*, 1998). Post cleavage the fragments are then connected together by a disulphide bridge yielding the GP1,2 protein (Malashkevich *et al.*, 1999). This then undergoes trimerization, through the coiled coil repeats in GP2, yielding the classical spiked GP trimer that is then trafficked to the cell membrane alongside membrane bound VP40. The nucleocapsids formed in inclusion bodies comprising of NP repeats with viral RNA, facilitated in their formation by VP35 and VP24, meet near membrane bound GP and VP40 (Noda *et al.*, 2005). VP24 also regulates RNA synthesis by binding to the RNP, altering conformation of the RNP, resulting in a switch between replication competent complex to a rigid form ready for packaging into virions (Banadyga *et al.*, 2017).

1.3.3 Budding and Egress

EBOV filaments have been shown to bud in two distinct modes. Many reports have shown budding to occur vertically, driven by VP40. However, another mode of budding results in horizontal egress and it appears that only one mode of budding occurs per cell, never both (Noda *et al.*, 2006). This mode of horizontal budding appears to occur for mature virions containing nucleocapsids, whereas VLPs without the nucleocapsid bud vertically. Its postulated that this occurs because the nucleocapsid structures interact with VP40 that is already present on the cell membrane, thus being anchored under the membrane horizontally (Noda *et al.*, 2006). The alteration of membrane dynamics for budding and egress are caused by VP40, resulting in a negative membrane curvature (R. V. Stahelin, 2014). Eventually, this leads to viral particles being pushed out of the membrane and into the extracellular environment [Figure 8].

1.4 Pathogenesis

1.4.1 Dysregulation of the Immune Response

Ebola virus can enter a host via mucosal surfaces as well as breaks and abrasions in the skin. The early targets are dendritic cells, macrophages and Kupffer cells

whereby infection remains sustained (Geisbert *et al.*, 2003). Macrophages and monocytes possess fusion factors that allow GP-mediated attachment and entry of EBOV such as cathepsins, NPC1 receptors, ICAMs and phosphatidylserine residues. Viral spreading in the host is highly contributed by monocytes, macrophages and dendritic cells as these cells migrate via the lymphatic systems, reaching several organs such as the liver and spleen. Interestingly, infection of dendritic cells resulted in little cell death over 6 days of infection, which may contribute to its dissemination (Mahanty *et al.*, 2003). It is believed that the early targeting of the innate immune system cells contributes to immunosuppression, a characteristic of EBOV infection (Bray and Geisbert, 2005). However, macrophage targeting unleashes a robust cytokine and chemokine response which is considered to be a lethal aspect of EVD. High levels of TNF-α, IL-6β, reactive oxygen species and nitrogen radicals have been associated with fatal cases. Furthermore, the cytokine and chemokine response also contributes to viral dissemination as their activation recruits myeloid cells to multiple sites of inflammation, allowing the virus to sustain its infection (Zampieri, Sullivan and Nabel, 2007). Infection of dendritic cells also prevents their maturation, resulting in impaired T-cell proliferation (Jin *et al.*, 2010). A massive decrease in lymphocytes during infection is likely due to triggering of apoptosis, of which several mechanisms may be responsible, such as EBOV GP interacting with TLR4, and exosomes containing VP40 (Pleet *et al.*, 2016; Iampietro *et al.*, 2017). A variant of GP that is cleaved by cellular metalloprotease TACE enzyme referred to as cleaved GP activates dendritic cells and macrophages that are not infected with the virus via TLR4 receptor stimulation, resulting in activation of pro and anti-inflammatory cytokines (Escudero-Pérez *et al.*, 2014). This contributes to the dysregulation of the inflammatory response, which ultimately contributes to pathogenicity.

1.4.2 Inhibition of the Interferon Response

Upon infection, VP35 blocks interferon production by binding to dsRNA that would have otherwise culminated in activation of the IRF-3 pathway (Basler *et al.*, 2003). It

can also block interferon responses by disrupting the RIG-I signalling pathway by directly binding to kinases IKKε and TBK-1, involved in the activation of IFN-β signalling pathway. VP35 binding to these kinases prevents phosphorylation of IRF-3 and IRF-7 (Prins, Cárdenas and Basler, 2009). Whilst VP35 is preventing endogenous antiviral signalling, VP24 interacts with several proteins that render the cell to be silent upon stimulation by interferons. VP24 binds to importins such as KPNA1, 5 and, 6, which during normal interferon receptor stimulation, would import STAT1 to the nucleus to activate interferon stimulating genes. However, by binding to importins, nuclear import of phosphorylated STAT1 is now blocked, and evidence has also shown that VP24 may directly bind to STAT1, preventing phosphorylation altogether (Reid *et al.*, 2006; Zhang, Bornholdt, *et al.*, 2012). This results in inactivation of the interferon-α/β and interferon-γ signalling. Consequently, the virus is able to disseminate with little hindrance from antiviral defences as the immune response is unable to activate in a sufficient manner to combat the virus.

1.4.3 Pathogenesis in non-immune system cells

Several proteins of Ebola virus have been implicated in pathogenesis on endothelial and epithelial cells. GP contributes to cellular detachment of endothelial cells by downregulation of adhesion molecules such as integrins, leading to cell rounding and ultimately death by anoikis, a form of apoptosis characterised by loss of adhesion (Simmons *et al.*, 2002; Ray *et al.*, 2004). In addition, GP present on virus-like particles have been shown to decrease the endothelial barrier function, due to reduced intercellular adhesions, which results in increased extravasation of water and macromolecules. (Wahl-Jensen *et al.*, 2005). This manifests as the haemorrhagic symptom of EVD and facilitates spread of the virus within the organism and transmission between organisms. Remarkably, Reston virus infection in humans has not be associated with any symptoms of disease compared to its deadly counterpart.

1.5 Reston, The Forgotten *Ebolavirus*

This section contains our published review in unedited form (Cantoni *et al.*, 2016)*. The figure legends have been renumbered for the purpose of this thesis*

1.5.1 Abstract

Out of the five members of the *Ebolavirus* family, four cause life-threatening disease whereas the fifth, Reston virus (RESTV), is non-pathogenic in humans. The reasons for this discrepancy remain unclear. In this review, we analyse the currently available information to provide a state-of-the-art summary of the factors that determine the human pathogenicity of Ebolaviruses. RESTV causes sporadic infections in cynomolgus monkeys and is found in domestic pigs throughout the Philippines and China. Phylogenetic analyses revealed that RESTV is most related to the Sudan virus (SUDV), which causes high mortality in humans. Amino acid differences between RESTV and the other Ebolaviruses are found in all nine Ebolavirus proteins, though no one residue appears sufficient to confer pathogenicity. Changes in the glycoprotein (GP) contribute to differences in Ebolavirus pathogenicity but are not sufficient to confer pathogenicity on its own. Similarly, differences in VP24 and VP35 affect viral immune evasion and are associated with changes in human pathogenicity. A recent *in silico* analysis systematically determined the functional consequences of sequence variations between RESTV and human-pathogenic Ebolaviruses. Multiple positions in VP24 were differently conserved between RESTV and the other Ebolaviruses and may alter human pathogenicity. In conclusion, the factors that determine the pathogenicity of Ebolaviruses in humans remain insufficiently understood. An improved understanding of these pathogenicity-determining factors is of crucial importance for disease prevention and for the early detection of emergent and potentially human-pathogenic Reston viruses.

1.5.2 Introduction

The recent Ebola virus (EBOV) outbreak in West Africa changed our perception of the global threat posed by the Ebolaviruses. The outbreak was of unprecedented size, resulting in 28,657 confirmed cases and 11,325 deaths (as of 8/5/2016 - www.who.int), with several reported deaths on other continents (CDC, 2016). Previous Ebolavirus outbreaks ranged from a very few infected individuals to a few hundred cases (Georges *et al.*, 1999). During this outbreak, evidence has emerged that Ebola viruses were able to persist and remain infective in immune-privileged sites in the body (including the eye, semen, vaginal fluid and breast milk), for over 6 months after disease resolution and clearance of the virus from the bloodstream, significantly complicating disease containment and control (Deen *et al.*, 2015; Varkey *et al.*, 2015). The combination of these factors (outbreak size and virus persistence) raises significant concern for the danger posed by future outbreaks. Advancing our understanding of Ebolaviruses is extremely important in order to ensure adequate surveillance and outbreak containment; however, much remains unknown about the mechanisms by which these viruses cause disease.

Ebolaviruses are filo (filamentous) -viruses with a single-stranded negative-sense RNA genome. The *Ebolavirus* family consists of five species: *Zaire ebolavirus* (type virus: Ebola virus, EBOV), *Sudan ebolavirus* (type virus: Sudan virus, SUDV), *Tai Forest ebolavirus* (type virus: Tai Forest virus, TAFV) and *Bundibugyo ebolavirus* (type virus: Bundibugyo virus, BDBV), and *Reston ebolavirus* (type virus: Reston virus, RESTV). EBOV, SUDV, TAFV, and BDBV cause severe haemorrhagic disease in humans with mortality rates ranging from 50% to 90% (Geisbert and Hensley, 2004; Kuhn *et al.*, 2010). RESTV is mildly virulent in pigs, avirulent in humans, but lethal in several but not all non-human primates, for example, African green monkeys (*Chlorocebus aethiops)* and baboons *(Papio hamadryas)* are resistant to RESTV, the latter showing resistance to EBOV as well (Rollin *et al.*, 1999; Barrette *et al.*, 2009; Bente *et al.*, 2009; Marsh *et al.*, 2011). In addition, RESTV is less virulent when directly compared to EBOV infections in non-human primates as RESTV was observed to have a slower onset of disease and viraemia (Fisher-Hoch *et al.*, 1992). Furthermore, coinfection may have a role in increasing

severity of disease, as a simian haemorrhagic fever virus coinfection with RESTV was detected in at least one of the non-human primates in RESTV outbreaks, which resulted in death (Dalgard *et al.*, 1992). Since current knowledge cannot elucidate the reason for RESTV being avirulent in humans means that it remains classified as a BSL-4 pathogen, as it may have pathogenic potential if ideal conditions are met, such as viral load, route of infection or other factors. The Ebolavirus genome is approximately 19 kb in length and encodes nine proteins: nucleoprotein (NP), glycoprotein (GP), soluble GP (sGP), small soluble GP (ssGP), RNA-dependant RNA polymerase (L), and structural proteins VP24, VP30, VP35, and VP40, many of which are associated with viral pathogenicity (Ikegami *et al.*, 2001; Feldmann and Geisbert, 2011; de La Vega *et al.*, 2015). Whilst the four human-pathogenic *Ebolavirus* species are all found in Africa, RESTV is known to be endemic in the Philippines and China. This makes RESTV the only Ebolavirus known to exist outside of Africa to date. RESTV was discovered by electron microscopic examination of infected cells during the 1989 epizootic outbreak in cynomolgus monkeys that had been imported from the Philippines into the United States and housed at a research facility in Reston, Virginia (Geisbert and Jahrling, 1990). The monkeys displayed the hallmark symptoms of Ebolavirus disease, including subcutaneous haemorrhaging, bloody diarrhoea, and sudden onset of anorexia (Dalgard *et al.*, 1992). In contrast, four handlers in the United States who became infected with RESTV did not show any signs or symptoms of illness, nor did the seropositive handlers at the Laguna export facility in the Philippines (CDC, 1990). Since then, several known minor outbreaks of RESTV have occurred in monkeys [Figure 9]: a subsequent outbreak in 1990 in Reston, Virginia, whereby four handlers developed antibodies to RESTV; a 1992 outbreak in Sienna, Italy in monkeys

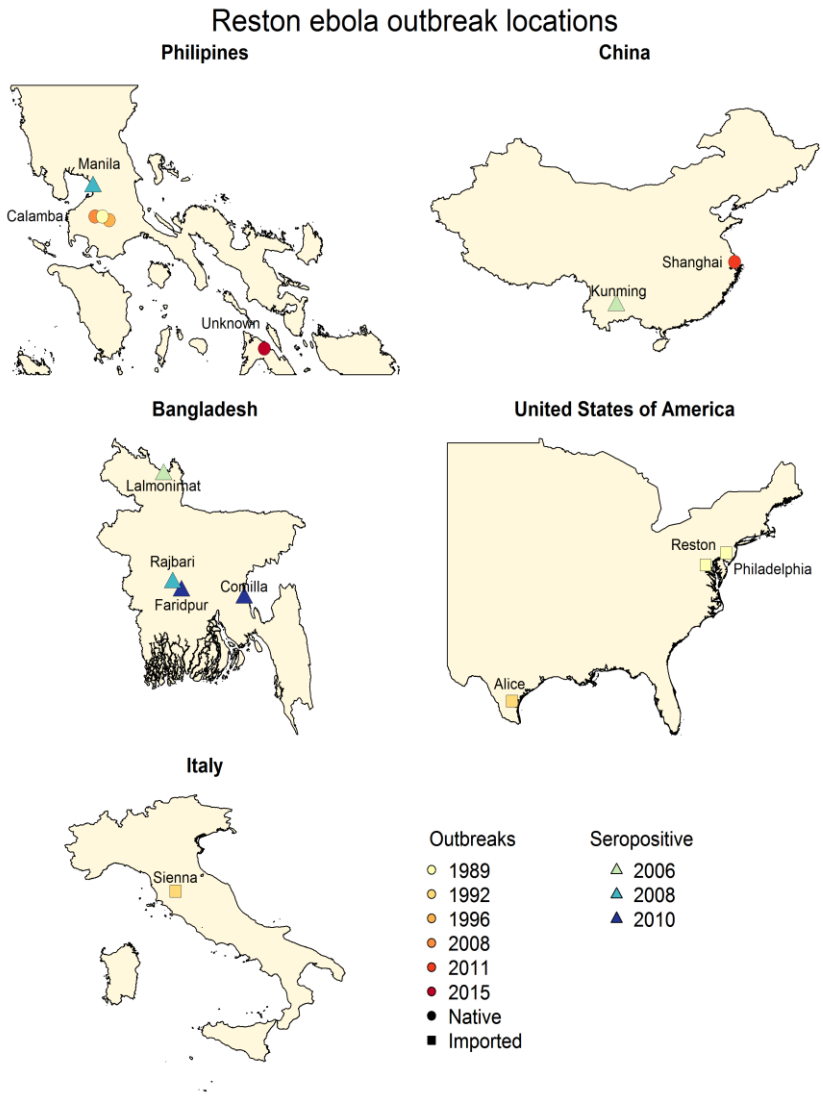

Figure 9. Detection of Reston Ebolavirus and Seropositive Evidence
This map shows that the virus, or seropositive evidence suggestive of virus infection, is more widely distributed that was previously thought (Rollin *et al.*, 1999; Yuan *et al.*, 2012; Olival *et al.*, 2013; Pan *et al.*, 2014). The distribution of RESTV appears to be in close proximity to the equator, similar to the other Ebolaviruses in Africa, though RESTV has never been detected in Africa

imported from the same facility in the Philippines that caused the 1989 outbreak; a 1996 outbreak in Alice, Texas, at the Texas Primate Centre; and two outbreaks in 1996 and 2015 in the Philippines (Geisbert and Jahrling, 1990; Dalgard *et al.*, 1992). In 2008, RESTV was found in farmed pigs in Manila, the Philippines (Barrette *et al.*, 2009)[Table 2]. Six handling personnel were found to be seropositive for RESTV, suggesting RESTV transmission from pigs to humans. Interestingly, RESTV was

Reston outbreaks

LOCATION	YEAR	ORGANISM	NO. OF SEROPOSITIVE HUMANS
PHILIPPINES	1989-90	Cynomolgus monkeys	3
USA, VA AND PA	1989-90	Cynomolgus monkeys	0
USA, TX	1989-90	Cynomolgus monkeys	4
ITALY	1992-93	Cynomolgus monkeys	0
USA, TX	1996	Cynomolgus monkeys	0
PHILIPPINES	1996	Cynomolgus monkeys	1
PHILIPPINES	2008	Pigs	6
CHINA	2011	Pigs	0
PHILIPPINES	2015	Cynomolgus monkeys	0

Locations with seropositive evidence only

PHILIPPINES	2008-2009	Fruit Bats	-
CHINA	2006-2009	Fruit Bats	-
BANGLADESH	2010-2011	Fruit Bats	-

Table 2. Outbreaks of Reston ebolavirus
(Jahrling *et al.*, 1990; Hayes *et al.*, 1992; Rollin *et al.*, 1999; Barrette *et al.*, 2009; Yuan *et al.*, 2012). The 1989 paper reports high mortality rates in the cynomolgus monkeys, whereas the infected pigs were found to be co-infected with PRRSV. The fact that there is additional seroevidence from countries further away from the Philippines strongly suggests migration of RESTV. No human handlers were reported to show any symptoms of disease (CDC, 1990).

only found in sick pigs that were also infected with porcine reproductive and respiratory syndrome virus (PRRSV), although histological analysis did not reveal colocalization of the two viruses in any body site. Whether RESTV contributed to the manifested symptoms remains to be determined (Marsh *et al.*, 2011). The viral genome sequences isolated from pigs in 2008 exhibited a 2.5% mean difference in nucleotide identity from the 1989 Reston monkey isolate. Three RESTV samples recently taken from infected pigs at different geographical locations in the Philippines

(Panganisan and Bulacan) showed even greater divergence from each other, with a 3.93% mean difference in nucleotide identity (Barrette *et al.*, 2009). It was suggested that the reason for this genetic diversity could result from both monkeys and pigs being infected from different unidentified reservoirs (Barrette *et al.*, 2009). In 2012, RESTV was again detected in pigs with PRRSV, this time in China, with 96.1%-98.9% sequence similarity to previous pig and monkey isolates from the Philippines (Pan *et al.*, 2014).

Despite the fact that the first known RESTV outbreak occurred almost 30 years ago, there is still relatively little known about this virus. This includes the natural reservoir for RESTV, the route of transmission from this reservoir to pigs and monkeys, and the reasons underlying its lack of pathogenicity in humans. Due to its similarity to the other four Ebolaviruses, there is a concern that RESTV could mutate to become pathogenic in humans, and that this Ebolavirus could then spread easily around the world through imported livestock or other animal hosts. In this review, we will discuss potential reservoirs for RESTV, its genetic relationship to other Ebolaviruses, and the molecular basis for its lack of pathogenicity in humans. We will also speculate on the potential risk of RESTV to human health and how this can be addressed.

1.5.3 RESTV Hosts and Reservoirs

Circulation of RESTV in reservoir species and other hosts may increase the probability that human-pathogenic RESTV variants emerge, in particular if selective pressures exerted by different hosts causes viral mutation or if the host range results in more frequent contact with humans. To date, it is known that RESTV can infect humans, monkeys, and pigs. However, it is often suggested that there are reservoirs for this virus that have not yet been identified (Barrette *et al.*, 2009; Yuan *et al.*, 2012). Bats are the most commonly implicated reservoir for filoviruses (Leroy *et al.*, 2005; Towner *et al.*, 2007; Negredo *et al.*, 2011). In 2008-2009 *Rousettus amplexicaudatus* fruit bats possessing RESTV-specific IgG antibodies were captured from the Philippine forests of Diliman and Cuezon, located within 60km from the Bulacan farm where RESTV-infected monkeys were identified in 2008 (Taniguchi *et al.*, 2011). *R. amplexicaudatus* are genetically similar to *R. aegyptiacus* bats, which are through to be the reservoir for Ebolaviruses in Africa (Taniguchi S,

Watanabe S, Masangkay JS, Omatsu T, Ikegami T, Alviola P, no date). In addition, RESTV as well as EBOV antibodies have been found in Bangladesh and in China in the related *R. leschenaultia* species of bats, suggesting that the Ebolaviruses may more widespread that previously believed.

1.5.4 RESTV genome evolution.

RESTV is thought to have originated in Africa and to have diverged from SUDV about 1400-1600 years ago before it migrated towards Asia [Figure 10.] (Sanchez, 2001; Geisbert and Hensley, 2004; Carroll *et al.*, 2013). The hypothesis that filoviruses have spread beyond the African continent was recently reinforced by the discovery of a new filovirus in bats in the Lloviu caves of Spain, as well as the

Phylogenetic analysis of the *Filoviridae* family.

Figure 10. Phylogenetic analysis of the Filoviridae family
RESTV is most closely related to SUDV (Carroll *et al.*, 2013). Bayesian coalescent analysis of viruses from the *Filoviridae* family.

presence of RESTV in bats, pigs and monkeys in Asia (Negredo *et al.*, 2011; Olival *et al.*, 2013; Pan *et al.*, 2014).

A recent phylogenetic study, analysed seven RESTV genomes, including four that were obtained from infected pigs (Carroll *et al.*, 2013). Whilst in one year on the same farm the virus showed genetic changes of 0.079%, in different farms there was a divergence of up to 4.5% (Carroll *et al.*, 2013). This study also showed that RESTV evolves at a rate of 8.21×10^{-4} nucleotide substitutions/site/year, similar to EBOV and much faster than the rate of nucleotide substitutions of SUDV, which could make the virus more susceptible to adaptation in humans.

The overall selection pressures between EBOV and RESTV show that amino acids on the main viral antigenic determinant, GP, were under increased selective pressure. EBOV selection pressure was found to be 0.299 whereas RESTV showed 0.329, whereby a ratio number >1 indicated increased selection, and <1 indicates decreased selection (Hurst, 2002). The EBOV GP showed selective pressure at mucin-domain residues 377 and 443, whereas RESTV GP was only under selective pressure at one glycosylated residue in the GP1 glycan cap, N229, though this residue was under stronger selection that any in EBOV GP (Li and Chen, 2014). These changes in GP may result in a different host tropism or may affect immune evasion, which may be a cause for concern for RESTV, though this has not been experimentally demonstrated.

1.5.5 Differences that may contribute to pathogenicity

A number of studies compared human pathogenic Ebolaviruses to RESTV in order to identify the underlying reasons for the observed differences in human pathogenicity (Reid *et al.*, 2007; Zhang, Abelson, *et al.*, 2012; Sandeep Chakraborty, Basuthkar J. Rao, Bjarni Asgeirsson, 2014). One of the proteins implicated in pathogenesis, VP24, acts by antagonising the host innate immune response. VP24 binds to the karyopherins (KPNA) 1, 5, and 6, inhibiting the nuclear import of phosphorylated (active) STAT1 and restricting the expression of interferon-stimulated genes (ISG) (Reid *et al.*, 2006). VP24 was also found to reduce binding of the heterogeneous nuclear ribonuclear protein complex C1/C2 (hnRNP C1/C2) to KPNA1, further restricting phosphorylated-STAT1 nuclear import as well as

relocating hnRNP C1/C2 from the nucleus into the cytoplasm (Shabman *et al.*, 2011). In viruses such as poliovirus and human papilloma virus, this relocation facilitates viral RNA replication and the translation of viral proteins (Gontarek *et al.*, 1999; Brunner *et al.*, 2005; Shabman *et al.*, 2011). In addition to blocking the STAT1 pathway, VP24 may also directly bind to STAT1 to prevent its nuclear import (Zhang, Bornholdt, *et al.*, 2012). EBOV VP24 may be more effective at suppressing the host interferon response than RESTV VP24 as EBOV-infected cells express lower levels of many ISGs than do RESTV-infected cells (Kash *et al.*, 2006).

Several amino acid differences between EBOV and RESTV VP24 may affect the virus's ability to inhibit STAT1 signalling, thus affecting pathogenicity (Groseth *et al.*, 2002). These variant residues appear to cluster at key sites involved in VP24 binding to KPNAs, such as the VP24 142-146 loop. In this region RESTV displays conserved amino acid changes (M136L, Q139R, R140S) compared to other Ebolavirus species (Zhang, Abelson, *et al.*, 2012). Changing the RESTV S140 residue to R140 modifies the hydrophobic moment of the protein and appears to be sufficient to enable KPNA binding (Sandeep Chakraborty, Basuthkar J. Rao, Bjarni Asgeirsson, 2014). These findings suggest that specific changes in RESTV VP24 may affect interactions with KPNAs, resulting in a reduced ability to inhibit interferon signalling. In 6-8-weeks old STAT1 knockout BALB/c mice, both EBOV and RESTV infections resulted in disease manifestation, causing lethargy, weight loss, and decreased survival rates after 6 days post infection. However, wild type BALB/c mice (6-8 weeks old) showed no manifestation of disease upon infection with either EBOV or RESTV (de Wit *et al.*, 2011; Raymond, Bradfute and Bray, 2011). EBOV was found to be lethal only in new-born mice or following several rounds of adaptation, however, the comparable experiments have not been performed with RESTV and thus the ability of RESTV to adapt and cause disease in mice remains unknown (de Wit *et al.*, 2011; Raymond, Bradfute and Bray, 2011). Moreover, when RESTV pathogenicity was tested in $IFNAR^{-/-}$ mice, only transient weight loss was observed between days 4-8, whereas EBOV showed to be uniformly lethal, with more severe symptoms, including weight loss, ruffled fur and hunched posture (Groseth *et al.*, 2012). Interestingly, $IFNAR^{-/-}$ mice challenged with RESTV became partially or completely protected from later mouse-adapted EBOV infections (Brannan *et al.*, 2015). This shows that RESTV

infections in different knockout mouse models are dissimilar, highlighting the complexity of testing RESTV pathogenicity in mice.

Bioinformatic investigation determined amino acid residues that are differently conserved (Specificity-Determining Positions, SDPs) between RESTV and the four human-pathogenic *Ebolavirus* species (Casari, Sander and Valencia, 1995; Rausell *et al.*, 2010). Several of these SDPs were located on protein surfaces, suggesting their possible involvement in molecular interactions (Pappalardo *et al.*, 2016). Whilst VP24 sequence identity between EBOV and RESTV is 80%, only 9 of 251 residues were identified as SDPs, possibly contributing to RESTV's lack of pathogenicity in humans (Ikegami *et al.*, 2001). Of the 9 SDPs found in VP24, three (T131S, M136L and Q139R) are located in the KPNA5 binding site. This supports the hypothesis that RESTV VP24 may be less effective at karyopherin binding and suppressing the interferon response. In addition, another SDP in RESTV VP24 results in the loss of hydrogen bonding between T226 and D48, potentially impacting protein stability and function (Pappalardo *et al.*, 2016). However, the SDPs were not restricted to VP24 and many SDPs were found in other protein interfaces that may affect interactions and stability [Table 3].

VP35 is an interferon antagonist that inhibits the activation of Interferon Regulatory Factor 3 (IRF3) following the sensing of viral RNA by the pattern recognition receptor RIG-I. RESTV VP35 has a 65% sequence identity with EBOV VP35 and shows 19 SDPs (Basler *et al.*, 2000; Cárdenas *et al.*, 2006; Prins, Cárdenas and Basler, 2009; Pappalardo *et al.*, 2016). Although, it was found that both RESTV and EBOV VP35 molecules were able to inhibit IRF-3 activation, blocking the IRF3-dependent transcription of the interferon sensitive genes (ISG) 54 and 56. In addition, neither RESTV nor EBOV VP35 could block signalling from the IFN-α/β receptor (Basler *et al.*, 2003). This implies that not all SDPs have an effect on pathogenicity; therefore, the consequences of these differences are not clear.

In addition to VP24, differences in the GP protein may also affect viral pathogenesis (Richman, DD. Cleveland, PH. McCormick, PB. Johnson, 1983; Feldmann, H. Kiley, 1999). EBOV GP contains a mucin-like domain that increases blood vesicle permeability by downregulating the expression of integrin β1 and other cell adhesion molecules (Chan, Ma and Goldsmith, 2000; Yang *et al.*, 2000; Simmons *et al.*, 2002).

RESTV GP has several conserved SDPs (R325G, H354L, Q403P, S418E, T448P) and was found to have a significantly weaker influence in downregulating integrin β1 expression, compared to EBOV GP (Simmons *et al.*, 2002; Pappalardo *et al.*, 2016). When examined *in vivo* it was seen that the presence of the RESTV GP attenuated EBOV pathogenicity, whereas the reverse genetics conversion of RESTV GP to EBOV GP was not sufficient to confer a pathogenic phenotype on RESTV, indicating that other proteins are involved in regulating Ebolavirus pathogenicity (Simmons *et al.*, 2002; Kash *et al.*, 2006; Groseth *et al.*, 2012).

Protein	Function	% SDPs
Nucleoprotein	Protects and packages the viral genome by encapsidation.	3.87
Glycoprotein	Class I viral fusion protein, responsible for binding and entry into host cells. Activated by proteolysis, creating GP1 and GP2. GP1,2 has extensive roles in modulating the immune response and altering the expression of cell surface adhesion molecules. Cleavage of GP1,2 from the plasma membrane creates a soluble variant.	4.3
sGP	Possible roles in immune evasion and alteration of endothelial permeability.	2.43
ssGP	Unknown role.	ND
VP24	Secondary matrix protein, minor component of virions. Key player in pathogenicity, inhibits components of immune response.	3.59
VP30	Viral nucelocapsid component. Key role in transcription depending on its state of phosphorylation	5.86
VP35	Polymerase cofactor in transcription and replication. Prevents antiviral response in cells by blocking IRF-3 and protein kinase EIF2AK2/PKR.	5.57
VP40	Regulates viral transcription, morphogenesis, packaging and budding.	2.72
Polymerase	Acts as a replicase and a transcriptase, whereby transcriptase is involved in subgenomic RNA capping and polyadenylation and the replicase function replicates the entire viral genome.	2.95

Table 3. Protein components of Ebolavirus and their roles

(Sanchez *et al.*, 1996; Han *et al.*, 2003; Watanabe, Noda and Kawaoka, 2006; Li *et al.*, 2008; Lee and Saphire, 2009; Prins, Cárdenas and Basler, 2009; Silva *et al.*, 2012)**.** The percentage of SDP sites in RESTV, as compared to EBOV, may offer clues as to the lack of RESTV pathogenicity in humans, though higher levels of specificity determining positions (SDP) do not necessarily indicate a change in protein function or activity. Furthermore, the percentage difference is likely to fluctuate regularly due to the viral mutation and evolution.

The functions of the two soluble and secreted Ebolavirus proteins sGP and ssGP remain the most elusive, with the structure of EBOV sGP only recently being solved (Pallesen *et al.*, 2016). sGP shares 295 N-terminal residues with GP, thus sGP is thought to contribute to evasion of the humoral system by absorbing GP antibodies (Sanchez *et al.*, 1996; Falzarano *et al.*, 2006). In addition, sGP seems to play an anti-inflammatory role by promoting recovery of the endothelial barrier during Ebolavirus infection (Wahl-Jensen *et al.*, 2005). RESTV appears to secrete more sGP than EBOV, suggesting that the anti-inflammatory role of sGP may have a more significant role on pathogenicity, considering its role on restoring the endothelial barrier (Wahl-Jensen *et al.*, 2005). The size of RESTV small soluble GP (ssGP), at 37kDa is significantly larger than that of the other Ebolaviruses (33kDa). However, the potential involvement of ssGP in pathogenicity remains unclear and thus the effect of the RESTV ssGP extension is unknown (Mahale and Patole, 2015).

It may also be that lack of RESTV virulence in humans is due to a delay in viral transcription and genome replication, as RESTV was found to have slower growth kinetics, suggesting a growth impairment that was not observed with EBOV (Boehmann *et al.*, 2005). The organisation of the RESTV genome differs from that of the other Ebolaviruses. Ebolaviruses contain gene overlaps between GP and VP30. In contrast, these two genes are separated by an intergenic region in RESTV (Sanchez, 2001). This change in genomic organization may affect the transcription of GP and VP30 or alter the efficiency of genome replication. Though, the relationship between EBOV gene overlap and genomic replication has not been tested, it is possible that the reduced efficiency of RESTV replication, combined with functional protein differences, could enable RESTV to infect humans without causing any detectable pathogenicity.

1.5.6 Conclusions

RESTV is unique among the Ebolaviruses in that it does not cause disease in humans. However, RESTV is infectious in several animal species that exist in close contact with humans, and humans can be asymptomatically infected with the virus, raising the question of whether humans can be carriers for Ebolaviruses and

suggesting that further adaptation of RESTV could cause a significant risk to human health.

An observed significant factor for the outbreak in West Africa was that infected bush meat provided a route of transmission of virus to humans (Alexander *et al.*, 2015). Humans and *R. leschenaultia* bats in Bangladesh share a common food source; date palm sap, which may be a potential route for viral transmission in humans. In addition, the ability of pigs to become hosts to RESTV means that the virus can be established in the human food chain, which is a cause for concern, as prolonged human contact may play a role for the virus to adapt to humans.

Furthermore, it may be the case that single amino acid substitutions in SDP sites can affect pathogenicity. This is concerning as many RESTV proteins had only a few SDPs that differed from EBOV, suggesting that a minimal number of mutations may be required to restore RESTV pathogenicity in humans. Thus, the investigation of the effects of individual SDPs is of great importance for understanding Ebola virus pathogenicity.

Whilst the likelihood that RESTV will become pathogenic in humans is not clear, given that it can establish itself in the human food chain in densely populated areas, the potential risk that the virus poses to human health worldwide is significant. This risk is even greater when considering that because RESTV is non-pathogenic in humans, the only people that have been screened for RESTV infection have worked at monkey and pig farms undergoing RESTV outbreaks, thus, the actual prevalence of RESTV in human and animal populations maybe significantly greater than anticipated. However, in response to the recent outbreak of EBOV in West Africa, research in treatments have shown promising advances, in particular vaccines and an antibody for pan-ebolavirus therapy, which has shown to be successful *in vitro* and *in vivo* in mice (Holtsberg *et al.*, 2015; Furuyama *et al.*, 2016).

1.6 Project outline

During this PhD course, we sought to explore the unknown reasons regarding differences in pathogenicity between EBOV and RESTV. Our experiments compared proteins from both species with the intent to elucidate the determinants of human *Ebolavirus* pathogenicity. This thesis will present the following projects:

1. Investigating cytotoxic properties of VP24

   This project was based on a statement made in Mateo et al. 2011 regarding VP24: “Our attempts to establish a cell line constitutively expressing VP24 also failed, probably as a result of as yet undefined cytotoxic properties of this protein (data not shown)”. Preliminary data in the laboratory showed that expression of VP24 in human cells caused cytotoxicity that was different with EBOV and RESTV VP24 proteins. We used multiple techniques in order to pinpoint the cellular pathways targeted by EBOV and RESTV VP24 proteins and uncover the mechanisms of VP24-induced cytotoxicity.

2. Solve the structure of delta-peptide.

   The delta peptide is a cleaved product of sGP. Current literature has shown that it is likely to act as a viroporin. However, no structures have yet been published. Given that this peptide retains an amphipathic helix, which binds to membranes either by full insertion or superficial interactions, we sought to solve the structure of the amphipathic helix and identify which residues are responsible for membrane interactions using NMR. Both EBOV and RESTV delta peptides will be compared to assess whether differences in sequence and structure contribute towards human pathogenicity.

2 Materials and methods

2.1 Materials

2.1.1 General Buffer Materials and Compositions

Deionized water and MiliQ grade water provided in house

General Buffer Materials	Company	Product Code
Acetic Acid	Sigma-Aldrich	A6283
Acetonitrile	Fisher Scientific	A/0627/17
Agar Technical	Oxoid	LP0012
Agarose	Sigma-Aldrich	A9539
Alpha-cyano-4-hydroxycinnamic Acid, 97%	Sigma-Aldrich	145505
Ampicillin Sodium Salt	Melford	A0104
Bacto Tryptone	BD Biosciences	211705
Bacto Yeast Extract	BD Biosciences	212750
Bovine Serum Albumin	Sigma-Aldrich	A2153
Bromophenol Blue	Sigma-Aldrich	114405
cOmplete mini Protease Inhibitor	Roche	04693116001
Deuterated Acetic Acid	Sigma-Aldrich	416886
DTT	Melford	MB1095
EDTA	Fisher Scientific	D/0700/53
Ethanol	Fisher Scientific	E/06500F/17
Formalin	Sigma-Aldrich	HT501128
Glucose	Fisher Scientific	10373242
Glycerol	Fisher Scientific	G/0650/17
HEPES	Sigma-Aldrich	H3375
Imidazole	Fisher Scientific	I/0010/53
IPTG	Melford	I56000

Kanamycin Sulfate	Sigma-Aldrich	K4000
L-Mimosine from Koa hoale seeds	Sigma-Aldrich	M0253
Phosphate Buffered Saline Tablets	Oxoid	BR0014G
phosSTOP phosphatase inhibitors	Roche	04906837001
Skimmed Milk Powder	Oxoid	LP0031
Sodium Chloride	Fisher Scientific	S/3160/60
Sodium Dodecyl Sulfate	Fisher Scientific	S/P530/53
Staurosporine	Abcam	Ab120056
Sucrose	Fisher Scientific	10638403
Tergitol (NP-40)	Sigma-Aldrich	NP40S
Trifluoro Acetic Acid	Sigma-Aldrich	302031
Tris Base	Fisher Scientific	T/P630/60
Tris HCL	Fisher Scientific	10060390
Triton X-100	Sigma-Aldrich	T8787
Tween-20	Sigma-Aldrich	P1379

General Buffers	**Composition**
Phosphate Buffered Saline	1 tablet per 100mL dH_2O
Tris Buffered Saline (20x) pH7.4	48g Tris Base 11.2g Tris HCL 176g NaCl dH_2O
TBS-T	TBS 1X 0.1% Tween-20
NP-40 Lysis Buffer	1% NP-40 in TBS 1X 1 tablet cOmplete protease Inhibitors 1 tablet phosSTOP phosphatase Inhibitor

5% Milk Blocking Buffer	5% (w/v) Skimmed Milk Powder, Laboratory Grade TBS-T
2% BSA Blocking Buffer	2% (w/v) Bovine Serum Albumin TBS-T
Laemmli Sample Buffer (4x)	40% Glycerol 240mM Tris HCL pH6.8 8% SDS 0.04% Bromophenol Blue
Miller LB Broth	NaCl Tryptone Yeast Extract dH_2O

2.1.2 Mammalian Tissue Culture Materials

Cell lines	Name	Source
HEK293T	Human Embryonic Kidney	ATCC
HeLa	Human Cervical Adenocarcinoma	ATCC
MEF	Mouse Embryonic Fibroblast	ATCC

Consumables and Reagents	Source	Product Code
T-75 Culture Flasks	Sarstedt	83.3911.002
T-175 Culture Flasks	Sarstedt	83.3912.002
6 Well Plate	Greiner	657160
12 Well Plate	Greiner	665180
24 Well Plate	Greiner	662102
96 Well F Bottom Plate	Greiner	655161
Dulbecco's Modified Eagle Medium	PanBiotech	P04-04510

Foetal Bovine Serum Good	PanBiotech	P40-37500
Trypsin	PanBiotech	P10-0235SP
Penicillin/Streptomycin	PanBiotech	P06-07100
Opti-MEM™	Gibco	31985070

2.1.3 Plasmids

Plasmids	Vector	Resistance	Source	Product Code
EBOV HA-VP24	pCAGGS	Ampicillin	BEI	NR-49207
RESTV HA-VP24	pCAGGS	Ampicillin	BEI	NR-49206
DsRed-MLKL	pDsRed-Monomer-C1	Kanamycin	Dr Zheng-Gang Liu, National Institute of Health USA	
RIP3-YFP	pEYFP-N1	Kanamycin	Dr Zheng-Gang Liu, National Institute of Health USA	
mCherry-Mito-7	mCherry	Kanamycin	Addgene	#55102
RESTV GP	pcDNA3.1	Ampicillin	Dr Elke Mulhberger, National Emerging Infectious Diseases Laboratories	
EBOV Delta Peptide	pUC19	Ampicillin	Synthesised Commercially	
RESTV Delta Peptide	pUC19	Ampicillin	Synthesised Commercially	

EBOV GFP-Delta Peptide	pCold	Ampicillin	Gibson Assembly

Bacterial Cells for Plasmid Generation	Source	Product Code
Escherichia Coli DH5 α	New England Biolabs	C2987I

2.1.4 qPCR Primers

All primers were gifted from Tim Fenton at University of Kent.

Primer	Sequence
Cyclin A2-F	CCAGAACCTGAGCCTGTTAAA
Cyclin A2-R	CTCGACATCAACCTCTCCAATC
Cyclin B1-F	ACTTTCGCCTGAGCCTATTT
Cyclin B1-R	CTGTGGTAGAGTGCTGATCTTAG
Cyclin D1-F	CCACTCCTACGATACGCTACTA
Cyclin D1-R	CCAATCAGATGACTCTGGGAAA
Cyclin E1-F	TTTGCAGGATCCAGATGAAGAA
Cyclin E1-R	GTCTCTGTGGGTCTGTATGTTG
TBP-F	CCCATGACTCCCATGACC
TBP-R	TTTACAACCAAGATTCACTGTGG

2.1.5 Antibodies

Primary Antibody	Supplier	Species	Product Code
HA	Santa Cruz Biotech	Mouse	Sc-7392

HA (HRP)	Santa Cruz Biotech	Mouse	SC-7392 HRP
PARP	Cell Signalling	Rabbit	9532
Cleaved Caspase 3	Cell Signalling	Rabbit	9661
Caspase 7	Cell Signalling	Rabbit	9492
p21	Cell-Signalling	Rabbit	2947
β-Actin-(HRP)	Sigma-Aldrich	Mouse	A3854
γH2AX	EMD Millipore	Mouse	05-636

Secondary Antibody	**Supplier**	**Species**	**Product Code**
Donkey Anti-Rabbit IgG (H+L) Cross-Absorbed Secondary Antibody, HRP	Invitrogen	Rabbit	A16023
Donkey Anti-Mouse IgG (H+L) Cross-Absorbed Secondary Antibody, HRP	Invitrogen	Mouse	A16011
Donkey Anti-Mouse IgG (H+L) Cross-Absorbed Secondary Antibody Alexa-488	Invitrogen	Mouse	A21202
Donkey Anti-Mouse IgG (H+L) Cross-Absorbed Secondary Antibody Alexa-594	Invitrogen	Mouse	A21207
Donkey Anti-Mouse IgG (H+L) Cross-Absorbed Secondary Antibody Alexa-647	Invitrogen	Mouse	A31571

2.1.6 Hardware and Software

Hardware	Application	Supplier
Accuspin Micro 17R Tabletop Centrifuge	Centrifugation	Fisher Scientific
Agilent 1100 HPLC	Peptide Purification	Agilent
Bruker 600Mhz NMR	Peptide Analysis	Bruker
CLARIOstar Plate Reader	BCA Fluo4 Assays Caspase Glo 3/7 Assays MTS assay	BMG Labtech
Function Generator	Giant unilamellar vesicle preparation	
G:BOX	Western Blot Imaging Coomassie Imaging	Syngene
Incucyte®	Live Cell Imaging	Sartorius
LSM-880 Confocal with AiryScan	Fluorescent Microscopy	Zeiss
Lumascope 600	Fluorescent Microscopy	Etaluma
Megafuge 40R centrifuge	Centrifugation	ThermoFisher
Nanodrop One^{C}	DNA/Protein Quantification	ThermoFisher Scientific
Optima™ LE-80K Ultracentrifuge	Ultra centrifugation	Beckman-Coulter
QuantStudio® 3 Real-Time PCR System	qPCR	ThermoFisher Scientific
UltrafleXtreme MALDI-TOF	Peptide Analysis	Bruker

Software	Application	Suppler
Agilent 1100 Method & Run	HPLC control	Agilent
Flex Analysis	MALDI-TOF analysis of peaks	Bruker
Flex Control	MALDI-TOF control	Bruker
GeneSys	Western Blot image acquisition	Syngene
ImageJ	Image Analysis	NIH (Schindelin *et al.*, 2015)
Microsoft Excel	Statistical Analysis	Microscoft
QuantStudio™ Design & Analysis v1.4.3	qPCR experiment design and analysis	ThermoFisher
Zen Black	Confocal Imaging	Zeiss
Zen Blue	Processing raw confocal data	Zeiss

2.1.7 Kits and Assays

Kit/Assay	Supplier	Product Code
Pierce™ BCA Protein Assay Kit	ThermoFisher Scientific	23225
Clarity™ Western ECL Blotting	Bio-Rad	1705060
Trans-Blot® Turbo™ 5x Transfer Buffer	Bio-Rad	10026938
MTS Assay Kit	Abcam	Ab197010
Fluo-4 Direct™	Thermofisher	F10471
Caspase-Glo® 3/7	Promega	G8090
Caspase-Glo® 8	Promega	G8200
Plasmid Midi Kit	Qiagen	12143
TransIT-LT1	Mirrus-Bio	E7-0002

Polyethylenimine, Linear, MW25000	Polysciences, Inc.	23966-2
Protein Ladder 10-245	Abcam	Ab116028
ProLong Gold Antifade Mountant with DAPI	ThermoFisher Scientific	P36935
RNAeasy Mini	Qiagen	74106
Criterion™ TGX™ Precast Gel	Biorad	5761124
GoScript™ Reverse Transcriptase	Promega	A5003
PowerUp™ SYBR Green 2X MasterMix	ThermoFisher	A25742
Peptide Calibration Standard II	Bruker	222570

2.1.8 Peptide Purification Materials

Buffers	Composition
Lysis Buffer	50mM Tris
	300mM NaCl
	dH_2O
Nickel Column Wash Buffer	50mM Tris
	300mM NaCl
	5mM Imidazole
	dH_2O
Nickel Column Elution Buffer	50mM Tris
	300mM NaCl
	400mM Imidazole
	dH_2O
Strep-Tactin Wash Buffer (Buffer W)	50mM Tris
	300mM NaCl
	dH_2O
Strep-Tactin Elution Buffer (Buffer E)	50mM Tris
	300mM NaCl
	2.5mM Desthibiotin
	dH_2O

M9 Salt Solution (10x)	66g $Na_2HPO_4(2.H_2O)$
pH7.2	33g KH_2PO_4
	5.5 NaCl
M9 Media	100mL M9 Salt
	800mL ddH_2O
	1mL 1M $MgSO_4$
	1mL 0.1M $CaCl_2$
	1mL 1M Thiamine
	10mL (100x) Trace Metal
	4g/L D-Glucose
	1g/L (15N) NH_4Cl
	1mL Ampicillin stock
HPLC Buffer A	0.1% TFA
	ddH_2O
HPLC Buffer B	0.09% TFA
	80% Acetonitrile
	ddH_2O
TEV Cleavage Buffer	50mM Tris
pH8	1mM EDTA

Materials	**Supplier**	**Product Code**
cOmplete™ His-Tag Purification Resin	Roche	05893682001
Strep-Tactin® Superflow®	IBA Lifesciences	2-1206-002
Econo-Pac® Gravity Column	Bio-Rad	7321010
Synthetic Peptide	BioMatik	

2.1.9 EBOV Delta Peptide Constructs

Vector	Sequence	Supplier
pUC57-Amp	TGGCTGCAAAAAATCCCGCTG CAGTGGTTCAAATGCACCGTC AAAGAGGGCAAACTGCAGTGC CGTATCTAG	Synbio Technologies

2.1.10 EBOV Delta Peptide Primers for PCR

Primer	Sequence	Tm (°C)	Supplier
zDelta Peptide Vector Reverse	AGCGGGATTTTTTGCAGCCAG CCTGCACCCTGGAAGT	60	Thermofisher
zDelta Peptide Vector Forward	AACTGCAGTGCCGTATCTAGT AAGGATCCGAATTCAAGCTTG TCGACC	60	Thermofisher
zDelta Peptide Fragment Reverse	AGCTTGAATTCGGATCCTTACT AGATACGGCACTGCAGTTTGC	60	Thermofisher
zDelta Peptide Fragment Forward	TGTACTTCCAGGGTGCAGGCT GGCTGCAAAAAATCCCGCTG	58	Thermofisher

2.1.11 Electroformation Consumables

Materials	Supplier	Product Code
Copper Foil	Sigma-Aldrich	GF28915421
Indium tin oxide coated glass slide	Sigma-Aldrich	703176-10PAK

FastWells™ reagent barriers	Sigma-Aldrich	GBL 664112-50EA

2.1.12 Lipidic Cubic Phase Crystallography Consumables

Materials	Supplier	Product Code
Laminex™ UV Plastic 200-micron Film Cover	Molecular Dimensions	MD11-53-200
Laminex™ UV Plastic Base 100 micron	Molecular Dimensions	MD11-51-100
MemGold2™ HT-96	Molecular Dimensions	MD1-64
MemGoldMeso™ HT-96	Molecular Dimensions	MD1-114
Monoolein (1-Oleoyl-rac-glycerol)	Sigma-Aldrich	M7765

2.2 Methods

2.2.1 Plasmid Preparation

To generate plasmid stocks, 100ng of plasmid were mixed with DH5-alpha E. Coli on ice for 20 minutes. Mixtures were then heat shocked at 42°C for 45 seconds then quickly returned to ice for 2 minutes. For plasmids containing a kanamycin resistance gene, an outgrowth was performed whereby cells were mixed with 1000µL of SOC media for 1 hour at 37°C with shaking at 200rpm to allow generation of antibiotic resistance. Lastly, cells were streaked on agar plates containing the appropriate antibiotic and plates were placed in an incubator at 37°C overnight for colony formation. The next day, single colonies were picked with a sterile pipette tip and dropped in 50mL Falcon tubes containing LB broth with the appropriate antibiotic resistance and incubated overnight in a shaking incubator at 200rpm, 37°C. The following day, the falcon tubes were centrifuged for 20 minutes at 4000G to pellet the bacteria, the supernatant was then removed. The pellets were then subjected a midiprep vacuum protocol supplied by the manufacturer (Qiagen) to recover plasmid

DNA. After elution, quantity and purity of DNA was measured using a nanodrop spectrophotometer.

2.2.2 Tissue Culture

2.2.2.1 Passaging Cells

HeLa, HEK 293t and, Huh-7s cell were grown in DMEM supplemented with 10% FBS, and1% P/S. Cells were maintained at 37°C and 5% CO_2. At 80% confluency all cells were split for passaging. For passaging, media from the flask was removed, cells were washed once with 5mL of warm PBS, followed by addition of 3mL of warm trypsin for 2-4 minutes until cells have detached. After detachment, 7mL of warm full DMEM was added to quench trypsin activity, and the cell suspension was placed in 15mL Falcon tubes for centrifugation at 300G for 5 minutes. Supernatant was discarded and fresh DMEM was added to resuspend the cells which were then added in appropriate tissue culture flasks in 1:10 ratio, then returned to the incubator. Cells were maintained up to a maximum of 50 passages. HEK293T cells were tested annually for mycoplasma contamination using the MycoAlert detection kit from Lonza. 2mL of cells were pelleted, 100 µL of supernatant was removed and placed in a new tube, 100 µL of MycoAlert reagent was added to the sample and incubated for 5 minutes, then luminescence was measured using a plate reading luminometer. Then 100 µL of MycoAlert substrate was added to sample and incubated for 10 minutes prior to taking another luminescence reading. Samples were run alongside a positive control supplied by the kit. The results confirmed the cells were mycoplasma free. HeLa and Huh-7 cells were sent for mycoplasma testing to Eurofins. Samples were certified mycoplasma free.

2.2.2.2 Freezing Cells

To generate frozen stocks of cells being used, a solution containing the media used for the cells with 10% DMSO was made. Stocks were made when required and carried out in tandem with passaging, usually during cell passage numbers 3 to 5. Half of the cell suspension in the falcon tube during passaging were removed and pipetted into a new falcon tube and counted using a haemocytometer under a light

microscope. The cells were then pelleted at 300G in a centrifuge for 5 minutes. The media was removed and cells were resuspended in DMEM with 10% DMSO and pippeted into cryovials at a density of 1,000,000 cells per ml. Cryovials were then frozen at -80°C and after 48 hours transferred to liquid nitrogen vats used to store cells for long term periods.

2.2.2.3 Thawing Cells

Cryovials were removed from the liquid nitrogen vats and placed in a box containing dry ice to prevent thawing as they were brought to the laboratory. The cryovials were thawed rapidly in a 37°C waterbath and visually inspected every minutes to ensure the cells were fully thawed. Afterwards, cells in the cryovial were pipetted into a falcon tube containing 4mL of prewarmed media and centrifuged at 300 x G for 5 minutes. The media was removed after centrifugation to remove DMSO and cells were resuspended in 5mL of fresh warm media. All of the cell suspension was transferred into a T-25 flask and left in the incubator at 37 °C and 5% CO_2. After 24 hours the media was replaced with fresh prewarmed media. Cells were passaged 3 times prior to use for experiments.

2.2.3 Transfection

Cells were grown to 80% confluency before splitting. Upon resuspension after trypsinisation, cells were counted using a haemocytometer and seeded in the appropriate plates for next day transfection (~75% confluency). The following description applies to transfections in 6-well plates. The table below summarises the values of cell number and reagents used in smaller plates. Transfection method using Polyethylenimine (PEI): 2000ng of plasmid DNA and 6µL of PEI were added in separate Eppendorf tubes containing 125µL filter sterilised 300mM NaCl solution and then mixed together into one tube and incubated for 15 minutes to allow the DNA complexes to form using a 1:3 DNA:PEI ratio. Full DMEM (10% FBS, 1% P/S) was removed from the cells which were then washed in warm sterile PBS media prior to adding 2mL of warm DMEM containing FBS only. 250µL of DNA:PEI complexes were added in a dropwise fashion to the cells, plates were gently rocked

to ensure even distribution and returned to the incubator. After 4 hours of incubation, media was replaced, cells were washed with warm sterile PBS to remove remaining PEI, and pre-warmed full DMEM was added to cells to incubate for indicated time periods.

Transfection method using Mirrus TransIT LT1: 2000ng of plasmid DNA was added to tubes containing 250µL of Opti-MEM, followed by addition of TransIT-LT1 at a 1:3 DNA:LT1 ratio and incubated for 15 minutes to allow DNA complexes to form. The 250µL solutions containing the DNA:LT1 complexes were then added in a dropwise fashion to the wells, plates were gently rocked to ensure even distribution and incubated for indicated time periods.

Plate	Cell Number (HeLa)	DNA Concentration	Transfection Buffer PEI (150mM NaCl)	Transfection Buffer LT-1 (Opti-MEM)
12 Well	125,000	1000ng	75µL for DNA 75µL for PEI	125µL
24 Well	75,000	500ng	Not Used	100µL
96 Well	10,000	100ng	Not Used	50µL

2.2.4 Cell lysis and Protein Quantification

6-well plates with transfected HeLa cells were removed from the incubator and media was aspirated, cells were washed once with 2mL of ice cold PBS and then lysed in 75µL of ice cold NP-40 lysis buffer (150mM NaCl, 50mM Tris pH8.0) containing protease and phosphatase inhibitors for 15 minutes on ice. For smaller plates, lysis buffer volume was scaled down appropriately. The lysate from the plates were pipetted into appropriately labelled Eppendorf tubes. Samples were clarified using a tabletop centrifuge at 4°C and 17,000 x G for 20 minutes. Supernatants were removed and placed into new Eppendorf tubes for downstream applications. All samples were subjected to BCA assay according to manufacturer's instructions for protein quantification. Briefly; 10µL of lysate samples were diluted in a 1:4 ratio with

lysis buffer, then added in wells of a 96-well plate in triplicate fashion. Protein standards supplied in the kit were added to separate wells of the 96-well plate. All samples were then treated using 200µL of Pierce™ BCA Protein Assay Reagent A/B and incubated for 30 minutes at 37°C. Afterwards, plates were removed from the incubator and absorbance of samples were measured using the Clariostar plate reader. Absorbances were then corrected against the blank wells and protein concentration was determined by comparing the resultant absorbance value against the standard curve. After the BCA assay, lysates were aliquoted and stored at -20°C.

2.2.5 RNA Extraction

Plates containing treated cells were removed from the incubator and media was aspirated. Cells were washed once with cold PBS and RNA was extracted using the RNAeasy Mini kit from Qiagen according to manufacturer's protocol. The optional step for DNA digestion was carried out to remove all DNA from the column prior to washing and eluting RNA. The concentration of RNA was determined using a nanodrop spectrophotometer.

2.2.6 Gel Electrophoresis and Western Blots

Cell lysates with known protein concentrations were mixed at a 4:1 ratio with 4x Laemmli buffer containing 200mM 2-mercaptoethanol and boiled at 95°C for 10 minutes. Samples containing 25µg of protein were loaded on Criterion™ TGX™ gels and subjected to gel electrophoresis at 200W in the presence of tris-glycine running buffer. When then blue dye front reached the bottom of the gel cassette, the gel was removed from the cassette and proteins were transferred from the gel onto polyvinylidene difluoride (PVDF) membranes using a Biorad Trans-Blot Turbo machine according to manufacturer's instructions. The membranes were blocked in 5% milk and 0.1% tween in TBS (TBS-T), or 5% bovine serum albumin in TBS-T for phospho-specific antibodies for 1 hour at room temperature. Primary antibody incubations were done overnight at 4C. Secondary HRP-conjugated antibody incubations were carried out for 1 hour at room temperature at 1:10,000 dilution in the same buffer used for primary antibody incubation. Western blots were developed

by incubating membranes in Clarity™ ECL reagent (BioRad) according to manufacturer's protocol; mixing the ECL reagents A and B in a 1:1 ratio, incubate PVDF membrane for 60 seconds in the dark and visualised using smart capture settings in the Gel Doc. Membranes were probed with anti-Caspase 3, anti-PARP1, anti-pMLKL. HRP-conjugated β-actin and anti-HA tag antibodies were used to verify equal gel loading and transfected protein expression.

Primary Antibody	Dilution	Dilution Buffer	Incubation
Cleaved Caspase 3	1:1000	5% Milk TBS-T	4°C Overnight
PARP-1	1:1000	5% Milk TBS-T	4°C Overnight
Cyclin E1	1:1000	5% Milk TBS-T	4°C Overnight
p21	1:1000	5% Milk TBS-T	4°C Overnight
RIP3	1:1000	5% Milk TBS-T	4°C Overnight
pMLKL	1:1000	5% BSA TBS-T	4°C Overnight
γH2AX	1:1000	5% BSA TBS-T	4°C Overnight
HA-Tag (HRP)	1:10,000	5% Milk TBS-T	1 Hour Room Temperature
β-Actin (HRP)	1:10,000	5% Milk TBS-T	1 Hour Room Temperature

2.2.7 Immunofluorescence Microscopy

Glass coverslips were autoclaved and subjected to UV sterilisation for 2 hours inside the tissue culture hood. Cells were counted and seeded on sterilised glass coverslips for next day transfection at the same densities described in *Transfections* section. After indicated incubation period post transfection, cell media was aspirated and the coverslips were washed in ice cold PBS prior to fixation using 4% formalin. After fixation coverslips were incubated in PBS containing 0.1% Triton X-100 for 15 minutes to permeabilise the cells unless otherwise stated. The coverslips were blocked using a buffer containing 5% BSA in TBS-T for 1 hour at room temperature. Primary antibodies were diluted in blocking solution and added at indicated ratios for either 1 hour at room temperature or overnight at 4°C. Coverslips were washed using TBS-T 4 times for 5 minutes on a rocker to remove non-bound antibodies. Secondary antibody staining was carried out using Alexa fluorophore-conjugated secondary antibodies in blocking solution at 1:1000 dilution for 1 hour at room temperature,

followed by four washes in TBS-T at 5 minutes each, in the dark. Coverslips were then mounted on glass slides using ProLong™ Gold Antifade mounting media containing DAPI (Invitrogen). All mounted coverslips were cured overnight at room temperature prior to imaging using either Etaluma Lumascope-600 or Zeiss LSM-880 confocal microscope. Images were analysed using Zen Blue software.

Primary Antibody	Dilution	Dilution Buffer	Incubation
HA-tag	1:500	5% BSA TBS-T	1 Hour Room Temperature
VDAC1	1:500	5% BSA TBS-T	1 Hour Room Temperature

Dye/Fluorophore	Excitation Max (nm)	Emission Max (nm)	Laser	Filter
DAPI	350	470	405	MBS-405
Alexa488	490	525	488	MBS-488
Alexa594	590	617	594	MBS-458/561
Alexa647	650	665	647	MBS-488/561/633
mCherry	587	610	594	MBS-458/561
eGFP	488	509	488	MBS-488

2.2.8 MTS Assay

HeLa cells were seeded at a density of 10,000 cells per well in a clear F bottom 96-well plate for next day transfection using TransIT and 100ng of DNA per well and incubated at 37°C. After 24 and 48 hours post transfection, 20µL of MTS ((3-(4,5-dimethylthiazol-2-yl)-5-(3-carboxymethoxyphenyl)-2-(4-sulfophenyl)-2H-tetrazolium) reagent (Abcam 197010) was added to each well and returned to the incubator for 4 hours at 37°C. After incubation, absorbance was measured with a plate-reader at OD_{490}. Blank wells were used to subtract background signal. Positive control wells were treated with 5µM staurosporine solution for 4 hours before performing the assay.

2.2.9 Quantitative PCR

RNA samples extracted from treated cells were converted to cDNA using the GoScript Reverse Transcription System (Promega) according to manufacturer's protocol. Where the option in the protocol was given, we opted to use both Random Primer and Primer [Oligo(dT)]$_{15}$. Also, we chose to add Recombinant RNAsin® Ribonuclease Inhibitor, another optional step in the protocol, as this would protect RNA from RNAase activity.

To perform the qPCR assays, we used SYBR Green PowerUp mastermix and followed the manufacturer's protocol. We carried out 10µL reactions, whereby 2 µL of cDNA (5ng/µL) was used. Primers for genes of interest were designed and purchased from Integrated DNA Technologies. Plate setup and raw data was set up using QuantStudio Design & Analysis software. Raw data was post processed in excel, where standard curves for each gene, kindly provided by members of the Fenton Research Group at University of Kent, were used to quantify the copy number of transcripts for each gene that was assayed.

2.2.10 Fluo4 Direct™ Calcium Assay

Intracellular calcium was measured using the Fluo4 Direct™ calcium assay according to manufacturer's protocol. Briefly, 24 well plates were seeded with HeLa cells at a density of 75,000 cells and transfected with either HA-zVP24, HA-rVP24 or empty vector control. Cells were incubated for 48 hours prior to assaying for intracellular calcium. After 48 hours, a 2x Fluo4 Direct™ calcium reagent was added directly to the well containing culture media at a 1:1 ratio. Plates were returned to the incubator for 30 minutes. After incubation, green intensity was monitored using a Lumascope-600 with a x10 lens Gain and exposure settings were kept identical for all conditions. Images were exported as TIFF and converted to 250bit greyscale to quantify signal intensity using ImageJ software.

2.2.11 Caspase Activity Assays

Caspase activity was monitored using the Caspase-Glo 3/7 Assay Systems kit ® and Caspase-8 Glo (Promega). HeLa cells were seeded at a density of 12,000 cells in a black F-bottom 96-well plate for next day transfection. 48 hours post transfection, 100µL of Caspase-Glo ® 3/7 was added to all the wells and the plate was gently shaken manually to ensure proper mixing. Plates were then incubated at room temperature for 2 hours prior to taking luminescent readings, Positive control wells were subjected to 2µM staurosporine for 4 hours before performing the assay.

2.2.12 Autophagy Bioinformatics

To find any LC3-interacting regions, the web resource iLIR (https://ilir.warwick.ac.uk/index.php) (Kalvari *et al.*, 2014) was used using the following Uniprot entries in FASTA format: EBOV VP24 (Q05322), RESTV VP24 (Q77DB4), and Influenza M2 protein (P0DOF8). The latter was used as a reference since M2 has been verified in-vitro in recruiting autophagy machinery (Beale *et al.*, 2014). Position Specific Scoring Matrices (PSSM) for each entry was tabled using Microsoft Excel.

2.2.13 STRING (Search Tool for the Retrieval of Interacting Genes/Proteins) Bioinformatics

To find binding partners of proteins that interact with EBOV VP24, STRING database (https://string-db.org/) was used with settings allowing results to appear that have been verified experimentally and with high confidence score (≥0.700). Searches were carried out for KPNA1 and KPNA5 genes in Homo sapiens. Results were exported as .png files.

2.2.14 Giant Unilamellar Vesicle Formation

GUVs were prepared by electroformation method. 26mg of Asolectin lipid pellets were dissolved with 1mL of chloroform in a glass tube. Chloroform was then evaporated in a nitrogen gas stream whilst rotating the glass tube at an angle to form a thin film. When the chloroform was fully evaporated lipids were resuspended in 50mM HEPES pH 7.4 buffer containing 1mM Nile red dye to a final concentration of 50mg/ml. 10µL of lipid mixture was placed on the conductive sides of two indium-tin oxide coated coverslips and evaporated in a vacuum chamber overnight. After complete evaporation, rubber O-rings were placed on the ITO coverslips and 70µL of 0.1M sucrose, 1mM HEPES buffer was added in the well, and coverslips were attached by bull clips to form a sealed chamber. The leads of the function generator were clipped onto the copper coated edges of the coverslip and the function generator was switched on with settings of 10Hz sine wave function, at 1.5V for 2 hours and 30 minutes to form GUVs. Voltage was monitored using a multimeter set to alternating current voltage. After electroformation, the GUVs were removed using a wide-bore pipette and diluted 1:100 in buffer containing 0.1M glucose, 1mM HEPES buffer. Successful formation of GUVs was confirmed by seeding 200µL of GUV solution in chamber slides and visualised using confocal microscopy using a 594nm laser with a x63 objective lens.

2.2.15 Oxidation of Delta Peptides

Method adapted from (J. He *et al.*, 2017). All peptides were purchased from Biomatik at 95% purity. To form the disulphide bonds between the c-terminus cysteine residues of the delta peptides, 1mg of peptide was dissolved in 15% acetic acid and made up to 300µL in ddH_2O. Then DMSO was added at 20% final concentration and tubes were incubated at room temperature overnight. To remove DMSO, samples were snap frozen in liquid nitrogen and lyophilised by placing the Eppendorf tubes inside the glass chamber that attaches to the vacuum lyophiliser. The air in the

chamber was vented out and samples were left overnight. The following day, the glass chamber was vented with air and Eppendorf tubes were removed.

2.2.16 Membrane insertion of Delta-peptide in GUVs

FITC tagged E23Δ_{red}, E23Δ_{ox}, R25Δ_{red}, and R25Δ_{ox} peptides were dissolved in ddH_2O with 20% acetic acid to 1mM at pH6.5. A multichamber slide was coated using 100µL of PBS containing 1% BSA for 1 hour prior. After successful coating the BSA solution was removed and FITC tagged z23Δ_{red}, z23Δ_{ox}, r25Δ_{red}, and r25Δ_{ox} peptide was mixed with GUVs in the chambers to a final concentration of 30µM and viewed after 15 minutes of incubation using a Zeiss LSM-880 confocal microscope using a Zeiss apochromat 63x objective with 488 laser, MBS-488 filter set for FITC excitation and 594 laser, MBS-594 filter set for Nile red excitation. Images were post-processed to normalise brightness across the samples using Zen blue software.

2.2.17 MALDI-TOF Mass Spectrometry

Matrix-Assisted Laser Desorption/Ionization-Time of Flight mass spectrometry was carried out by spotting peptide samples diluted in TA30 solution (30:70 [v/v] acetonitrile:0.1% trifluoroacetic acid) at 1:100 on the AnchorChip target plate. The plate was calibrated by adding 0.5µL of Peptide Calibration Standard II solution on a grid spot adjacent to our experimental sample. When the spots dried on the AnchorChip plate, 1µL of working matrix solution (alpha-cyano-4-hydroxycinnamic acid in TA30) was added to both experimental peptide samples and calibration samples. After drying, the AnchorChip plate was inserted into the Bruker Flextreme MALDI-TOF. Data collection was carried out after calibrating against the Peptide Calibration Standard II spot and was acquired using a preset program (RP700-3500) on Flex Control software by the in-house technician to detect peptides up to 3500kD in size. FlexAnalysis software was used to label peaks and extract the results into TIFF format.

2.2.18 Gibson Assembly

To clone the EBOV 23 amino acid C-terminus DNA fragment from the pUC57 vector into a pCold vector expressing 6x His tag, twin strep tag and GFP, Gibson assembly was carried out according to manufacturer's protocol. Thermocycler settings for amplifying pCold vector were as follows: 2 minutes 95°C, followed by 30 cycles of 45 seconds at 95°C, 30 seconds at 55°C, 11 minutes at 73°C. Final elongation step was 5 minutes at 73°C. For amplification of the EBOV delta peptide fragment, the thermocycler settings were as follows: 2 minutes 95°C, followed by 30 cycles of 45 seconds at 95°C, 30 seconds at 55°C, 1 minutes at 73°C. Final elongation step was 5 minutes at 73°C. The pCold amplified product was subjected to a PCR cleanup step, using a PCR CleanUp Kit, whereas the amplified EBOV delta peptide fragment was not subjected to the PCR cleanup step. Gibson Assembly was carried out by mixing amplified products in a 1:4 ratio between amplified vector and amplified fragment, to a total 0.25pmols of DNA, followed by mixing with 2X Gibson Assembly Mastermix and volumes were raised to 20µL per PCR tube using ddH_2O. The thermocycler settings were set to 50°C for 15 minutes as per manufacturer's protocol. After the reaction, the resulting DNA solution was transformed using competent cells to generate plasmid DNA to ship for sequencing. Sequence data returned by Eurofins confirmed successful generation of the pCold-EBOV delta peptide plasmid.

2.2.19 Peptide Expression and Extraction

BL21 competent E. coli were transformed with pCold EBOV Delta-peptide plasmid by mixing 100ng of plasmid DNA with 100µL of BL21 cells on ice, followed by heat shocking the mixture at 42°C for 45 seconds in a water bath, followed by returning samples on ice for 10 minutes. Samples were then streaked onto ampicillin (100µg/ml) treated agar plates for colony formation. The following day, a colony was transferred by stabbing with a sterile pipette tip to grow overnight in 50mL of LB broth containing 100µg/mL ampicillin in a shaking incubator at 37°C. The next day 15mL of the overnight growth sample was then added to 1L of LB broth and returned to the shaking incubator at 37°C, periodically checking the OD of the culture. When the

OD_{600} was recorded to have an absorbance of 0.7, the 1L culture was quickly cooled to 15°C in ice water for 30 minutes. Then 1mL of IPTG was added to the 1L culture, yielding a final concentration of 1mM to induce peptide production. The 1L culture was returned to a shaking incubator set to 15°C and incubated overnight to allow peptide expression.

The day after peptide expression the 1L culture was removed from the flask and cells were pelleted by centrifugation at 5000G. The supernatant was removed and cell pellets were resuspended in 50mL of lysis buffer. Cells were lysed by sonication on ice for 10 minutes, and debris was removed from the lysate by ultracentrifugation at 117734G using a Type 70i rotor for 1 hour at 4°C. The supernatant was transferred into appropriately labelled falcon tubes and the pellet fraction was discarded.

2.2.20 Nickel Column Purification

cOmplete™ His-Tag purification resin was loaded onto a gravity chromatography column to a final bed volume of 2.5ml. The column was washed by adding 4 column volumes (CV) of ddH_2O (80ml) to remove the storage buffer containing 20% ethanol. Then, the column was equilibrated using 4 CV of lysis buffer. After equilibration, 4 CV of lysate were then added to the column, and flowthroughs were collected in 15mL falcon tubes. The resin was washed by adding 4 CV of Wash buffer containing 5mM imidazole two times and collected in 15mL falcon tubes. To elute bound sample, 4CV of Elution buffer containing 400mM imidazole was added to the column twice and all samples were collected in 15mL falcon tubes. To check purity of samples, 10µL fractions from each falcon tube was subjected to gel electrophoresis using a Criterion™ TGX™ gel. The gel was removed from the cassette then stained with Coomassie blue for 4 hours at room temperature on a shaker plate and incubated in destain overnight to detect protein bands on the gel.

2.2.21 Strep-tactin column Purification

Strep-Tactin® Superflow® resin was added to a 20mL gravity chromatography column to a final column bed volume of 5ml. The column was then equilibrated with

2 column volumes (CV) of Buffer W. Lysates were then added and flowthrough was collected in 15mL falcon tubes. After running the lysate, the column was washed with Buffer W 4 times at 1 CV (20ml) per wash, with all flowthroughs collected in 15mL falcon tubes. After washing the column to remove non-specific bound contaminants, the bound strep-tagged peptide was eluted using 0.5 CV of Buffer E 4 times and collected in 15mL falcon tubes. All collections throughout the purification were kept on ice. To check purity of the samples, 10µL fractions from each falcon tube was subjected to gel electrophoresis using a Criterion™ TGX™ gel. The gel was removed from the gel cassette and then stained with Coomassie blue for 4 hours at room temperature on a shaker plate and incubated in destain overnight to detect protein bands on the gel.

2.2.22 HPLC Purification

Reverse phase HPLC was carried out on an Agilent 1100 HPLC machine. Peptide sample was injected into a Vydac™ Protein and Peptide C18 column and eluted based on a gradient increase of buffer B (1% TFA in acetonitrile) against buffer A (10% TFA in ddH_2O). Sample elution was monitored by fluorescence at 280nm wavelength. Peak intensity was recorded at 35 minutes, therefore elutions at 35-38 minutes were collected.

2.2.23 Nuclear Magnetic Resonance

Reduced 23 amino acid EBOV delta-peptide was dissolved in ddH_2O containing 20% deuterated acetic acid to a final concentration of 650µM and loaded into a Bruker Advance3 spectrometer operating at a 1H frequency of 600MHz equipped with a TCI-P cryo- probe. 1H -1H TOCSY experiment with excitation sculpting for water suppression was used with a mixing time of 60 ms, with 4096 points in the direct dimension and 1020 in the indirect dimension. 1H -1H NOESY experiment with excitation sculpting for water suppression was used with a mixing time of 120mS, with 4096 points in the direct dimension and 864 in the indirect dimension.

2.2.24 Lipid Cubic Phase Crystallography

Technique performed in collaboration with Dr Jose Ortega-Roldan. Monoolein lipid was warmed up to 40°C and transferred into a gas-tight Hamilton syringe. Special care was taken to prevent formation of air bubbles. Synthetic RESTV 25aa delta peptide dissolved in 15% acetic acid to 20mg/mL at pH 5 was pipetted into the Hamilton syringe containing the prewarmed monoolein lipid to final mixture volume of 40µL, 40% weight:volume between lipid and peptide. The final mixture was moved to the very tip of the Hamilton syringe to remove residual air prior to coupling with another Hamilton syringe for mixing. Once the two opposing Hamilton syringes were successfully coupled without presence or air, the plungers were pressed to move the mixture into the opposite Hamilton syringe and vice-versa repeatedly to mix the solution until the mixture becomes transparent. Once completed, the syringe was attached to a Mosquito® High Throughput Screening robot. The Mosquito® robot was programmed to pipette 800nL volume from 96 well plates containing the precipitant screens for crystallisation; MemGold2™, MemGoldMeso™, onto a 96 well plastic bases. The Mosquito® robot was also calibrated to dispense 50nL of lipid:peptide mixture onto the 96 well plastic bases containing the precipitants. The plastic bases were then covered with a plastic film cover and incubated at 18°C. Plates were checked every week under a light microscope for crystal formation.

3 Cytotoxicity of VP24 - Metabolism and Proliferation.

3.1 Abstract

Ebola virus VP24 is a protein that is involved in suppression of the interferon signalling pathway. However, a group has reported that failure to establish a stable cell line expressing VP24 was likely due to unreported cytotoxic effects. In order to verify whether there are cytotoxic effects displayed by VP24, we carried out simple assays that would give us insight into how cells are affected in response to VP24 transfection. Using live cell imaging we detected a decrease in cell proliferation after 24 hours post transfection. Furthermore, analysis of metabolism by MTS assay revealed a decrease in metabolic activity of cells transfected with VP24 between 24 and 48 hours post transfection. Analysis by immunofluorescent microscopy showed a morphological change in mitochondrial architecture with cells transfected by VP24. Therefore, our data in this chapter confirms that VP24 does negatively affect cells, and further work would be needed to assess which pathways would be responsible.

3.2 Introduction

Due to the ambiguity of the term cytotoxicity with regards to specific pathways and mechanisms, we sought to verify what events were displayed by cells that express zVP24 protein and where possible rVP24 protein as we would need to initially confirm whether VP24 is cytotoxic to cells. We hope that these experiments may elucidate whether these cytotoxic effects are species specific, due to multiple potentially pathogenic-adapting amino acid mutations between EBOV and RESTV. After the information given to us from running these broad screens we hope to pinpoint the pathway by which VP24 is interfering with normal cellular function. The literature we gave particular attention to is a protein-protein interaction study that reported numerous binding partners to zVP24 by mass spectrometry (García-Dorival *et al.*, 2014). Despite lack of published evidence of VP24 cytotoxicity, many binding targets of VP24 that were identified in the study are involved in key pathways that ensure cell viability and proliferation, some of which are highlighted [Table 4]. A more recent study (Batra *et al.*, 2018) has also mapped the interactome of VP24, of which the authors stated their results matched 9 targets out of 50 found by García-Dorival *et al.*, 2014. However, the majority of these binding targets have only been verified in high throughput mass-spectrometry with little to no follow up in the context of VP24 interfering with pathways of the binding proteins in question. We aim to identify the VP24 interacting pathways and explore potential impact on cell function.

In this chapter we describe our experiments investigating the impact of VP24 on overall cell metabolism, proliferation and viability, as these characteristics are very informative for assessing cytotoxicity. If VP24 displays a cytotoxic phenotype, it would be detected in these assays. This would then allow us to navigate our experimental design towards identifying the key mechanisms responsible for cytotoxicity.

Protein	Name	Role	Implication in cell death
ATP1A1*	ATPase Na^+/K^+ transporting subunit alpha 1	Membrane protein, maintains electrochemical gradient across plasma membrane	-
VDAC1	Voltage Dependent Anion Channel 1	Facilitates exchange of ions and metabolites across outer mitochondrial membrane. Also found on plasma membrane	Involved in apoptosis.
VDAC2	Voltage Dependent Anion Channel 2	Facilitates exchange of ions and metabolites across outer mitochondrial membrane.	Involved in apoptosis
COX5B	Cytochrome C Oxidase Subunit 5B	Terminal enzyme of mitochondrial respiratory chain.	Loss or suppression may cause cell senescence
ANP32A*	Acidic Nuclear Phosphoprotein 32 Family Member A	Involved in cellular proliferation and differentiation.	Involved in apoptosis

Table 4. Mass Spectrometry Pull Down Data
A selection of proteins we deemed of interest are presented in this table, based from García-Dorival *et al.*, 2014. Given that these proteins have functions related to cell metabolism and have been implicated in cell death functions (except ATP1A1), we hypothesised that VP24 interacting with any of these proteins inside host cells may display detrimental effects. * indicates hits also verified in Batra *et al,* 2018.

3.3 Results

3.3.1 VP24 decreases cell metabolism and proliferation

In order to ascertain if VP24 has any effect on cell proliferation and viability, we monitored cell cultures in real-time using the Incucyte® live-imaging system. HEK 293T cells were transfected with either HA-tagged zVP24, rVP24 or empty vector. Plates were returned to the incubator containing the Incucyte® live imaging system in order to monitor cell proliferation over a 72-hour period at 37°C and 5% CO_2. The images captured every 24 hours using a x10 lens during incubation appear to show reduced proliferation in both zVP24 and rVP24 cells after the 24-hour period whereas the mock cells showed ordinary growth day after day [Figure 11]. These results suggest VP24 of both EBOV and RESTV are likely to be interfering with cellular mechanisms resulting in a decrease of cell numbers after the 24-hour period, though it could not be determined from this experimental setup if this was due to decreased cellular proliferation or viability.

Following the live-cell imaging results, we decided to investigate cell viability by MTS assay as this would give us insight into any changes of cellular metabolism via colorimetric changes of the reagent. Cells were transfected with either HA-tagged zVP24 and rVP24 for 24 and 48 hours. At indicated timepoints the plates were subjected absorbance readings at optical density of 490nm in a plate reader to quantify the levels of formazan dye, as only metabolically active cells are able to

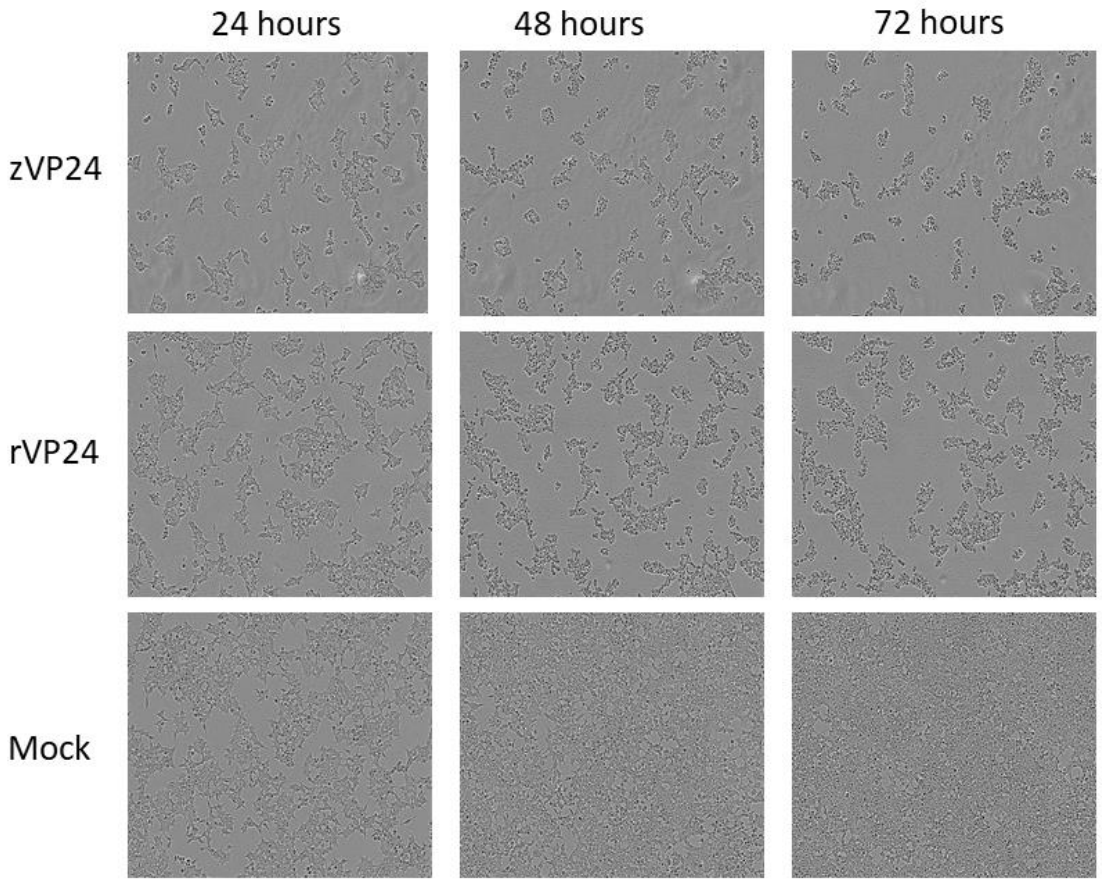

Figure 11. Live cell monitoring from 24 to 72 hours post transfection.

Cell confluency was monitored using Incucyte® Live cell imaging system with a x10 in 12 well plates for 24, 48, and 72 hours post transfection using 1000ng DNA of zVP24, rVP24 and empty vector. Stunted cell growth and loss of typical HEK293t morphology was observed at from 48 hours onwards with zVP24. By comparison, rVP24 shows a similar, yet less pronounced, sequence of events. Empty vector transfection of pCAGGS shows normal and consistent rate of growth by which the cells also retain a healthy-looking morphology. Experiment was repeated 3 times.

convert the MTS tetrazolium salts into the purple formazan dye by dehydrogenase enzymes.

The positive control was made by treatment of cells with 8μM staurosporine, a strong kinase inhibitor that induces apoptosis 4 hours prior to subjecting the plates to the MTS reagent. At the 24-hour incubation period there appears to be no significant change between zVP24, rVP24 and the empty vector transfected cells, indicating that VP24 has no adverse effects on cell metabolism within this incubation period [Figure 12]. However, at 48 hours incubation there was a statistically significant decrease in absorbance signal for both zVP24 and rVP24 transfected cells of 20-25% in comparison to the mock cells. These results suggest that both zVP24 and rVP24 cause a decrease in metabolic activity of cells, which starts to occur only after 24 hours post-transfection. In comparison to the results of Figure 11, the MTS assay showed that RESTV and EBOV have comparable impacts on cellular metabolic activity. To confirm that zVP24 and rVP24 have similar expression levels, the MTS samples were lysed and subjected to Western blotting for the VP24 HA epitope tag and a β-actin loading control. Results show equal transfected protein expression [Figure 12].

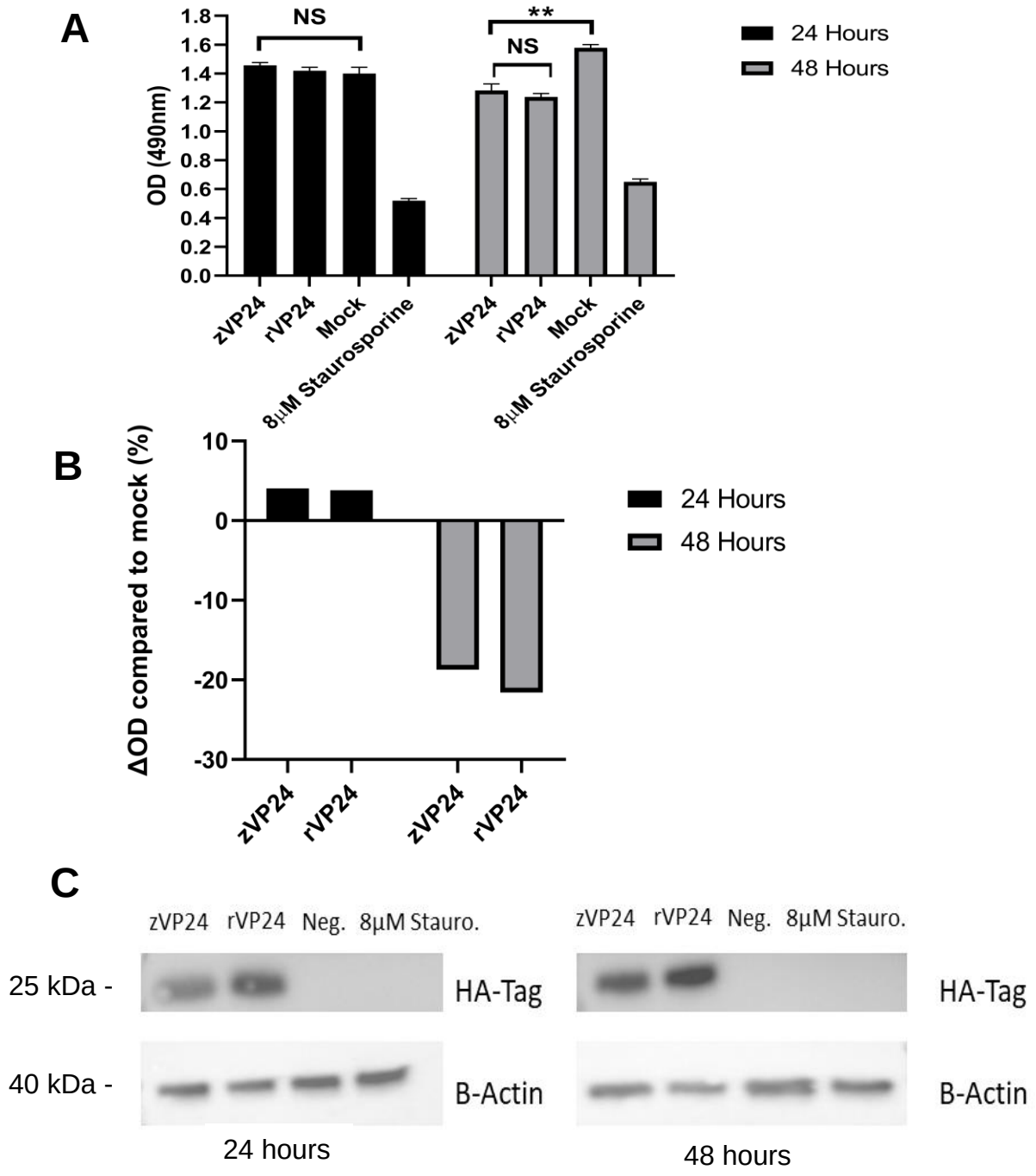

Figure 12. Analysis of cell viability in VP24 transfected Hela cells.

(A)Hela cells transfected with either HA-tagged zVP24 or rVP24 were subjected to MTS assay after 24 and 48 hours post transfection. Mock samples were transfected with empty vector. Positive controls were transfected with empty vector and treated with 8µM staurosporine for 3 hours to induce apoptosis. Results are shown as OD from the plate reader. (B) Fold changes show decrease in OD at 48 hour time point. (C)Experiments were done in triplicate and transfections were verified by western blot analysis. N=3. Values were subjected to one way ANOVA statistical method. **=p value <0.01. T-test statistical analysis was carried out between zVP24 and rVP2 only.

3.3.2 VP24 alters mitochondrial morphology

Due to MTS assay results showing differences in cellular metabolism, we chose to observe the mitochondrial architecture to see whether VP24 is affecting metabolism at the mitochondria. Seeing as mitochondrial architecture has been implicated in indicating cellular stress, therefore the mitochondria of HeLa cells transfected with HA-tagged zVP24, rVP24 or empty vector was examined by confocal microscopy. The mitochondrial architecture was examined by co-transfecting all samples with mito7-mcherry plasmid, whereby a mCherry tag is expressed on mitochondrial marker protein cytochrome *c* oxidase subunit 8A. VP24 was detected by immunofluorescence staining of the HA epitope tag. Cells with either zVP24 and rVP24 appear to show altered mitochondrial morphology [Figure 13]. The mitochondria seem to be punctate in structure whereas in the negative control we can see the characteristic tubular morphology typically associated with healthy cells. Due to the reported data showing VP24 binding to VDAC1 (García-Dorival *et al.*, 2014), we assessed whether we could see colocalization between VP24 and VDAC1, as this could suggest a pathway by which VP24 might be adversely affecting the cells. HeLa cells were transfected with HA-tagged zVP24, rVP24 or empty vector for 48 hours before immunofluorescent staining for HA and endogenous VDAC1 protein. Confocal imaging of the samples suggest that both zVP24 and rVP24 co-localise with VDAC1 in parts of the cell, predominantly the perinuclear regions [Figure 14].

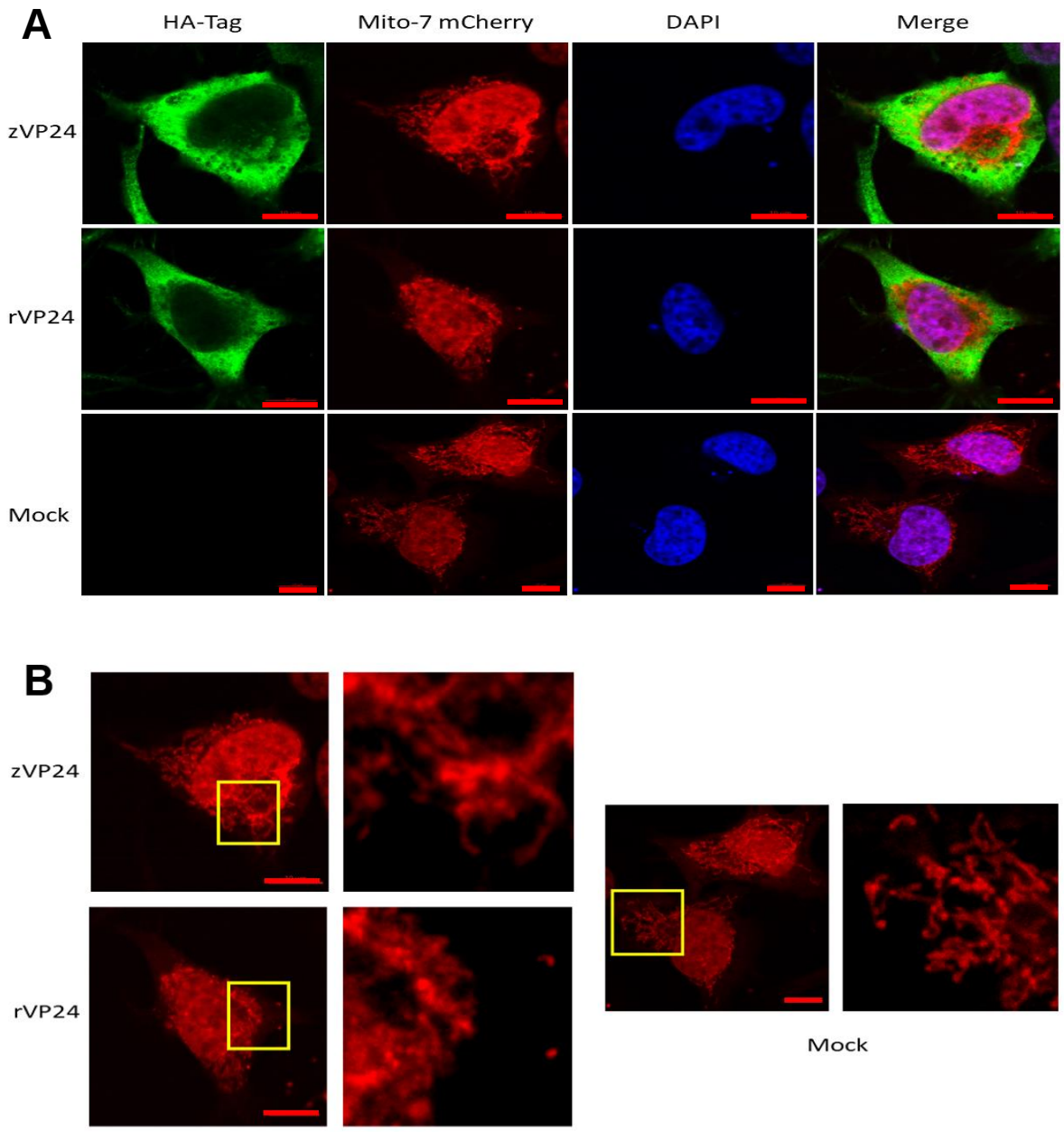

Figure 13. Analysis of Mitochondrial architecture in VP24 transfected Hela cells.

Hela cells were co-transfected with Mito7-mCherry and either zVP24-HA, rVP24-HA or empty pCAGGS vector and incubated for 48 hours. Coverslips were then stained with anti-HA and counterstained with DAPI prior to mounting on glass slides. (A) Cells positive for either zVP24 and rVP24 show punctate mitochondrial morphology whereas the negative control shows typical tubular morphology. These findings appear more pronounced in the zoomed in region of interests (B). Scale bars represent 10μM. N=3

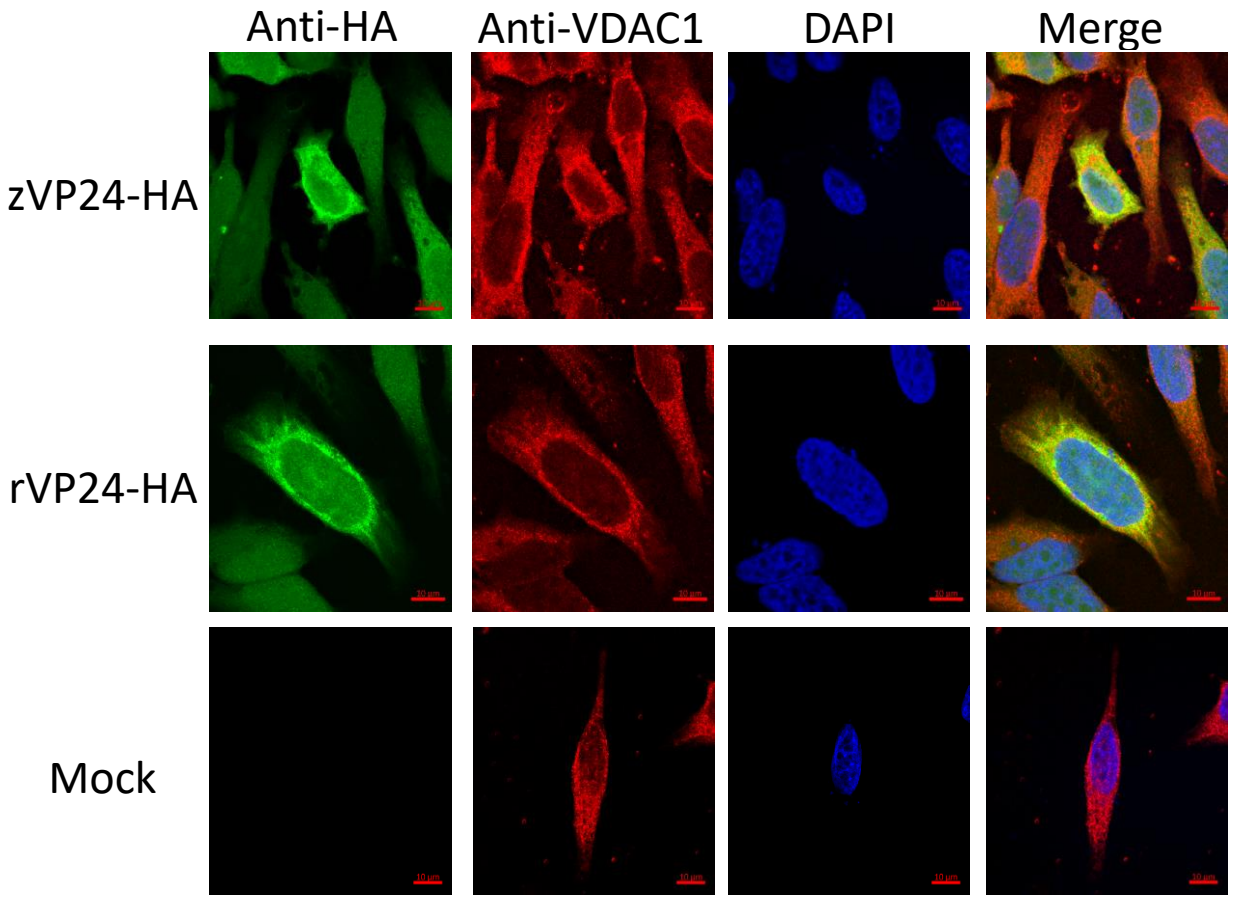

Figure 14. VP24 immunostaining with VDAC1

HeLa cells transfected with either zVP24 and rVP24 were grown for 48 hours prior to fixation. Cells were probed for VDAC1 and HA tag. The images appear to show similar localisation of VDAC1 and VP24, suggesting that there may be some interaction, however, further experiments would need to be done to fully verify these interactions. Scale bars denote 10μM. Images captured by confocal microscopy. N=3

3.3.3 VP24 does not affect intracellular calcium levels

Due to the extensive roles calcium has in cells regarding proliferation, metabolism and cell death, we decided to investigate whether VP24 has any effect on intracellular calcium we subjected transfected HeLa cells to the Fluo4 Direct™ assay kit which measures intracellular calcium and monitored fluorescence. HeLa cells were transfected with either HA-tagged zVP24, rVP24 or empty vector and incubated for 48 hours prior to running the assay. Both zVP24 and rVP24 do not appear to have any influence on intracellular calcium levels as Fluo4 intensity was comparable

to the negative control [Figure 15]. By comparison, the positive control that has cells treated with ionomycin, a powerful calcium inducer, showed increased fluorescent intensity. The western blot analysis confirmed successful transfection of both zVP24 and rVP24 during the assay. As a result, we believe that VP24 does not induce cytotoxicity by increasing intracellular calcium at 48 hours post transfection.

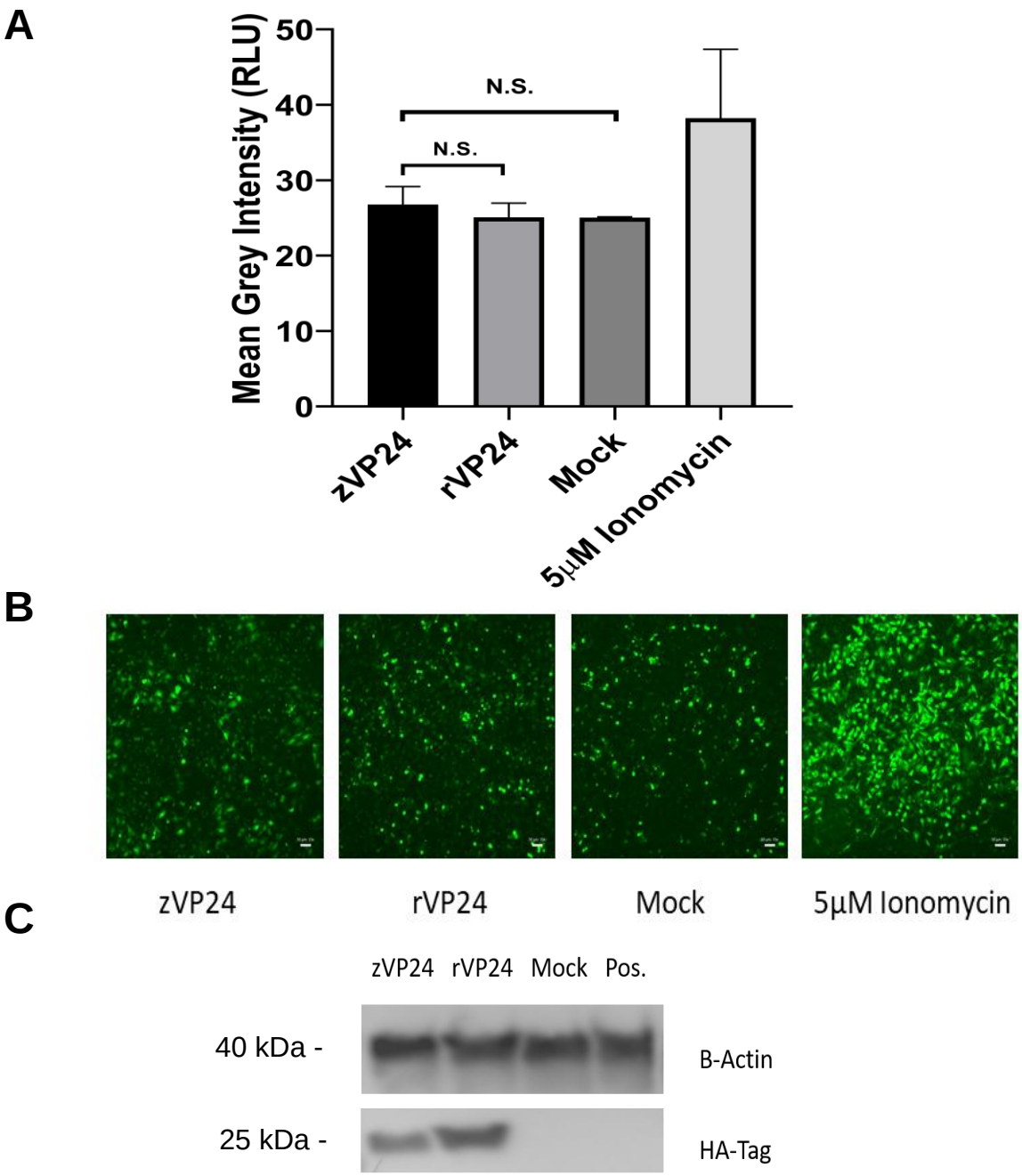

Figure 15. Fluo-4 Calcium Assay.
Cells transfected with either zVP24-HA, rVP24-HA or empty vector pCAGGS for 48 hours prior to assaying with Fluo-4 Direct™. (A) After 48 hours Fluo4 intensity was measured using ImageJ. The intensities were subjected to ANOVA statistical analysis. N=3. There is no significant increase in levels of intracellular calcium between the zVP24, rVP24 and the negative control. The positive control using 5μM ionomycin shows high levels of intracellular calcium. (B) Live cell imaging shows Fluo4 fluorescence of the cells in each sample. (C) Western blots verified that the transfection had successfully resulted in comparable protein expression. N=3

3.4 Discussion

3.4.1 Cell Proliferation and Viability

Due to the previous inability to create a stable cell line expressing VP24 (Mateo et al. 2011), we decided to monitor in real time what happens to VP24 transfected cells incubated over a 72-hour period using the Incucyte®^{TM} live imaging system. Monitoring of cellular proliferation revealed a gradual decline in cell density in both zVP24 and rVP24 cultures predominantly after the 48 hour time point [Figure 11]. The larger contrast in cell proliferation displayed at 72 hours between VP24 (z and r) and mock suggests that VP24 may have cytotoxic properties. Whilst live imaging provided us with observational evidence of changes in proliferation, we cannot deduce what pathways are involved.

In order to further investigate VP24 cytotoxicity we examined cell viability by MTS assay as this experiment would indicate if VP24 causes cytotoxicity through alterations in cellular metabolic activity. The colourimetric MTS assay was derived from the MTT assay with a variation of the tetrazolium salts of which are soluble in cell culture medium, yet retains the initial principle of measuring mitochondrial enzymatic activity of only viable cells (Mosmann, 1983; Cory *et al.*, 1991). Despite the predominant use of MTS assays to screen cells against drug compounds, particularly in realms of cancer research, this technique has been used to investigate effects of viral proteins, therefore making this assay a suitable choice to use despite the slightly cytotoxic effects of transfection reagents (Honda *et al.*, 2000). In order to minimise any background cytotoxicity caused by transfection reagents, we used TransIT-LT1, known for its low toxicity. We observed significant changes of cellular metabolism in samples transfected with both HA-tagged zVP24 and rVP24 at 48 hours, yet at 24 hours there appears to be no difference, highlighting temporal or protein level-dependent effects of VP24 [Figure 12]. Despite a stronger band intensity for rVP24-HA, likely due to unequal DNA concentration, it does not appear to have any difference with regards to metabolism compared to zVP24. Previous

transcriptomic experiments have shown that VP24 differently affects immune response gene expression in human dendritic cells depending on the time point in which the analysis was carried out (Ilinykh *et al.*, 2015). Whilst we are not specifically investigating the immune response of cells, we consider the underlying principle to be of value in that different subset of genes may be affected depending on length of incubation periods. Furthermore, based on the fact that the MTS compound changes colour in relation to mitochondrial viability, we find it interesting that we observe a decrease in signal upon VP24 transfection, as previous studies investigating the VP24 interactome by immunoprecipitation and mass spectrometry have identified several mitochondrial proteins (García-Dorival *et al.*, 2014). The authors reported VP24 binding to proteins VDAC1 and VDAC2, both involved in metabolite regulation across the mitochondrial membrane. These reported interactions may offer insight as to where and why VP24 is causing a decrease in cell viability, especially given that the MTS assay is based on mitochondrial activity. However, another research group more recently investigated VP24 binding partners also by coimmunoprecipitation and mass spectrometry did not report VDAC1 nor VDAC2 as binding partners, though differences may be due to the experimental procedures as the two groups used different tags on VP24 , the former group used both N and C terminal GFP tags in separate experiments (27kDa) whereas the latter used 2x strep tag (2kDa) (Batra *et al.*, 2018). Nonetheless the latter group identified ATP1A1 and ATP2A2 as VP24 binding partners, also confirmed by García-Dorival et al. 2014. There is some evidence whereby ATP1A1 was implicated in cytotoxicity (Takase *et al.*, 2017; Zhang *et al.*, 2018), though to assume that the MTS assay result was due to the VDACs or ATP1A1 interactions would be speculation. Whilst the actual mechanisms in question for our reported reduction in cell viability remain to be elucidated, we can state that prolonged expression of VP24 in HeLa cells results in a decrease in cellular metabolism and viability.

3.4.2 Mitochondrial Architecture

Using immunofluorescent microscopy techniques we observed mitochondrial morphology as a marker for cellular stress, given their canonical role in generating ATP and many other metabolites, as well as acting as calcium stores in the cell (Brookes *et al.*, 2004). Morphological changes of mitochondria often occur when the cellular environment has been altered due to stress factors (Youle and van der Bliek, 2012). Regulated by GTPases in the dynamin family, mitochondrial fusion or fission occurs as a form of quality control, where fusion rescues damaged mitochondria and fission is needed to create new mitochondria and under stressed conditions lead to apoptosis (Bleazard *et al.*, 1999; Meeusen *et al.*, 2006; Youle and van der Bliek, 2012). By using Mito7-mCherry, we were able to observe the mitochondria using confocal microscopy in order to deduce whether there was a change in morphology attributed to the presence of VP24. Our data show a disturbed mitochondrial morphology in comparison to the mock transfected cells, which we believe supports our hypothesis that VP24, both EBOV and RESTV, has cytotoxic properties. Interestingly, we do not see any colocalization between VP24 and mitochondria, despite the reported presence of VDAC1 and VDAC2 on the outer mitochondrial membrane and the known association between VP24 and VDAC1. An explanation for this could be that the interactions between VDAC1, VDAC2 and, VP24 did not occur, as reported by Batra et al. 2018. We noticed red signal arising from the nucleus for Mito7-mCherry. This was due to incompatible filter sets used at the time of the experiments, due to a logistical issue at the time with the confocal microscope kit.

We also immunostained transfected cells for endogenous VDAC1 [Figure 14]. There appears to be colocalization in some parts of the cell but the microscopy data is not sufficient to prove that VP24 is indeed interacting with VDAC1. Furthermore, VDAC1 has also been found to localise in the plasma membrane, therefore we cannot differentiate whether the previously reported interactions are occurring on the mitochondria or in the plasma membrane.

One of the drawbacks of assessing morphology of organelles such as mitochondria is that it becomes difficult to distinguish between morphologies during apoptosis and cell cycle regulation, as mitochondria undergo fission during the M and S phase of the cell cycle (Antico Arciuch *et al.*, 2012). Therefore, our conclusions cannot point

towards a singular cause for this altered morphology. Nevertheless, our results strongly suggest that VP24 has cytotoxic effects.

3.5 Conclusion

From the data generated in this chapter we see that VP24 has cytotoxic properties and may affect cellular death signalling pathways. Whilst we do see some colocalization with VDAC1 in the cells, this does not appear to occur at the mitochondrial membrane and so did not focus on this interaction with regards to cytotoxicity. We next sought to investigate the impact of VP24-induced cytotoxicity, such as cellular death activation. Therefore, we assessed VP24 activation of three key signalling pathways; apoptosis, necroptosis and autophagy, as they culminate in cell death.

3.6 Future Work

Due to the decrease in proliferation and metabolism as seen by the live imaging and MTS assays, it would be interesting to carry out further follow-up experiments. Many assay kits are now commercially available that would be informative to carry out, in this instance, an ATP assay kit could indicate whether VP24 causes decrease in ATP levels in cells compared to the mock. This may explain the reduced proliferation of cells. Furthermore, another experiment that would be interesting to carry out despite being more time consuming would be a metabolomics experiment by nuclear magnetic resonance imaging, as this would allow us to see changes in specific metabolites in cells transfected with VP24. Having this data can give us more insight how VP24 reduces cell proliferation and metabolism.

4 Cytotoxicity of VP24 – Cell Death Signalling Pathways

4.1 Abstract

Observations of VP24 causing a decrease in metabolic activity and proliferation in the previous chapter has led us to verify whether there is any activation of cell death. Many cell death signalling pathways have been uncovered, such as apoptosis, one of the most understood forms of cell death, necroptosis, a form of violent death involving swelling and lysis, and, autophagic death, a new form of cell death involved during cellular starvation. Our immunoblots reveal an activation in caspase 8, an initiator of the apoptosis cascade, however no activation of key apoptotic markers; PARP and caspase 3. We detected by immunofluorescence localisation of MLKL differed in cells transfected with VP24 compared to the mock, however this did not lead to necrotic death. From our results collected in this chapter, we believe that VP24 cytotoxicity does not lead to cell death, and that other pathways are responsible for the decrease in metabolic activity and cellular proliferation.

4.2 Introduction

Programmed cell is a terminal event undertaken by cells for several biological processes, one of which is to eliminate cells that pose a threat, be it by pathogen infection or disruption of cellular processes. Currently, three main types of programmed cell death are known; apoptosis, necroptosis and autophagic death. Each mode has unique morphological characteristics and often occur in different situations.

Apoptosis is one of the most understood modes of cell death. It has characteristic morphological features such as cell shrinkage, plasma membrane blebbing and fragmentation of chromosomal DNA (Kerr, Wyllie and Currie, 1972) [Figure 16]. The two main pathways are intrinsic apoptosis and extrinsic (receptor mediated) pathways, of which either pathway initiates a series of cascades between caspases, with the final cleavage of executioner molecules caspase 3 and caspase 7 indicating manifestation of apoptosis (Strasser, O'Connor and Dixit, 2002). The intrinsic pathway can be triggered by several factors such as oxidative stress, DNA damage or presence of pathogens. Markers to detect initiation of apoptosis include the caspases 2, 8, 9, and 10. Their activation results in cleavage of downstream executioner caspases 3, 6 and, 7. Other markers for apoptosis include cleavage of poly-ADP-ribose polymerase (PARP) by caspases, resulting in inhibition of its DNA repair properties.

Necroptosis was once considered to be an accidental form of death, though nowadays it is widely accepted to be a programmed form of cell death. The key markers for activation of the pathway is phosphorylation of receptor-interacting serine/threonine-protein kinase 3 (RIP3) by RIP1, which both interact with mixed lineage kinase domain-like protein (MLKL) to form the necrosome. Following this, the executioner molecule MLKL becomes phosphorylated by RIP3. This leads to MLKL oligomerisation and subsequent transport to the membrane, acting as a pore. The cell cytoplasm then swells, leading to rupture of the cell [Figure 16]. This is a violent event that spills large amount of signalling molecules called damage-associated molecular patterns (DAMPs) (Dhuriya and Sharma, 2018) that recruit

immune system cells to the site of damage. This results in high inflammation and affects nearby tissues. Necroptosis can be activated by extrinsic factors such as TNF-α binding to its receptor, oxidative stress and DNA damage.

Autophagic death or autosis has been subject to intense debate as this pathway was primarily known to be activated for cell survival (Debnath, Baehrecke and Kroemer, 2005). This occurs by degradation of macromolecules in the cell, taking place in autophagosomes that fuse into lysosomes which ultimately undergo lysosomal degradation, releasing oxidizable substrates to be used if nutrients are sparse (Codogno and Meijer, 2005). In regard to cell death, most of the evidence is correlative with other modes of cell death as these pathways are energy intensive, ergo, starving the cell of metabolites which would increase autophagy. So far, it appears that two forms of death have been attributed to autophagy: Autosis, and type II autophagic cell death. Morphological features are often used to distinguish the two such as moderate chromatin condensation (late autosis/ not present in type II) and ER disappearance (autosis). However, many of these morphologies are also seen in apoptotic and necrotic cells thus adding fuel to the debate (Liu and Levine, 2015). Lastly, autophagy has been shown to have both pro-viral and anti-viral properties for influenza and dengue viruses (Kudchodkar and Levine, 2009). Currently, autophagic death is morphologically defined, and conclusive evidence for the actual mechanism responsible for cell death by autophagy remains elusive (Debnath, Baehrecke and Kroemer, 2005). It is for these reasons that this mode of death is subject to debate. Ultimately, the principle for this form of cell death is based on a prolonged activation of autophagy machinery due to starvation or exposure to cytotoxic agents. Once exposed to these factors, phagophores form which engulfs material in the cell, leading to the formation of an autophagosome, of which the marker LC3-b is exposed on the inner membrane (Tanida, Ueno and Kominami, 2008). Protein interactions with LC3-b occur through a LC3-interacting region (LIR) on the protein and are crucial for recruitment of LC3 and autophagosome maturation. Following this, the autophagosome fuses with lysosomes, forming the autolysosome, where the contained cargo is degraded by acid hydrolases. The degraded contents can then be used by the cell as a source of nutrients. Activation

of autophagy can be detected by seeing increased number of LC3 foci by microscopy.

In this chapter we will explore various cell death markers in order to identify whether prolonged expression of VP24 leads to cell death and if so, by which pathway.

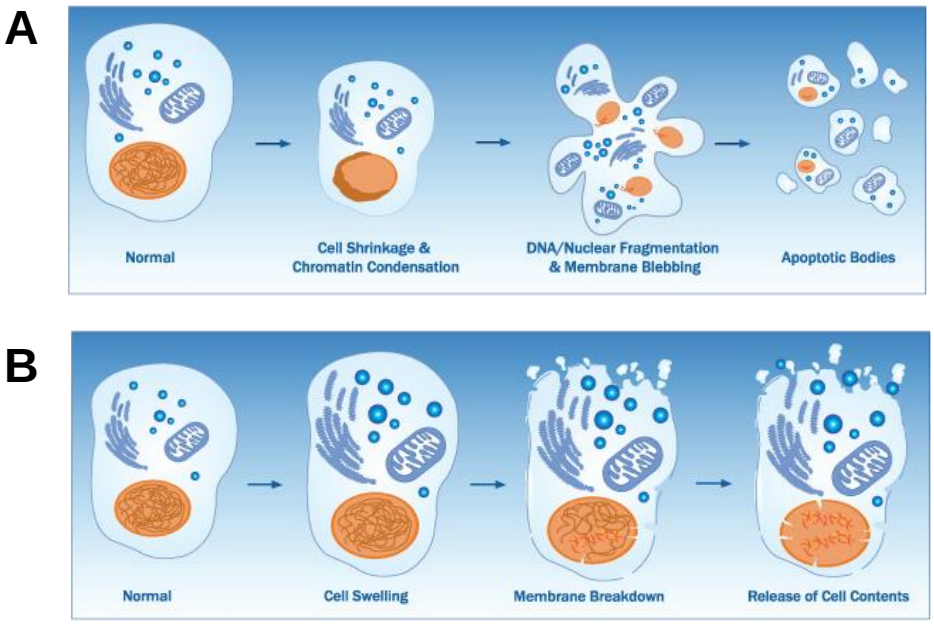

Figure 16. Morphological differences between Apoptosis and Necroptosis

This figure highlights the distinct morphological features observed from cell dying by apoptosis (A) or necroptosis (B). One of the key differences is that apoptosis leads to cell shrinkage and fragmentation, whereas necroptosis leads to cell swelling and rupture. (Taken from Novus Biologicals Poster)

4.3 Results

4.3.1 VP24 does not activate intrinsic apoptosis

To investigate whether VP24 activates cellular death pathways, we opted to assay for apoptosis. We initially used fluorescent assay techniques that detect several different apoptotic factors: caspase 3, 7 and 8 cleavage. Using a 96 well plate, HeLa cells were transfected with either HA-tagged zVP24, rVP24 or empty vector and incubated for 48 hours. The cells were then assayed using fluorescence detection kits Caspase-Glo 3/7 and Caspase-Glo 8. We report that Caspase-Glo 3/7 does not show activation of apoptotic pathway in either zVP24 and rVP24, comparable to the empty vector control [Figure 17 A]. However, the Caspase-Glo 8 assay revealed increased caspase-8 activity when compared to the empty vector control, suggesting that VP24 from both species cause activation of caspase 8 [Figure 17 B]. This would appear to tell us that the initiation of apoptosis is active, but we do not report execution of apoptosis.

We decided to confirm the Caspase-Glo results by western blot, using antibodies that specifically detect cleaved forms of apoptotic execution proteins (PARP-1, CASP3 and CASP7). Our blots show no cleavage of any of the aforementioned proteins, confirming the results of fluorescent assays [Figure 18]. Furthermore, lack of PARP-1 cleavage confirms that apoptosis is not activated since its cleavage is dependent on caspases. Lastly, our confocal imaging shows no morphological changes of the cell nucleus, therefore it appears that VP24 does not induce apoptosis after 48 hours post transfection [Figure 18 B].

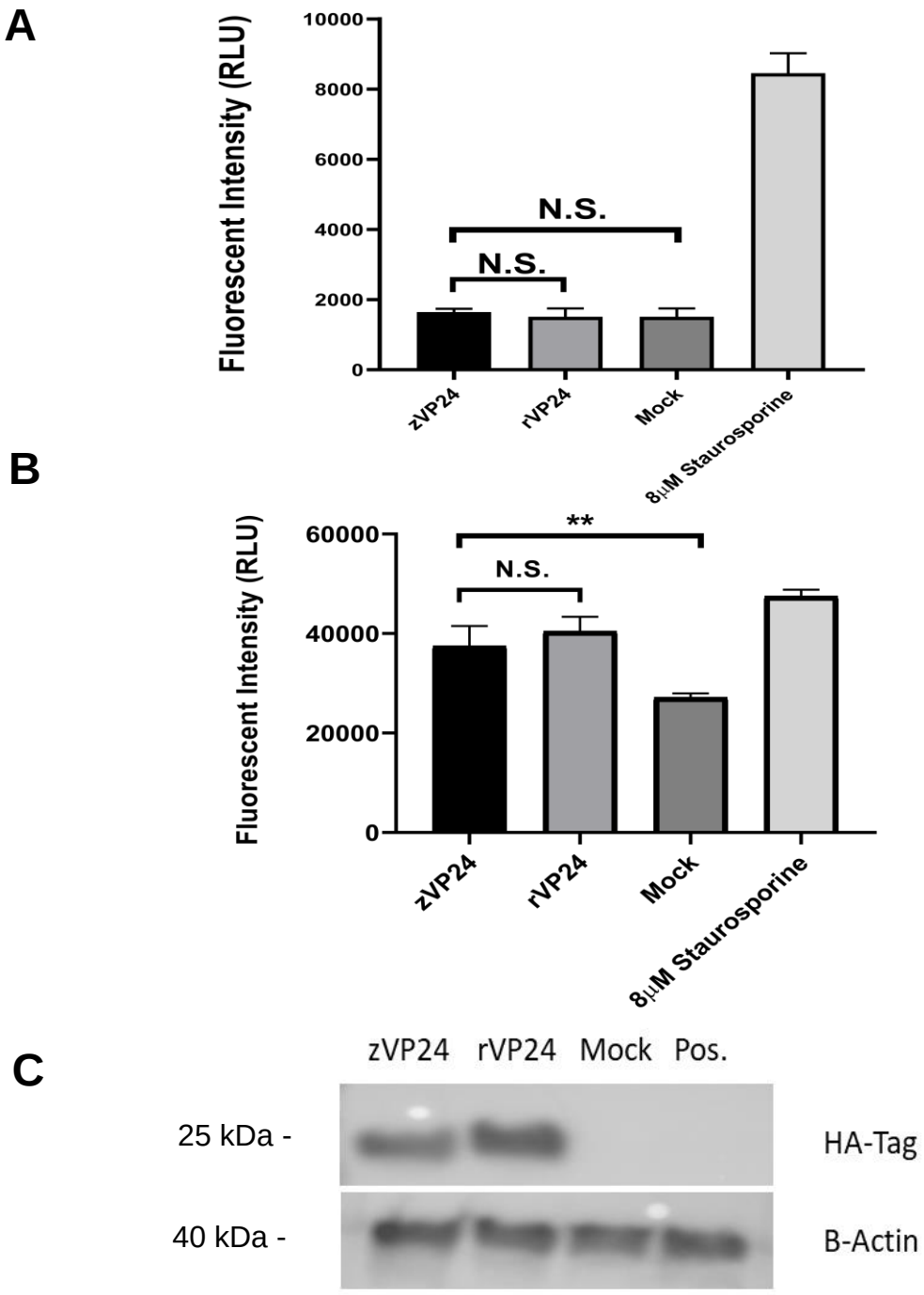

Figure 17. Caspase Glo Assays

To detect activation of key apoptotic markers, cells transfected with HA-taggedzVP24 and rVP24 and incubated for 48 hours prior to assaying with fluorescent assay kits Caspase-Glo 3/7 and Caspase-Glo 8. (A) Caspase Glo-3/7 assay shows no activation of the apoptotic executioner markers caspase 3 and 7, therefore apoptosis does not appear to be taking place. Caspase-Glo 8 assay however reveals activation of caspase 8 (B), a protein known to be involved in regulating several pathways involving cell viability, depending on its interacting partners. Western blots were carried out in tandem to confirm successful transfection (C). Results were subjected to ANOVA statistical method. N=3, p=<0.01

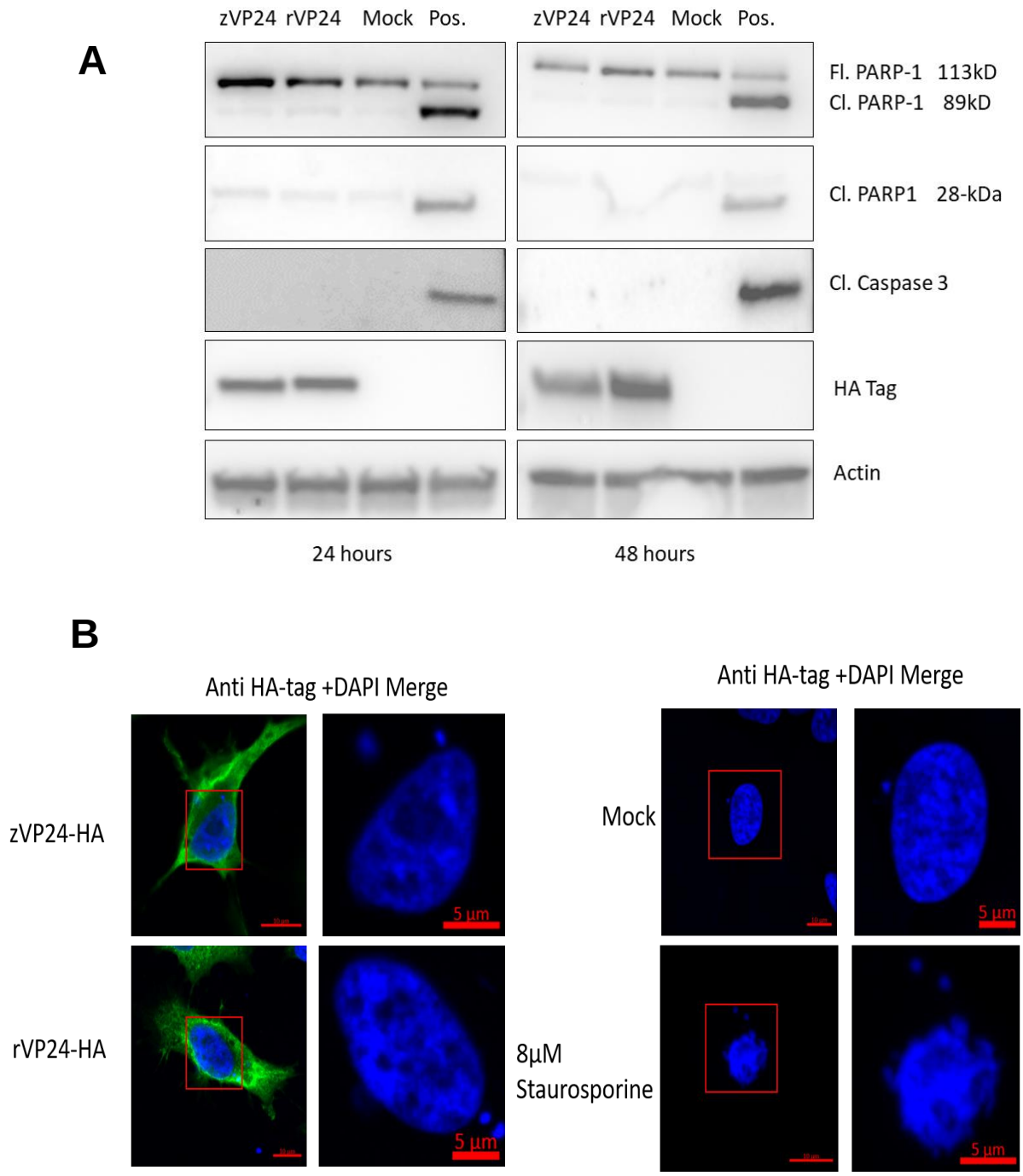

Figure 18. Western Blot Analysis of Key Apoptosis Markers
Cells were transfected with either HA-tagged zVP24, rVP24 and, empty vector pCAGGS and incubated for 24 and 48 hours prior to lysis or fixation. A western blot was carried out to detect any markers for apoptosis (A). Due to the lack of bands in the zVP24 and rVP24 samples for cleaved caspase 3 and cleaved PARP, we can confirm that there is no activation of apoptic pathways. The nuclei of cells positive for VP24 do not show morphological features associated with apoptotic cells ass seen in the positive control (B). Cells were treated with 8µM of staurosporine to generate positive controls. N=3

4.3.2 VP24 does not activate the autophagy pathway

As LIR domains are a well-defined mechanism for virus-manipulation of autophagy, we first screened for potential LIR domains in VP24 using the iLIR online database, which also return a position-specific scoring matrix (PSSM). The PSSM score is useful to ascertain the validity of a possible LIR domain, as the higher the PSSM score, the more genuine the LIR domains are from the screen. Results showed W-x-x-L motif hits for both zVP24 and rVP24, suggesting that there may be LC3 interaction sites between LC3 and VP24, despite lower position-specific scoring matrix (PSSM) scores compared to the canonical viral LC3-interacting protein, influenza M2 [Figure 19 A]. To verify the bioinformatic screening, we used immunofluorescent microscopy to detect whether autophagosome formation is occurring using an LC3 plasmid fused with GFP. Autophagic activity is monitored by the formation of autophagosomes, seen as green puncta in the cell cytoplasm. HeLa cells were co-transfected with LC3-GFP and either HA-tagged zVP24 or empty vector, and incubated for 48 hours prior to fixation. Cells were stained for anti-HA to probe for HA-tagged VP24. The positive control was generated removing full culture media of the LC3-GFP transfected cells and replaced with 2mL Earl's Balanced Salt solution (EBSS) for 4 hours as to starve the cells and induce autophagy. Our confocal imaging results suggest zVP24 causes minor activation of the autophagic pathway as LC3-GFP retains a predominantly diffuse cytosolic localisation with only small occasional foci seen, in contrast to the induction of autophagy in starved cells incubated in EBSS. [Figure 19B].

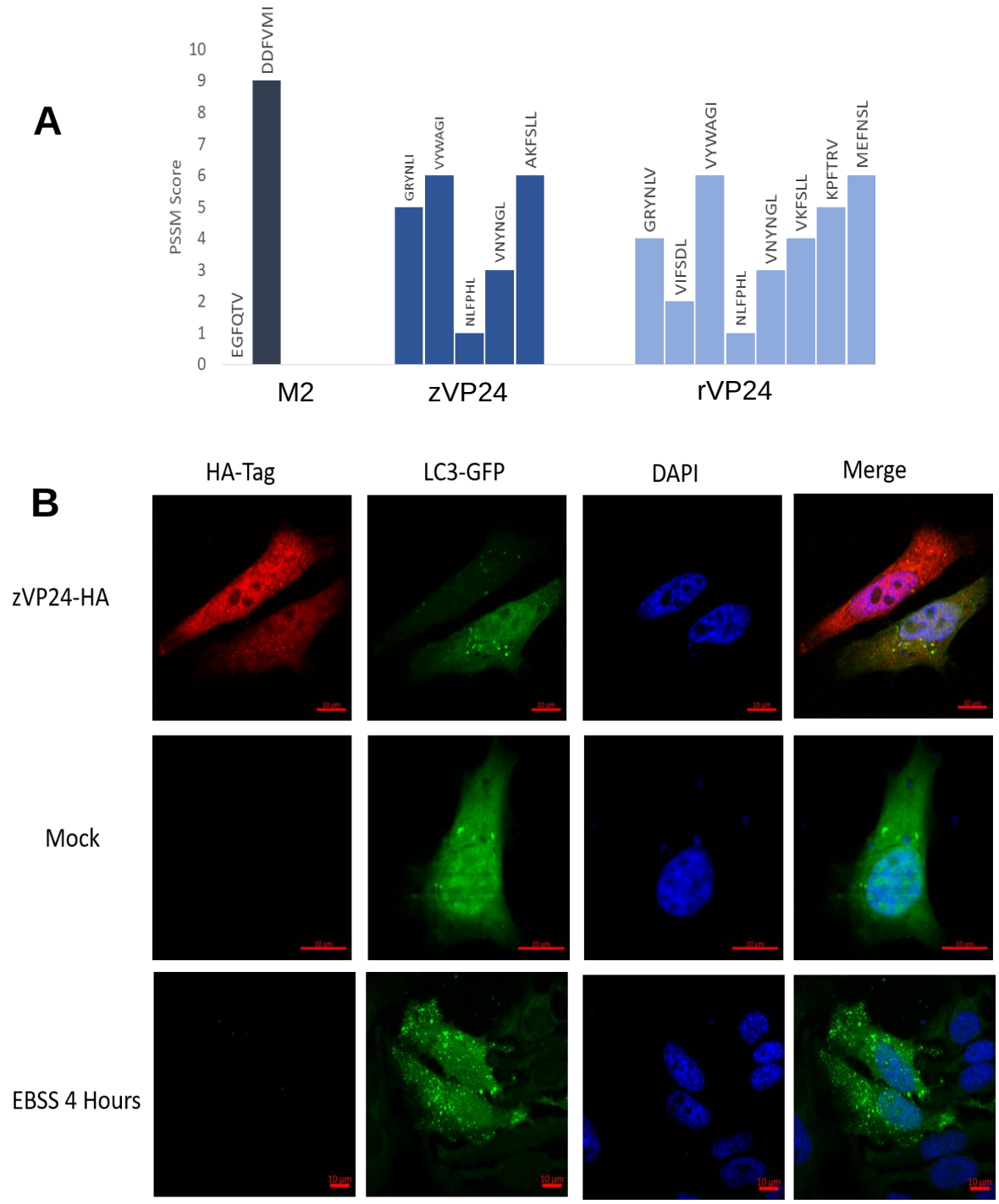

Figure 19. Identification of LC3 Interacting Domains
Screening for potential LIR domains returned several motifs in both zVP24 and rVP24, though the PSSM score is not as high as the Influenza M2 protein (A). HeLa cells were transfected withHA-tagged zVP24 and LC3-GFP for 48 hours prior to fixation for microscopy. zVP24 transfected cells do not show increased levels of autophagy compared to the mock, which represent basal autophagy levels. Cells treated with EBSS have numerous LC3-GFP puncta, showing strong activation of autophagy (B). These results show that VP24 is not causing any changes with regards to autophagy activity within the cells. N=3

4.3.3 VP24 rearranges localisation of necroptosis markers

Another form of programmed cell death is necroptosis whereby the cells swell and lyse. Phosphorylation of mixed lineage kinase domain like pseudokinase (MLKL) allows for oligomerisation and formation of pores in the cell membrane. Using western blot techniques, we sought to detect any phosphorylation of MLKL in the presence of either zVP24 or rVP24. HeLa Cells were co-transfected with HA-tagged zVP24, RIP3-YFP to reconstitute the necroptotic pathway as HeLa cells do not express RIP3, and dsRED-MLKL for 48 hours prior to lysis and immunoblotting. The Western blot reveals phosphorylation of MLKL within the zVP24 cell lysate, whereas rVP24 and mock reveal dim signal intensity by comparison [Figure 20]. This suggests that zVP24 may be cytotoxic because it triggers activation of necroptotic programmed cell death.

To confirm MLKL phosphorylation by western blot, we used fluorescent microscopy for assessing localisation of MLKL in zVP24 transfected cells, as MLKL localises to the plasma membrane upon phosphorylation and activation. Based on the MLKL Western blot data, only zVP24 induction of MLKL relocalisation was investigated. Our imaging does not show membrane localisation of MLKL in either zVP24 or mock treated cells [Figure 21]. However, there seems to be an increase in MLKL fluorescent intensity near the plasma membranes as well as the formation of MLKL puncta in the cytoplasm in zVP24 transfected cells whereas mock cells retain a diffuse level of cytoplasmic MLKL expression [Figure 21]. This suggests zVP24 in cells may lead to activation of MLKL, though in a slow or non-canonical process.

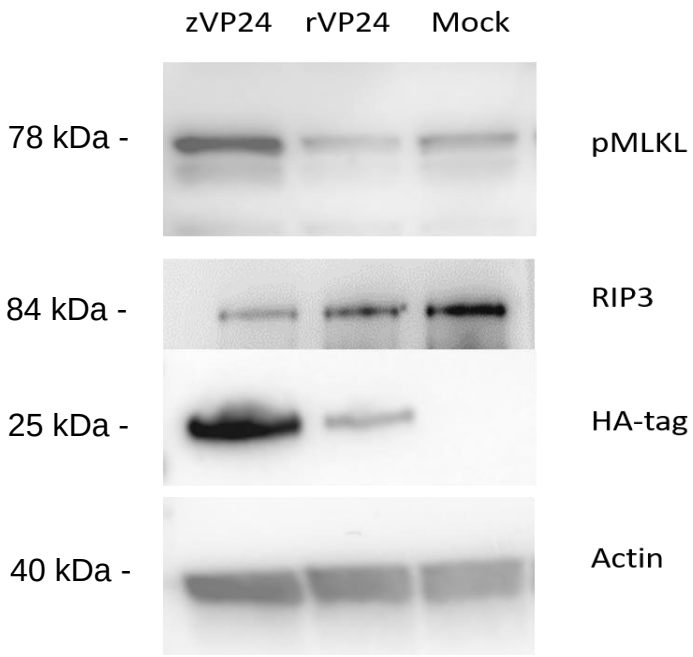

Figure 20. Western blot analysis of pMLKL
HeLa cells were co-transfected using PEI with either zVP24 or rVP24, as well as RIPK3-YFP and dsRED-MLKL for 48 hours prior to lysis for western blot analysis. Membranes were probed with antibodies for pMLKL, RIP3, HA-tag and β-actin. The pMLKL band intensity is highest in zVP24 treated cells which suggests that presence of zVP24 leads to activation of the necroptosis pathway. The molecular weight for pMLKL is 50 kDa, though since this protein was overexpressed for detection, it also contains a dsRED tag (28 kDa), therefore the band appeared at around 78 kDa. Similarly, RIP3 (57 kDa) is not endogenously expressed, therefore a YFP-RIP3 expression plasmid was used, so the antibody band appeared at around 84 kDa.

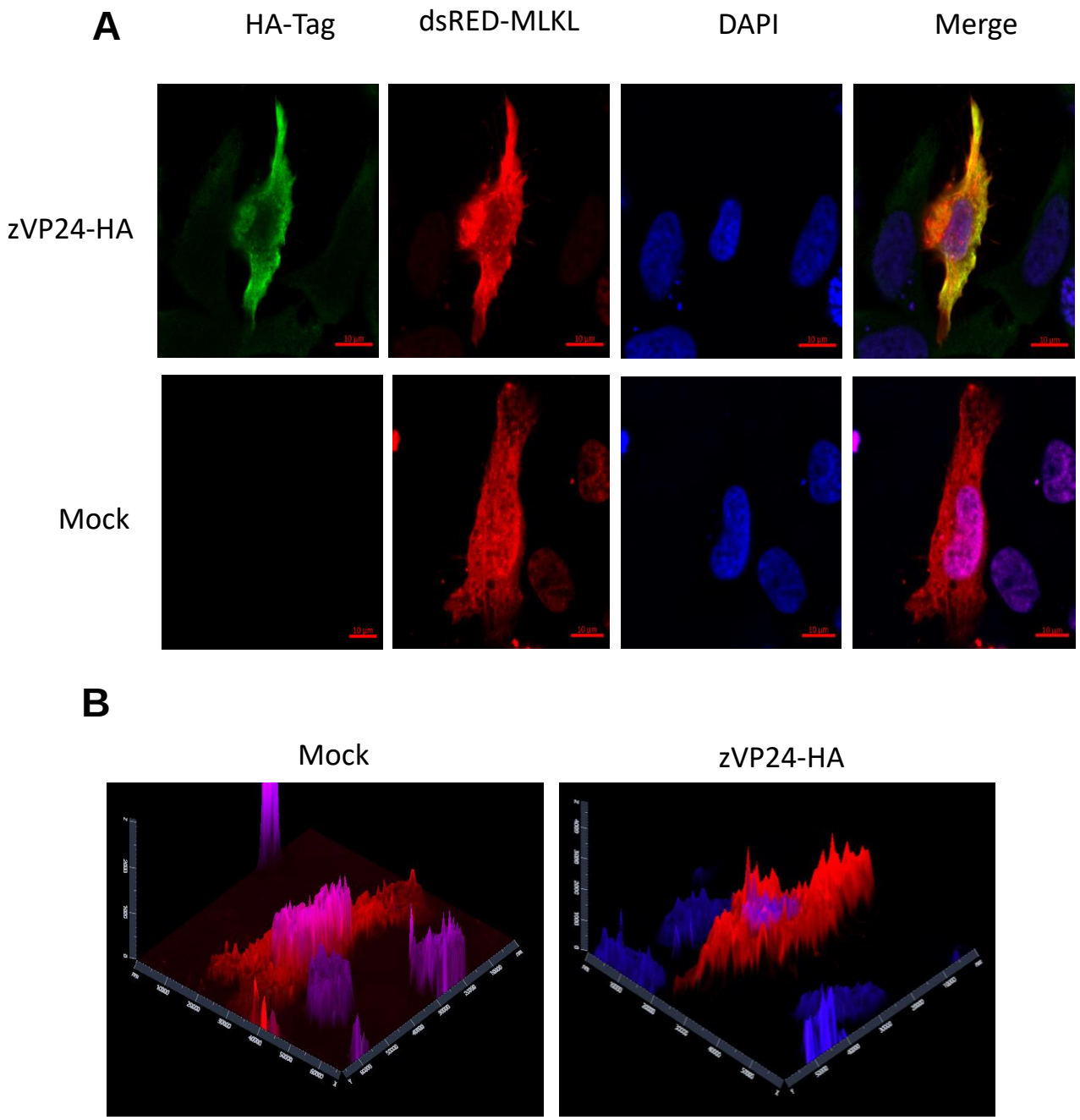

Figure 21. Immunofluorescent analysis of MLKL localisation
Assessing localisation of MLKL can give insight as to whether the cells are undergoing necroptosis, due to its localisation in the plasma membrane. (A) HeLa cell were co-transfected with HA-tagged zVP24 and dsRED-MLKL and incubated for 48 hours prior to fixation and immunofluorescence staining for HA. The negative control shows a diffuse cytoplasmic localisation of MLKL. Cells positive for zVP24 show rearrangement of MLKL but don't appear to have full membrane localisation around the cell. (B) 2.5D representation of MLKL (red) and DAPI (blue) channels taken from images in A highlight the increased fluorescent intensity and localisation of dsRED-MLKL in zVP24 positive cells compared to the diffuse uniform cytoplasmic localisation in the mock sample. N=3

4.4 Discussion

4.4.1 Autophagy

Given that we saw a change in metabolism as seen by MTS assay [Figure 12], coupled with the roles of pathogen induced autophagy, we wanted to verify whether the autophagy pathway was responsible for VP24-mediated cytotoxicity. An initial screen by the online database iLIR generated predictions that would suggest the multiple presences of motifs that may bind to proteins of the ATG8/LC3 family. Noticeably, rVP24 returned 8 hits compared to the 5 from zVP24. Both zVP24 and rVP24 domain hits retain the W-x-x-L motif, though the scores do not appear to be of high confidence compared to M2, of which the LIR domain has been verified *in vitro* (Beale *et al.*, 2014). In addition, our immunofluorescent results revealed only minimal increase in autophagosome formation for zVP24 as the GFP-LC3 marker retains a predominantly diffuse cytoplasmic localisation like the negative control, whereas the positive control displays the typical punctate distribution. Therefore, it appears likely that the VP24's cytotoxicity is not induced by autophagic stress, despite possessing a minimal capacity to active autophagy.

4.4.2 Apoptosis Pathway

Several EBOV proteins induce host cell death, such as exosomal secreted VP40 inducing death in bystander lymphocytes (Pleet *et al.*, 2016). Furthermore, GP has been shown to induce anoikis, a form of apoptosis, resulting in downregulation of adherence molecules such as integrins (Ray *et al.*, 2004). Our caspase-glo 3/7 kit shows no activation of apoptosis in the presence of either zVP24 or rVP24. However, there are many different mechanisms of apoptosis that are independent of caspase 3 and/or caspase 7. For example, extensive DNA damage that is beyond repair can activate apoptosis. This can be detected by blotting for cleaved fragments of PARP-1, a protein involved in DNA repair by adding poly (ADP ribose) polymers. If the DNA damage is extensive and beyond repair, full length PARP-1 (113kDa) is broken down

into smaller fragments, with each fragment being unique depending on necrotic or apoptotic death (Chaitanya, Alexander and Babu, 2010). During apoptosis, PARP-1 is cleaved into a 89-kDa catalytic fragment, and a smaller 24-kDa containing a DNA-binding domain. Our results show that PARP-1 is not being cleaved when the cells are incubated with VP24, whereas the positive controls show the characteristic fragments of PARP-1 during apoptosis. Lastly, our confocal imaging on nuclear morphology shows no nuclear fragmentation, therefore our data strongly suggest that VP24 does not induce apoptosis within a 48 hour incubation period.

Interestingly, we see activation of Caspase-8 despite lack of caspase 3/7 cleavage. Caspase-8 is only considered active when present in the cleaved form. This would indicate that the apoptosis pathway is being initiated. However, we do not see any execution of apoptosis upon the cells. There are reports of active caspase 8 during inhibition of autophagy (Hou *et al.*, 2010) which is interesting because we show VP24 does not induce autophagy but unsure as to whether it inhibits autophagy. Therefore, if we had more time, we would need to carry out further experiments such as inducing autophagy in cells transfected with VP24 to see whether VP24 actually inhibits this pathway. We would also attempt to induce apoptosis in cell transfected with VP24 to see if there is inhibition of apoptosis. However, we did not pursue this route at this moment as we felt it didn't fit the context of the current story.

4.4.3 Necroptosis Pathway

Necroptosis is another mode of programmed cell death that is distinct from apoptosis. Characterised by osmotic imbalances leading to cellular swelling and lysis, necroptotic cell death is often considered to be a 'violent' type of cell death affecting neighbouring cells and leading to high inflammatory response. EBOV infection in cells have shown typical signs of necrotic cell death, such as cell swelling and membrane rupture (Olejnik *et al.*, 2013), however this has yet to be experimentally verified by investigating the activity of key mediators involved in this pathway. The downstream executioner protein of this pathway is MLKL, whereby its phosphorylation results in oligomerisation, leading to pore formation in the membrane. Our results show that MLKL is being phosphorylated in cells positive for

zVP24 compared to rVP24 and the negative control. However, we also detected faint bands for pMLKL in rVP24 and the negative control though we believe this is due to cytotoxic effects likely exerted by the PEI transfection method, as reports have shown activation of cell death pathways in A431 cells (Kafil and Omidi, 2011). At the time of these experiments we were limited in our choice of reagent, as this experiment would have been carried out with TransIT-LT1, which is considered to be more gentle to the cells during transfection. Recent data also suggests that MLKL is involved in the ESCRT-III pathway and that limited phosphorylation of MLKL resulted in generation of vesicles from the ESCRT-III pathway to counteract the cell death pathway and sustain survival of the cells (Gong *et al.*, 2017). Our immunofluorescence results appear to show a rearrangement of MLKL near the plasma membrane in zVP24 expressing cells. However, we did not detect full plasma membrane localisation as has been reported previously for MLKL activation (Cai *et al.*, 2014). Therefore, it is not possible to state if the presence of zVP24 is cytotoxic because of the activation of necroptosis but it is possible that a longer incubation period may have resulted in full membrane insertion. Using a longer incubation period with transfected cells however may cause more noise in the results, due to the harshness of transfection, therefore we did not attempt to assay for results past 48 hours. Unfortunately, most cancer cell lines do not express RIP3 due to silencing by genomic methylation at its transcriptional start site (Koo *et al.*, 2015), and our attempts to establish a fully reconstituted necroptosis pathway by transfecting cells with RIP3-YFP led to high amounts of cell death in the negative control despite many attempts at optimisation, making this option impractical to pursue. It is possible that the presence of RIP3 would allow for full membrane localisation of MLKL upon zVP24 expression. Increased levels of intracellular calcium have been reported to occur during necroptotic death (Cai *et al.*, 2014), however, given that we do not see increase in calcium levels in the cells [Figure 15], we believe that zVP24 may not be directly inducing necrotic cell death but could potentially sensitize the cells to this mode of death. This could happen if VP24 is either blocking apoptotic signalling pathways, eventually forcing the cell to enter necroptosis, or due to increase in reactive oxygen species (Christofferson and Yuan, 2010). However, we did not assay for apoptosis inhibition by VP24 as at the time it did not fit within the scope of

the project, though we did see caspase-8 activation, which is known to interact with RIP1 to mediate both apoptosis and necroptosis. Ultimately, it remains difficult to determine the intensity of VP24-induced MLKL phosphorylation without comparison to a known positive control necroptosis inducer. Therefore, we attempted to repeat the experiment with an extra sample of cells that have been treated with a cocktail of Z-VAD, an apoptosis inhibitor, SMAC mimetic BV6, an apoptosis inducer, and TNF-α, which together are known to activate the necroptosis pathway, however, we did not see MLKL phosphorylation and due to time constraints were unable to optimise the experiment.

4.5 Conclusion

Our observations from the previous chapter led us to hypothesise that cell death signalling pathways were being stimulated by expression of VP24. However, we can see with the current results that this hypothesis is not correct. Whilst zVP24 induces the activation of components of multiple cell death pathways (Caspase 8 cleavage, minor LC3 foci and MLKL phosphorylation), no cell death pathways were fully induced to the execution phase. There is the possibility VP24 may prime cells for cell death upon additional exposures or upon longer duration exposure to VP24. However, the initial live cell imaging results presented in Figure 11 highlight that the reduced cell densities may be either from increase cell death or decreased cell proliferation, which brings into question whether the cell cycle is being impaired by VP24 expression. Therefore, in order to reconcile the data found in chapter 3, our new hypothesis of VP24 cytotoxicity is that the protein negatively affects cell cycle.

4.6 Future Work

Despite not observing any activation of executioner caspases, it would be interesting to see if VP24 may have anti-apoptotic properties. Experiments whereby activation of the extrinsic apoptosis pathway by adding inducers into the cell culture medium such as Fas ligand or TNF-receptor apoptosis inducing ligand (TRAIL) in the presence of VP24 transfected cells, followed by western blotting the same executioner proteins of the apoptosis pathway as done in this chapter. This could be

informative since we observed activation of caspase 8 only. In addition, a follow up experiment regarding necroptosis would be warranted since we saw by western blot and increase in phospho-MLKL compared to rVP24. This would be repeated, possibly in a cell line that expresses endogenous RIP3 so that we could minimise the harshness of cell transfection, especially when restoring a cell death pathway. However, as the current data shows, we believe that its very unlikely VP24 induces cell death. As a result, moving onwards to cell cycle dysregulation would make more sense to follow up.

5 Cytotoxicity of VP24 – Cell Cycle

5.1 Abstract

Many viral proteins have been found to interfere with the cell cycle in order to dedicate host machinery towards viral replication, resulting in efficient generation of viral progeny. With regards to Ebola virus, nothing is known about whether there is a cell cycle arrest during infection. With the knowledge generated so far, we decided to assess for markers involved in cell cycle arrest in cells transfected with VP24 such as p21, a protein that is overexpressed to induce cell cycle arrest. We found that VP24 from both Zaire and Reston increases expression of p21 at 48 hours post transfection. This strongly suggests that a cell cycle arrest is taking place. We also detected an increase in γH2AX, a marker for DNA damage. This data suggests that the unreported cytotoxic effects of VP24 and the inability to generate a stable cell line is due to VP24 causing cell cycle arrest, which we consider to be a novel finding. We hope these observations would result in follow up research using live virus to verify cell cycle arrest and how that would be to the benefit of the virus upon infection.

5.2 Introduction

In the first chapter of this investigation we had identified a decrease in metabolic activity by MTS assay and a decrease in cell density by live imaging. However, in the second chapter we did not observe activation of apoptosis, minimal activation of autophagy and inconclusive data regarding necroptosis activation. This leaves us to explore the last area we suspect that VP24 may be interfering with, the cell cycle. The cell cycle is split into four stages; G1 phase, S phase, G2 phase and M phase [Figure 22]. Within each of these phases, cyclins form complexes with cyclin-dependant kinases (CDKs). The complexing of these proteins can be used to identify stages of cell cycle (Reddy, 2014). Many different proteins can promote or block cell cycle progression, depending on certain factors, such as DNA damage or pathogen-host interactions.

Many viruses have been known to modulate the cell cycle, such as HIV, which arrests cells in G2 phase, resulting in increased virus production (He *et al.*, 1995). Thus, we decided to look for any evidence to suggest whether VP24 may affect cell cycle. Both mass spectrometry results from García-Dorival *et al.*, 2014 and Batra *et al.,* 2018 identified ANP32a as a binding partner of VP24. ANP32a protein has been shown to be involved in cell proliferation, through interactions with the retinoblastoma complex (Adegbola and Pasternack, 2005). Furthermore, we wondered whether the most well-known interactive partners of VP24; KPNA1 and KPNA5 were responsible for shuttling proteins into the nucleus that have important roles for cell cycle regulation. We then hypothesised that if VP24-KPNA1 or VP24-KPNA5 interactions prevents KPNA mediated nuclear import of STAT1, could there be another binding partner of both KPNAs involved in the cell cycle that are blocked from nuclear import?

To verify changes in cell cycle we will use qPCR to check expression levels for cyclins. Cyclins are a family of proteins that have a regulatory role in cell cycle progression. Each cyclin is known to have distinct expression levels at various checkpoints of the cell cycle [Figure 22] as they form complexes with cyclin-dependant kinases (CDK) to drive progression into the next stage.

A

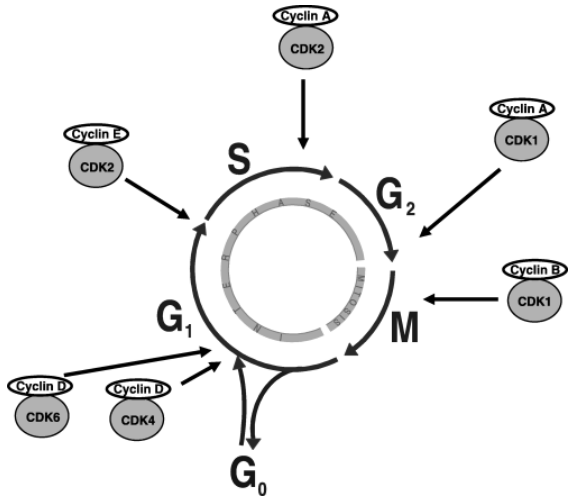

B

Cyclin	Cell Cycle Stage
Cyclin D1	G1 Phase
Cyclin E	Late G1/S phase transition
Cyclin A	S phase, G2/M phase transition
Cyclin B	Mitosis

Figure 22 Cyclins during Cell cycle stages

Expression levels of cyclins differ during the various stages of the cell cycle due to their regulatory role in progression from one stage to the next (A)(adapted from Vermeulen *et al.,* 2003. Assaying expression levels of cyclins may offer insight as to what stage of the cell cycle the population is currently in. Our hypothesis lies on a possible G1 arrest by VP24.

5.3 Results

5.3.1 KPNA1 and KPNA5 Binding Partners using STRING database

STRING is a database that shows reported protein-protein interactions based on the protein query that a user would be interested in. By using STRING database for interactive partners of KPNA1 and KPNA5, we screened for any protein that may have potential roles in cell cycle regulation [Figure 23]. We chose to use stringent filters for the listing of binding partners; so that we could collect datasets derived from experiments only, combined with high confidence threshold (≥0.700). The results identified ANP32B protein, from the same family as ANP32A, to interact with KPNA5. Current literature shows that ANP32A knockdown and ANP32B deficiency results in G1 arrest (Wang *et al.*, 2013; Yang *et al.*, 2016).

A

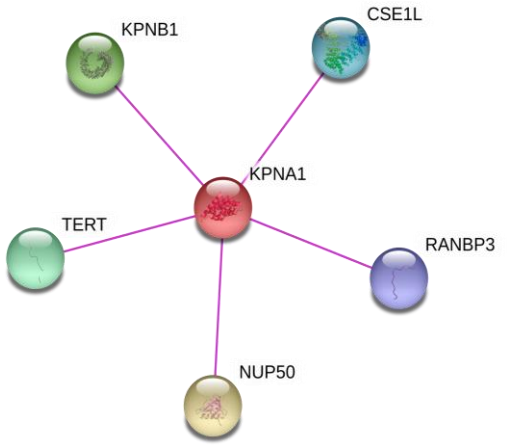

B

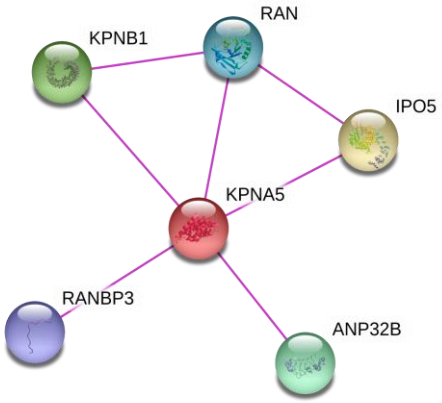

C

Gene	Name	Role
KPNB1	Karyopherin Subunit Beta-1	Nuclear import protein.
TERT	Telomerase Reverse Transcriptase	Replication of chromosome termini.
ANP32B	Acidic Nuclear Phosphoprotein 32 Family, Member B	Cell cycle factor for progression from G1 to S phase. Cell survival factor.
RAN	Ras-related Nuclear protein	GTPase involved in nucleocytoplasmic import/export. GTP-bound form required for mitotic progression
RANBP3	Ran-binding Protein 3	Cofactor for XPO1/CRM1-mediated nuclear export.
NUP50	Nucleoporin 50	Nuclear pore complex component, facilitates importin cargo complex.
CSE1L	Chromosome Segregation 1 Like protein	Export Receptor for importin alpha. Mediates export.
IPO5	Importin 5	Nuclear import transporter, Receptor for nuclear docking and import

Figure 23. Binding Partners for KPNA1 and KPNA5
By using STRING we screened for binding partners to KPNA1 (A) and KPNA5 (B) with the intention of identifying any protein by which impeding its nuclear import may result in adverse effects to the cells. By using datasets derived from experiments only, combined with high confidence threshold (≥0.700) we found the ANP32B protein that interacts with KPNA5 to be of interest due to its role in cell cycle and cell survival.

5.3.2 Analysis of cyclin mRNA expression levels

To verify whether there is any change in cell cycle regulation, we opted to carry out a qPCR experiment to assess expression levels of cyclins using primers specific for Cyclins; A2, B1, D1, and E1. HeLa cells were transfected with either HA-tagged zVP24 or empty vector and incubated for 48 hours prior to lysis for RNA extraction. The CT values were analysed using excel and plotted on a graph to show fold changes against the mock samples that were transfected with empty vector plasmid. The results show that zVP24 expression causes an observable increased mRNA levels of Cyclin E1 comparable to the positive control generated by treating the cells with 500µM mimosine which arrests the cells at late G1 phase [Figure 25]. However statistical analysis did not reveal any significance as the p-value from an unpaired t-test was 0.3346. As a result, it is suggestive but not conclusive that VP24 interferes with Cyclin E1 expression at the mRNA level and causes G1 phase arrest.

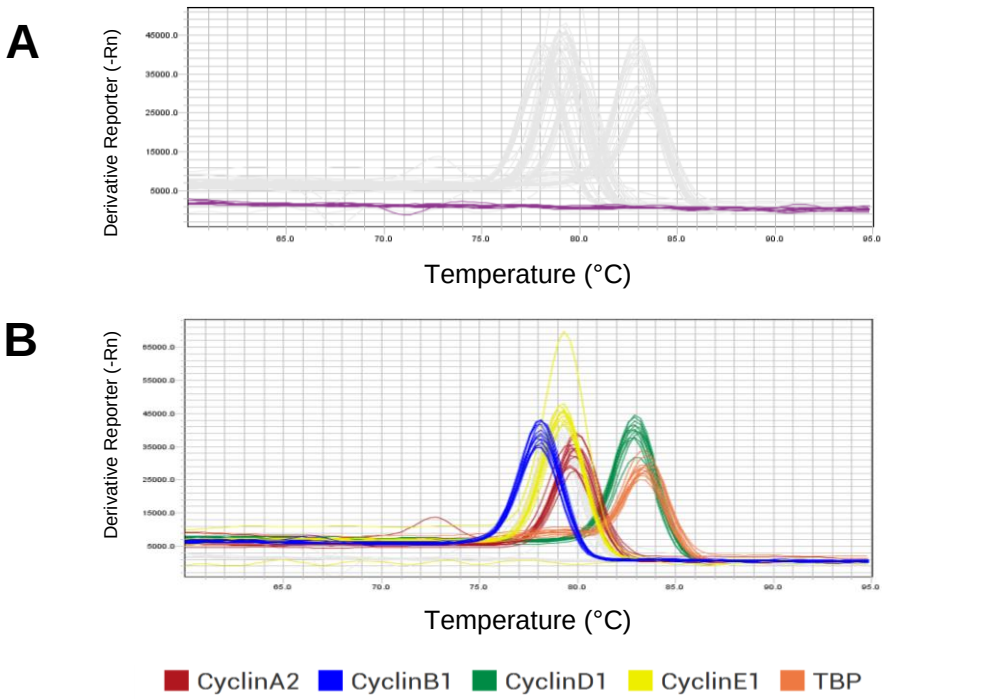

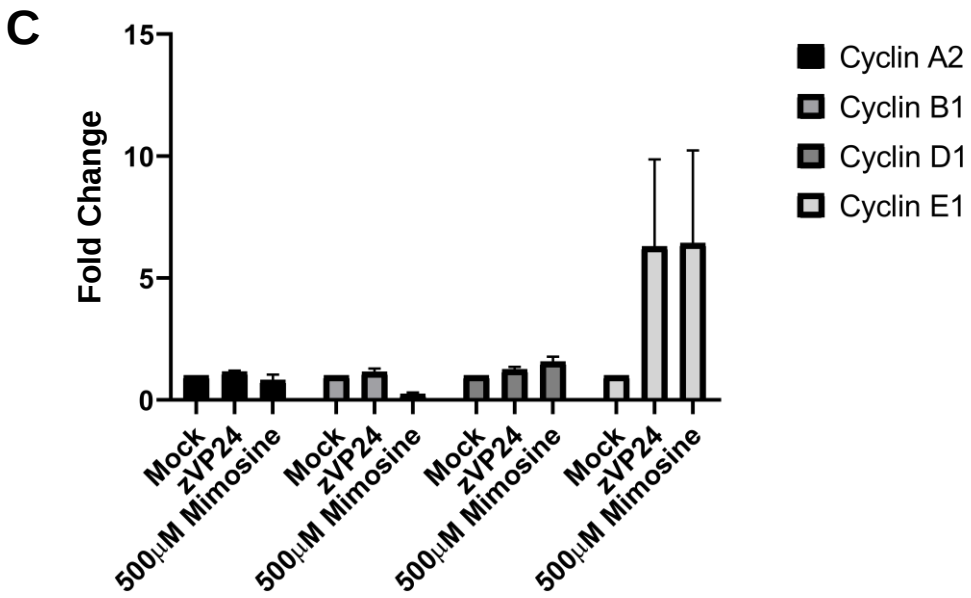

Figure 24. Quantitative PCR analysis of Cyclin mRNA expression levels. Cells transfected with either HA-tagged zVP24, rVP24 or empty vector were lysed for RNA extraction at 48 hours post transfection. A positive control was generated by incubating mock transfected cells with 500μM mimosine for 24 hours to synchronise cells in G1 arrest. Melt curves for the water only samples tested negative for contamination during preparation for qPCR (A). Melt curves for primers specific to their target show similar Tm's, which means they are amplifying one specific target (B). Fold changes of cyclin mRNA expression levels show increased Cyclin E1 in VP24 positive samples (C), suggesting that VP24 may be blocking cells in late G1 stage of the cell cycle. N=3

5.3.3 VP24 expression leads to increase p21 expression

As the qPCR experiments on cyclin mRNA levels were not able to conclusively prove VP24 alterations of cell cycle progression, we opted to carry out a western blot on p21, a cyclin-dependent kinase inhibitor that inhibits activity of cyclin-CDK complexes, resulting in cell cycle arrest. Our results show an increased expression level of p21 in both zVP24 and rVP24 samples compared to the mock, though zVP24 appeared to induce p21 to slightly greater levels than rVP24 [Figure 25]. The strong induction of p21 also appears in the positive control where cells were arrested by 500µM mimosine, a compound known to arrest cells in late G1 phase. Therefore, our results show that presence of VP24 increases intracellular levels of p21, likely leading to a cell cycle arrest at late G1. In addition, VP24 does not affect expression of cyclin E1 at the protein level, which was confirmed in figure 25.

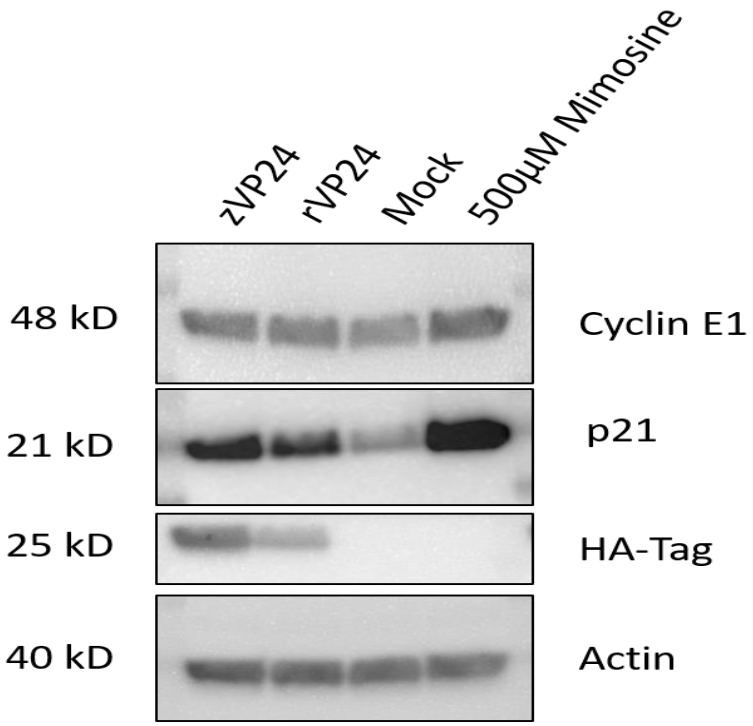

Figure 25. Western Blot for p21 expression levels
To investigate dysregulation of cell cycle, Hela cells were transfected with either HA-tagged zVP24, rVP24 or empty pCAGGS vector for 48 hours prior to lysis. To block cells in G1 arrest 500µM mimosine was added to cells to generate a positive control sample. Cells transfected with zVP24 and rVP24 show increased expression of p21, suggesting that VP24 is blocking the cell cycle at G1 phase whereas the mock represents p21 expression levels in an asynchronous cell population. N=3

5.3.4 VP24 expression leads to DNA Damage

In order to detect whether VP24 induces DNA damage that would then result in cell cycle arrest, we attempted to immunoblot against γH2AX, a biomarker for double-strand DNA breaks. HeLa cells were transfected with either HA-tagged zVP24, rVP24 or empty vector and incubated for 48 hours prior to lysis for western blot. We detected increased signal intensity for γH2AX in both zVP24 and rVP24, whereas the negative control showed a weaker signal, therefore showing us that VP24 is inducing double strand breaks in host cells, leading to overexpression of γH2AX [Figure 26].

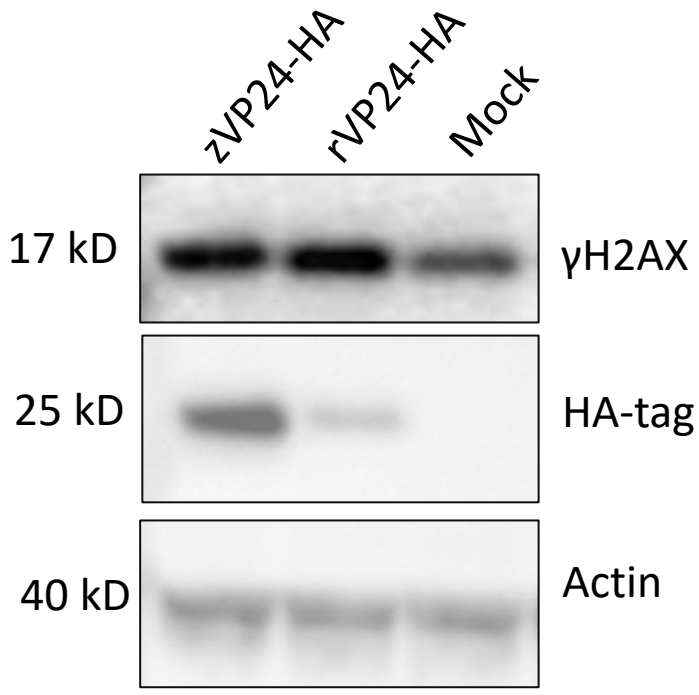

Figure 26. Western Blot for DNA double strand breaks biomarker γH2AX.

Double strand breaks of DNA damage lead to increased levels of γH2AX, a phosphorylated form of H2AX. To verify whether VP24 causes DNA damage, we transfected Hela cells for 48 hours prior to lysis with either zVP24, rVP24 and empty vector plasmid. Our immunoblot shows increased intensity of the γH2AX band compared to the mock control, suggesting that expression of zVP24 and rVP24 in cells lead to DNA damage.

5.4 Discussion

5.4.1 Cell Cycle Markers

We had initially thought that by screening the mRNA levels of the different cyclins would give us insight into what stage of the cell cycle that cells would be in after transfection with VP24. However, literature has shown that in certain circumstances their expression levels are not directly correlated with cell cycle phase; for example, rapamycin induced G1 arrest in B-CLL cells was associated with decreased expression of cyclin E1, whereas histone deacetylase inhibitor FR901228 induced G1 arrest with increased expression of cyclin E1 (Sandor *et al.*, 2000; Decker *et al.*, 2003). By taking this information into account, we still believe that qPCR of the different cyclins is important to examine in conjunction with Western blot analysis of protein expression [Figure 25]. In our experiments we can see that there is a non-statistically significant increase in Cyclin E1 mRNA but not protein expression in the presence of VP24. Based on our initial screening of interacting partners presented in the introduction section of this chapter, we decided to probe for markers for G1 arrest. p21, also known as WAF1/CIP1, is known to promote cell cycle arrest at G1 and G2/M stage by inhibiting the cyclin-CDK complexes from forming (Karimian, Ahmadi and Yousefi, 2016). Multiple viruses have been reported to induce cell cycle arrest associated with p21 overexpression, such as HIV-1 Vpr protein, arresting cells at G2/M stag (Chowdhury *et al.*, 2003). Furthermore, p21 has been shown to be overexpressed during activation of the DNA damage response, which then leads to cell cycle arrest (Karimian, Ahmadi and Yousefi, 2016). For these reasons we proceeded to blot for p21. The fact that p21 was overexpressed in both zVP24, rVP24 and the positive control suggests that VP24 may cause cell cycle arrest through modulation of p21 expression, further experiments need to be done to validate cell cycle arrest. The ideal experiment that should be carried out to ascertain the stage of cell cycle would be propidium iodide assay by flow cytometry. However,

during the time of this PhD project, we were unable to use the flow cytometer in the department. Whilst other chemicals and compounds can be used to induce G1 arrest such as thymidine by double blocking, we chose mimosine for its simplicity as it relies on a single treatment on cells and that it is G1 arrest specifically by p21 induction, which was detected by western blot in Figure 25.

5.4.2 Detecting DNA Damage

The overexpression of p21 had made us question the possibility of VP24 causing DNA damage in the cell. The localisation of VP24 in cells has predominantly been reported to be cytoplasmic, though a small minority of groups have reported nuclear localisation by immunofluorescence (F. He *et al.*, 2017). In our experience, we do not detect any nuclear localisation of VP24, therefore we believe that the DNA damage caused by the protein is independent of its subcellular localisation. The biomarker for double strand breaks of DNA is phosphorylation of histone H2AX. Its phosphorylation by several kinases such as ataxia telangiesctasia mutated (ATM) and ATM-Rad3 related (ATR) result in recruiting DNA repair proteins into the nucleus (Kuo and Yang, 2008). Many viruses have been reported to interfere with the DNA damage response of the host cell, including negative sense single strand RNA viruses such as Influenza A virus, Rift Valley fever virus and La Crosse virus (Ryan *et al.*, 2016). In the case of Rift Valley Fever virus, infection causes DNA damage via ATM kinase pathway. It was found that the subsequent cell cycle arrest stemming from the DNA damage was beneficial for viral replication (Baer *et al.*, 2012). Whether VP24 is inducing DNA damage for the benefit of viral replication is yet to be determined, however our data appears to be promising for future follow up work.

5.5 Conclusion

The results presented in this chapter, in tandem with the live cell imaging and MTS in chapter 3, would suggest that VP24 is interfering with the cell cycle by causing DNA damage, leading to detection of γH2AX and overexpression p21. Whether the cell cycle is being blocked at a specific checkpoint is impossible to say at this stage and due to time constraints, we were not able to investigate further. Nonetheless, here we find the first pieces of evidence that VP24 is negatively affecting the cells, which is displayed via components of the DNA damage response pathway and likely resulting in a block of the cell cycle at the G1 phase.

5.6 Future Work

The data gathered in the VP24 cytotoxicity chapter has given us a glimpse into how the protein is affecting the cell cycle and DNA damage response pathway. We find this very encouraging because to our knowledge, there is no literature focusing on *Ebolaviruses* and the DNA damage response pathway. Despite our data being preliminary with regards to the conclusion presented in Chapter 5, this thesis presents many experiments that returned negative results. We deem these results to be also of high value because it helps to remove possible biases and increase the validity of the positive results. For example, our MTS assay has shown a decrease in signal that was deemed to be statistically significant. Coupling the aforementioned results alongside the cell death pathways such as autophagic and apoptotic death which returned negative results gave us the impetus us to explore different avenues. This ultimately led us down the path of investigating cell cycle regulation and DNA damage, which we did not initially consider during this project. Ultimately, presenting scientific data that encompasses a mixture of negative and positive results helps to communicate a much broader overview of the project in question.

In terms of future work, we would primarily centre the focus around p21, as its overexpression can indicate cell cycle arrest, DNA damage response and suppression of apoptosis. Therefore, the first experiment would be to carry out flow cytometry experiments with propidium iodide to ascertain if and where the cell cycle arrest occurs and in which stage. Following this, further data to support the evidence of the flow cytometry result, such as immunoprecipitating the CDK-cyclin complexes, as p21 can inhibit their formation. This would yield strong evidence with regards to cell cycle arrest. Subsequent experiments would include western blotting for expression levels of p53, as this would verify whether VP24 is overexpressing p21 via p53 dependant or independent pathway, using suitable positive controls such as bleomycin, a drug that induces double strand breaks. We would also like to verify whether VP24 may localise in the nucleus to cause DNA damage, therefore carrying out a nuclear extraction treatment on VP24-transfected cells could give us more insight as to its localisation. It would greatly increase our understanding of VP24 if a

mutation in a particular residue or domain of the protein could be identified that would then abrogate the findings in this thesis. In this case we would attempt the same experiments using VP24 with mutations within the KPNA interacting domain, as this would tell us whether the phenotype we observed is dependent on these protein-protein interactions. Lastly and most importantly, experiments using either the transcription and replication-competent viral-like-particle (trVLP) system or engaging with collaborators that have access to category 4 biocontainment labs for live virus experiments would have to be carried out in order to complete the full story because ultimately, why would the virus block the cell cycle or engage the DNA damage response pathways? Is it to modify the host cell for optimal viral replication or is it a self-defence mechanism of the infection by the host? These questions would help us understand pathogenic mechanisms during EBOV infection, and by comparing between non-human and human pathogenic strains we could hopefully understand key differences that determine pathogenicity.

6 Structure Function of the Ebola Virus Delta Peptide

The Ebola virus delta-peptide is a viroporin, derived from proteolytic cleavage of sGP. Little is known about delta-peptide with regards to structure and function. Here, we decided to employ several different techniques to allow us to analyse the structure of delta peptide. We attempted to generate delta-peptide by recombinant methods using bacteria, which failed to generate the quantities required for suitable NMR methods. However, by purchasing synthetic delta-peptide in reduced form allowed us to attempt a unique type of crystallography called lipidic-cubic phase crystallography. This technique differs from traditional crystallography as it revolved around crystallisation in a lipid environment, a valuable technique for membrane bound proteins and peptides. We were successful in generating several crystals with different screening conditions, for both reduced and oxidised forms of the peptide. We hope to carry out X-ray scattering to derive a structure of the 23 amino acid c-terminus Zaire delta-peptide and 25 amino acid c-terminus of Reston delta-peptide. This would allow us to investigate how their structures might result in pore formation in membranes and whether there is a difference in cytotoxicity between the two species.

6.1 Introduction

The delta peptide of Ebolavirus is a small peptide produced during protein processing of sGP [Figure 28]. This occurs in the final stages of processing as the enzyme furin recognises a motif for cleavage on the C-terminus of sGP that results in mature sGP and delta peptide, both of which are secreted extracellularly (Volchkova, Klenk and Volchkov, 1999). The role of the delta-peptide is currently unknown, however bioinformatic analysis would suggest that it acts as a viroporin (J. He *et al.*, 2017). Viroporins are peptides or proteins that are involved in pathogenesis and viral replication, of which their characteristic feature is forming pores in lipid bilayers. These pores can have ion-channel activity, as seen with Influenza Virus M2, forming a tetrameric channel that conducts protons, and rotavirus NSP4, which increases intracellular calcium (Nieva, Madan and Carrasco, 2012). Viroporins are known to possess amphipathic helices, which are important for promoting insertion into membranes and forming pores when oligomerisation of multiple viroporins occurs. In terms of viral replication, viroporins can alter membrane properties, allowing for morphogenesis and budding, as seen with Influenza Virus M2 (Rossman and Lamb, 2011). Current literature on the delta-peptide is sparse. Since its discovery in 1999, only three studies have been completed. Whilst none have solved the structure of the delta-peptide, other properties have been investigated. Gallaher and Garry, 2015 conducted a bioinformatic analysis that modelled the structure of delta peptide from EBOV and RESTV. From their investigation, they identified a potential lytic activity of the peptide. He *et al.,* 2017 used a synthetic peptide to determine its pore forming capability and lytic properties. They showed that the delta-peptide is active in an oxidised state, suggesting that formation of the disulphide bond between the cysteines is important for pore formation and insertion. Pokhrel *et al.,* 2019 used molecular dynamics simulation to explore how oligomerisation states affect pore formation and activity. Their data suggests that hexameric pores can be formed that have high selectivity to chloride ions.

It is our intention to solve the structure of the 23-25 amino acid delta peptide fragment containing the suspected amphipathic structure of delta-peptide from both EBOV and RESTV, in oxidised and reduced states. We hope this structural determination would help shed more light on the function of the delta-peptide, its potential role in viral pathogenesis and show how the structure and function is affected by the disulphide bond formation [Figure 27].

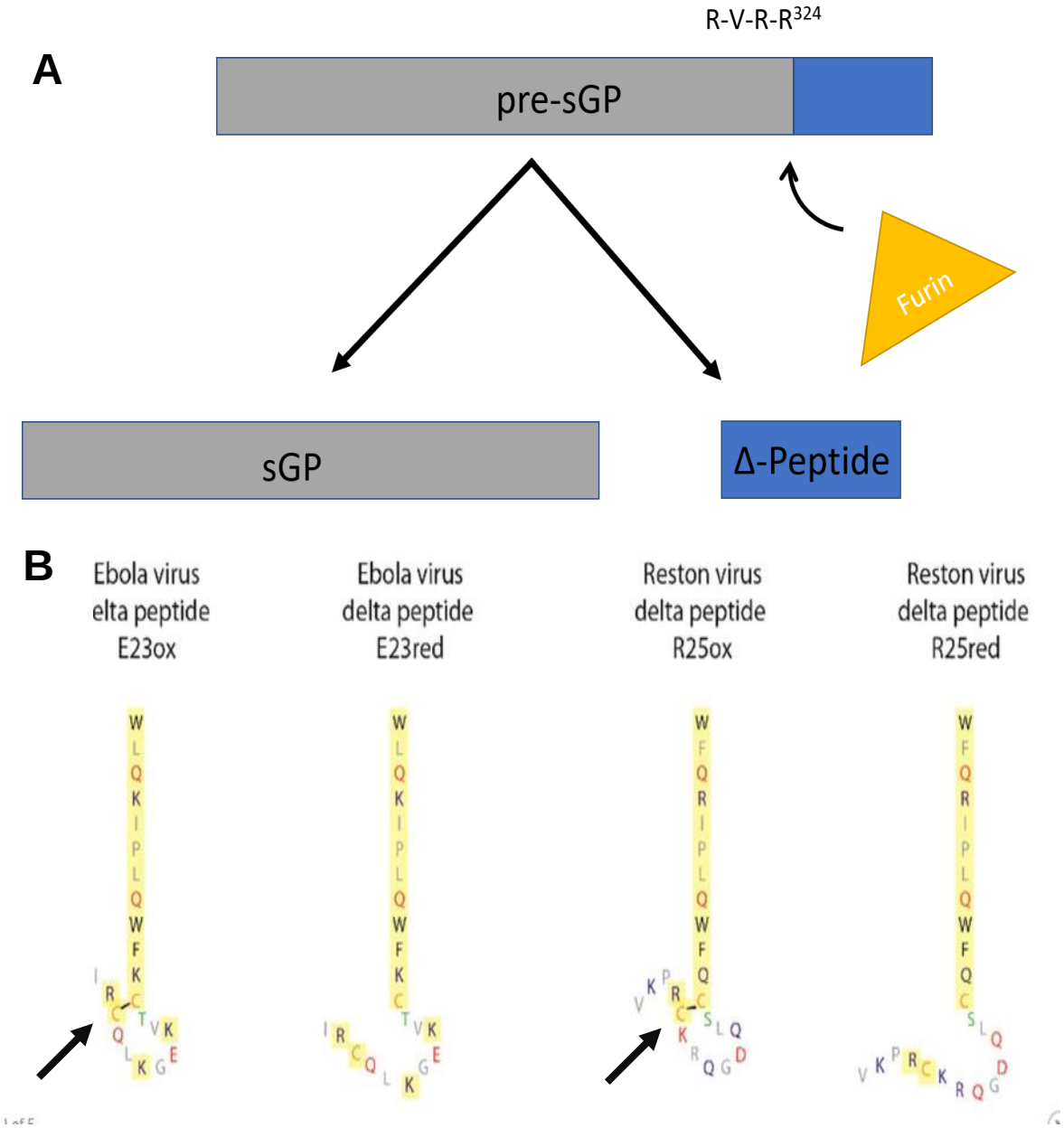

Figure 27. Ebolavirus Delta-Peptide is a product of sGP processing.

During expression of 7U GP gene, 80% of protein produced is sGP. This results in a furin-like cleavage site at position 324. Furin then cleaves the C-terminal end of sGP to yield a mature sGP protein and a ~40 amino acid Delta-Peptide (A). Delta-peptide from both EBOV and RESTV contain a region in their C-termini believed to form an amphipathic structure (B). It is hypothesized that this structure could occur by the formation of a disulphide hairpin loop between the cysteines. (Panel B adapted from He *et al.,* 2017.

6.2 Results

6.2.1 TOCSY and NOESY NMR Imaging

We first obtained chemically synthesised peptides corresponding to the last 23 C-terminal amino acid residues for EBOV and last 25 C-terminal amino acid residues for RESTV in their reduced form. Then, before starting to collect spectrums on all of the delta-peptides from EBOV and RESTV in their reduced and oxidised states, we decided to carry out a total correlation spectroscopy (TOCSY) and nuclear overhauser effect spectroscopy (NOESY) experiment on the reduced EBOV delta peptide as a proof of concept. Therefore, we resuspended EBOV delta-peptide in ddH_2O containing 20% acetic acid to a final concentration of 650µM and ran the experiments on the NMR machine. The spectra generated from the experiments show the peaks corresponding to the delta peptide, suggesting that this experiment is possible [Figure 28]. However, we would need to confirm whether the delta-peptide interacts only superficially with the membrane, which would allow for non-labelled NMR experiments, otherwise, in a situation whereby the peptide fully inserts into a membrane these NMR experiments will not detect the peptide.

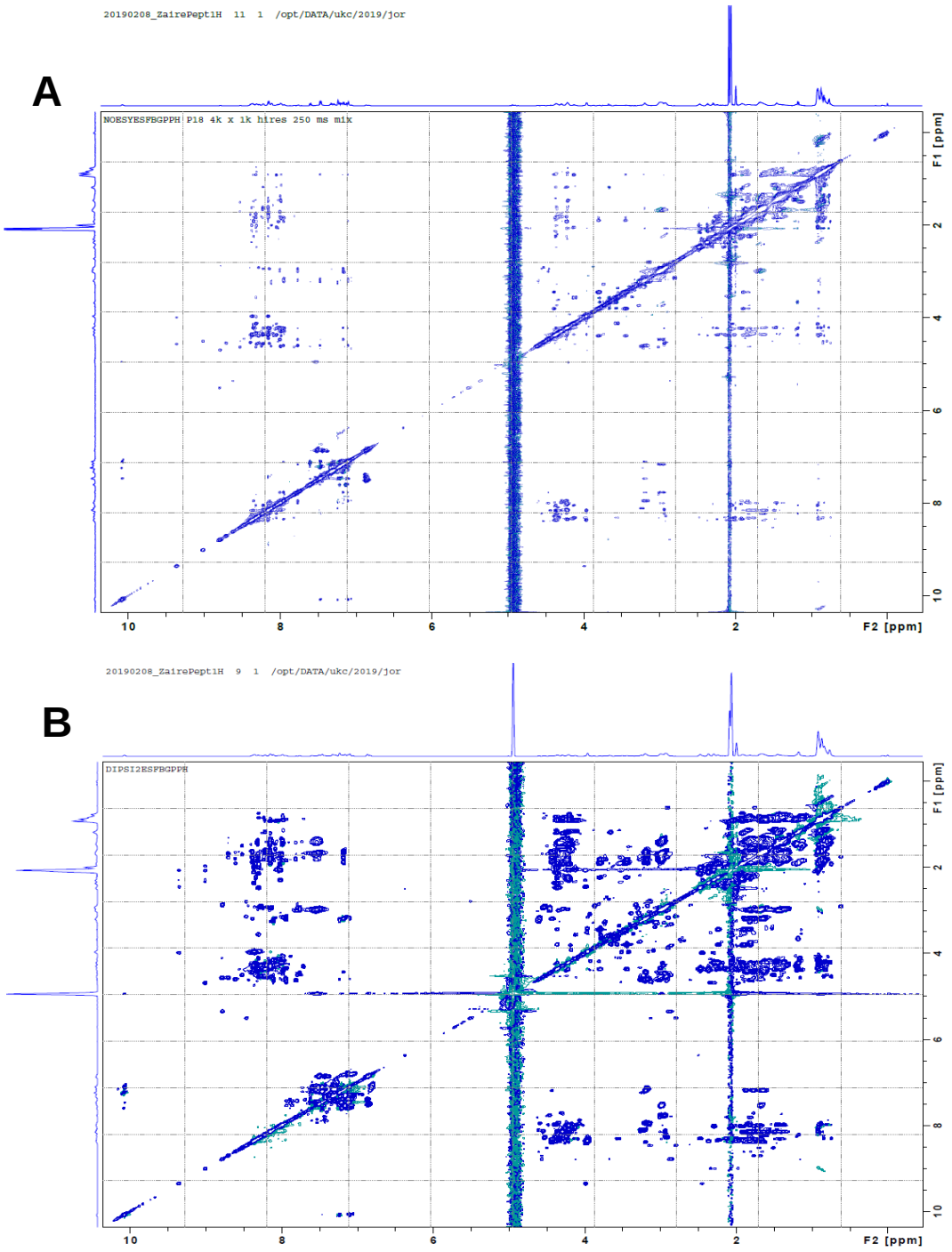

Figure 28. TOCSY and NOESY NMR Spectra of reduced EBOV Delta-Peptide

To confirm whether in-solution NMR experiments could be carried out, we attempted to generate TOCSY (A) and NOESY (B) spectra of the EBOV delta-peptide. Our spectra detected the delta-peptide, therefore these experiments can be carried out once we verify whether the peptide interacts superficially with membranes or whether it fully inserts.

6.2.2 Delta Peptide Membrane insertion

To assess whether the structure of the delta peptide C-termini can be observed by NMR we first screened for membrane interactions using Nile Red stained giant unilamellar vesicles. The principle of unlabelled NMR based structure studies is that if the interactions remain superficial rather than full membrane insertion then it would be possible to generate the required spectra as the signal from the peptide would not be blocked by the lipid environment. However, full membrane insertion would not permit proton-proton experiments by NMR due to the signal generated by the lipids which would mask the signal generated from the peptide. Therefore, by using confocal microscopy we can understand the type of interaction with greater detail. Current research suggest full membrane insertion which would then require the generation of recombinant peptide with ^{13}C and/or ^{15}N labelling. We opted to generate GUVs using asolectin lipids as they contain a mixture of phospholipids. The results show insertion into the membrane as the FITC-delta peptide signal was present throughout the entire membrane, overlapping the red signal from the lipid bound dye [Figure 29]. This confirms previous results suggesting full membrane insertion and suggests why channel formation may be why the delta peptide has lytic properties (J. He *et al.*, 2017). Due to this result, unlabelled NMR experiments would not be possible and so we endeavoured to generate recombinant labelled peptide for our NMR structural studies by using BL21 strain of *Escherichia coli*. For practical reasons, we opted to attempt this procedure using the EBOV delta peptide and, if successful, to follow up with RESTV delta peptide.

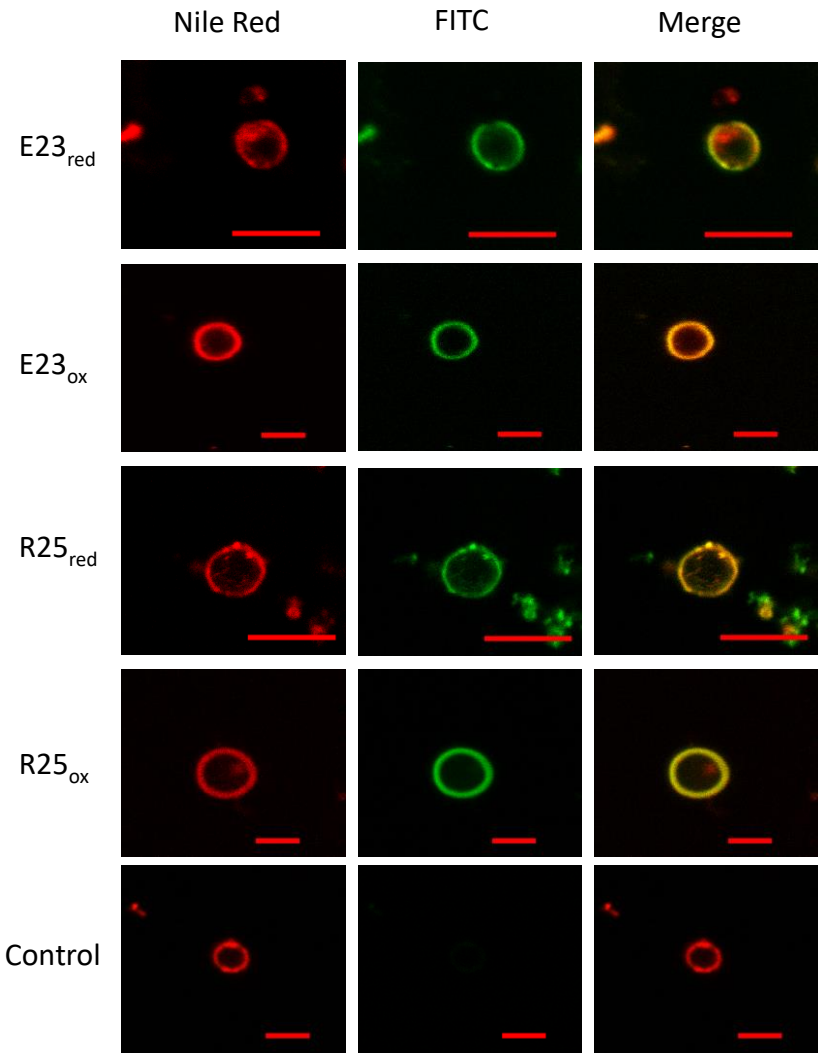

Figure 29. Peptide Membrane interactions using Asolectin Lipid GUVs. 20µM oxidised and reduced forms of FITC-labelled EBOV (E23) and RESTV (R25) delta peptides were incubated in the presence of Nile Red stained asolectin GUVs for 15 minutes prior to viewing on the confocal microscope. All forms of peptide colocalise with the GUV membranes which shows membrane insertion. This is consistent with previously published literature. Scale bars represent 5µm.

6.3 Recombinant Production of 23 amino acid C-terminus Delta Peptide

6.3.1 Gibson Assembly

We opted to use a pCold bacterial expression vector from Ortega-Roldan research group for recombinant peptide production, due to the cold expression properties that reduces protease activity after induction to produce peptide in bacteria. To remove the delta-peptide gene insert from the pUC57 vector into a pCold vector expressing 6x His tag, twin strep tag and GFP, Gibson assembly was carried out using the correct primers with overhangs. Two PCR reactions for amplifying our vector and construct were carried out, one for the pCold vector and one for the EBOV delta-peptide. The thermocycler settings used are presented in Figure 31. We subsequently used a PCR cleanup kit to remove contaminants. However, we found that after PCR cleanup we did not see any of the 72bp fragment encoding the delta peptide. This is likely due to a minimum bp retention size of the membrane present in the PCR cleanup centrifugation tubes. Therefore, we attempted the experiment again, omitting the PCR clean up step and ran the product on a 3% TAE agarose gel treated with treated with SYBR Green to visualise DNA bands on the UV transilluminator [Figure 30].

We detected a band around the 100bp marker for the sample that was not subjected to the PCR cleanup kit, therefore we decided to carry on the final steps of the Gibson assembly using that sample.

This involved mixing our amplified products in a 1:4 ratio between amplified vector and amplified fragment, to a total 0.25pmols of DNA, followed by mixing with 2X Gibson Assembly Mastermix and volumes were raised to 20µL per PCR tube using ddH_2O. The thermocycler settings were set to 50°C for 15 minutes as per manufacturer's protocol. After the reaction, the resulting DNA solution in the tube was used to transform competent cells to generate plasmid DNA that was sent off for sequence to Eurofins to confirm successful generation of the plasmid to be used for recombinant production [Figure 31C].

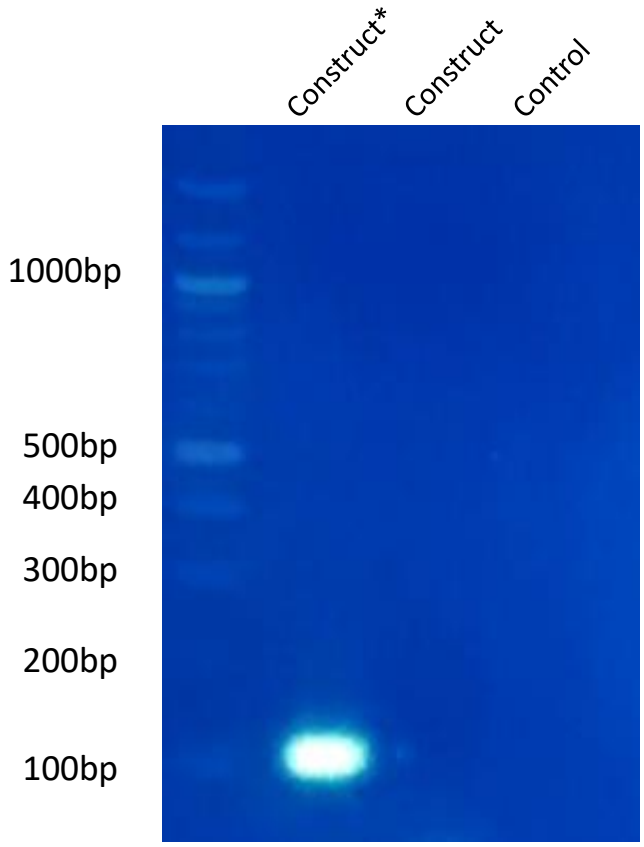

Figure 30. DNA Agarose Gel of delta-peptide PCR products
Delta-peptide PCR products were mixed with 6X loading dye and 5µL were run on a 3% TAE Agarose gel stained with SYBR Safe Green DNA stain. *denotes no PCR cleanup sample. Control sample was water mixed with 6X loading dye. We detected a band around the 100bp marker for our construct that was not subjected to the PCR cleanup kit.

A

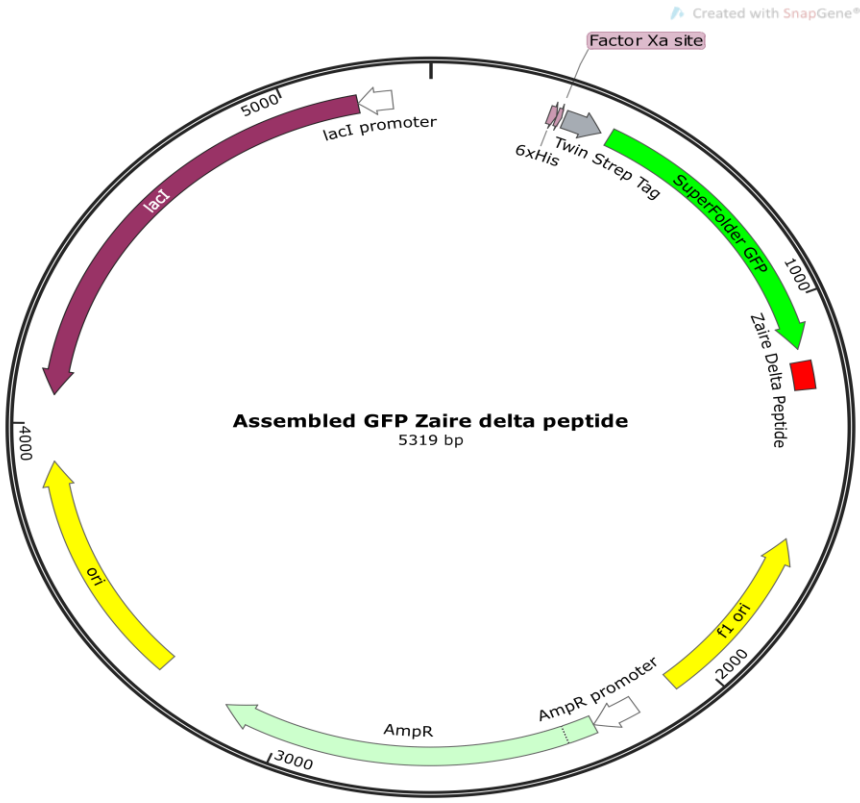

B

Condition 1: pCold Vector			Condition 2: Zaire Δ-peptide		
2 minutes	95°C		2 minutes	95°C	
45 seconds	95°C	30 Cycles	45 seconds	95°C	30 Cycles
30 seconds	55°C		30 seconds	55°C	
11 minutes	73°C		1 minutes	73°C	
5 minutes	73°C		5 minutes	73°C	
4°C Hold			4°C Hold		

C

```
Seq_1   1     GCaGGCTGGCTGCaAAAAATCCCGCTGCAGTGGTTCaAATGCACCGTCAAAGAGGGCAAA  60
              ||||||||||||||||||||||||||||||||||||||||||||||||||||||||||||
Seq_2   1     ------TGGCTGCAAAAAATCCCGCTGCAGTGGTTCAAATGCACCGTCAAAGAGGGCAAA  54

Seq_1   61    CTGCAGTGCCGTATCTAGTAAGGATCCGAATTCAAGCTTGTCGACCTGCAGTCTAGATAG  120
              ||||||||||||||||||
Seq_2   55    CTGCAGTGCCGTATCTAG------------------------------------------  72
```

Figure 31. Thermocycler Settings for Gibson Assembly
Construct Map of pCold vector expressing 6His-, twin-strep, GFP tagged EBOV Delta peptide (A).Conditions used to generate products for downstream Gibson assembly (B). The final product was sent for sequencing by Eurofins to verify successful assembly using custom primers from Jose Ortega-Roldan laboratory group (C). Sequences were aligned using SerialCloner software. Seq_1 denotes final product sequence. Seq_2 denotes the 72bp sequence for the 23aa C-terminus of EBOV Delta-Peptide.

6.3.2 Purification by Nickel Column

In order to produce pure GFP fused delta peptide, we first transformed BL21 competent *E. coli* with pCold zDelta-peptide plasmid. Protein expression was induced with IPTG at 15°C overnight followed by lysis through sonication and debris removal by ultracentrifugation. In order to purify the GFP fused delta peptide, a series of column purification techniques were used; starting with a nickel column. The lysates were added to the column and all follow-throughs during purification were collected as the capture of the desired protein is never 100% efficient, and therefore allowing us to re-run any flowthroughs that were visibly green in order to maximise efficiency of peptide production, as the green colour indicated presence of GFP tagged delta peptide. After ultra-centrifugation was carried out to remove any cell debris, the lysate was initially purified through a nickel column due to the presence of a histidine tag. Two washes were carried out using wash buffer containing 5mM imidazole to remove any non-specific bound proteins. After the 2 washes using 5 column volumes (CV) of wash buffer, the remaining bound proteins were eluted using 1CV of wash buffer containing 400mM imidazole, three times. Prior to starting the second step of purification by strep-tactin column to increase the purity of our sample for downstream application, we ran 10µL of lysates from each step on a tris-glycine gel and Coomassie stained to determine the purity of the samples [Figure 32]. We noticed that the elution portion of the purification still had many protein bands, suggesting that the purification has worked compared to the flowthrough sample, but not to optimum levels, as usually you would want to see a single band of your expressed protein. Following the result of the Coomassie stained gel, the elutions were subjected to a dialysis using a 7.5kD cutoff dialysis tubing. Dialysis was performed against 5 litres of lysis buffer overnight at 4°C using a 30kD cutoff dialysis tube in order to remove the imidazole present in the elution as this would interfere with the strep-tactin purification beads.

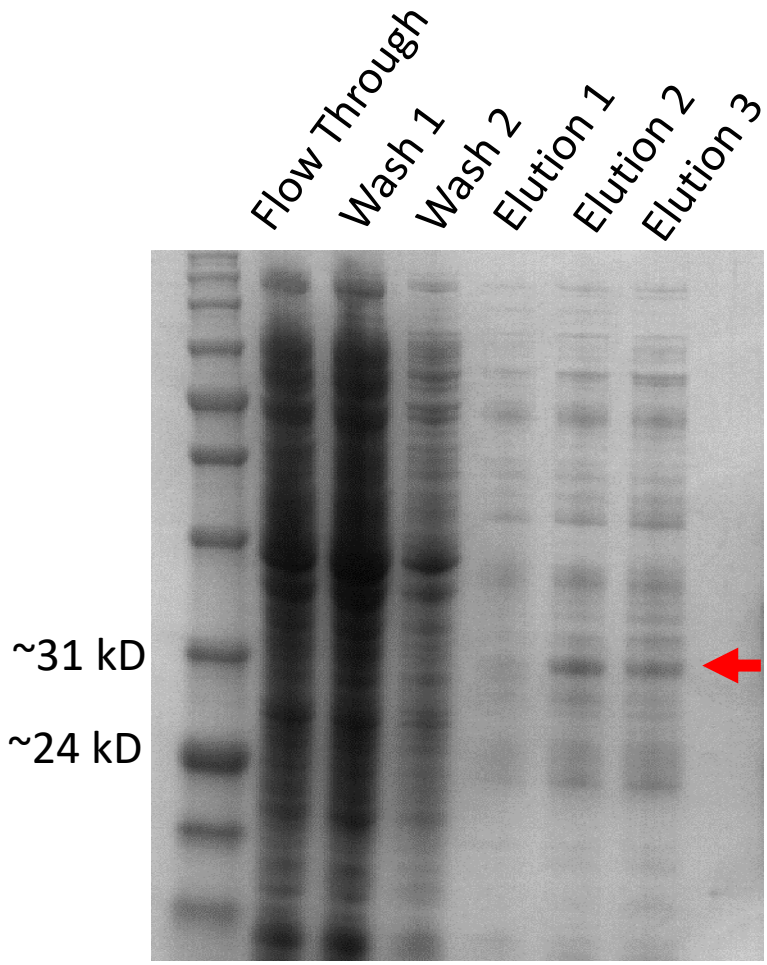

Figure 32. Nickel Column Purification of Delta Peptide
BL21 cells were transformed with pCold GFP delta peptide and induced with IPTG overnight prior to lysis and purification by nickel column. 10µL of samples collected at each stage of the purification were subjected to gel electrophoresis using SDS-PAGE Criterion™ TGX™ gels rated at AnyKD by the supplier (Biorad). Coomassie staining was carried out on the denaturing gel for four hours followed by overnight destaining at room temperature to assess purity. Most of the tagged peptide appeared in elution 2 and 3 but samples need further purification from background protein content due to the presence of multiple bands at different molecular weights in the elution lanes.

6.3.3 Strep-Tactin purification

To further purify the GFP-fused delta peptide we used a strep-tactin column as the construct expresses a twin strep tag. The column contained 5mL of packed beads, and was primed using the strep-tactin wash buffer prior to loading the lysate. Following the priming, the lysate eluted from the nickel column (elutions 2 and 3) was added to the column and washed using 10CV of wash buffer to remove any non-specific bound proteins. All flowthroughs were collected for analysis by Coomassie staining. To elute the bound GFP-fused peptide, 2.5mM of desthibiotin was added to the wash buffer and elution was carried out at 1CV in steps. Then, 10µL of elutions were subjected to gel electrophoresis using a tris-glycine gel and

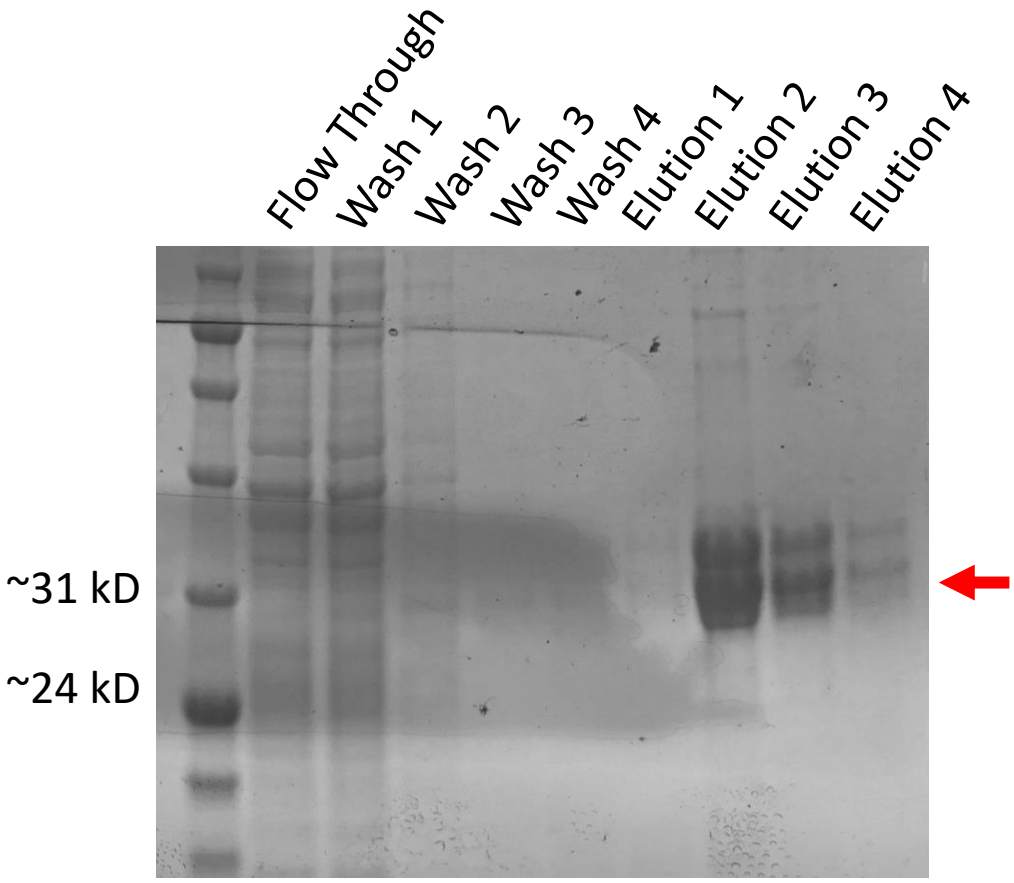

Figure 33. Strep-Tactin Purification of Delta Peptide
10µL samples were taken from each stage of strep-tactin purification and subjected to Coomassie staining on a denaturing gel to assess purity. Due to the purity of samples during elution 2 and 3 were used for TEV cleavage of peptide from the His-Strep-GFP tag. Red arrow points to the band containing the tagged delta peptide.

Coomassie stained to determine the purity [Figure 33]. We saw two bands in the elutions. We suspect that the lower band is likely due to autocleavage of the TEV site, possibly due to presence of proteases still in the sample.

6.3.4 TEV Cleavage

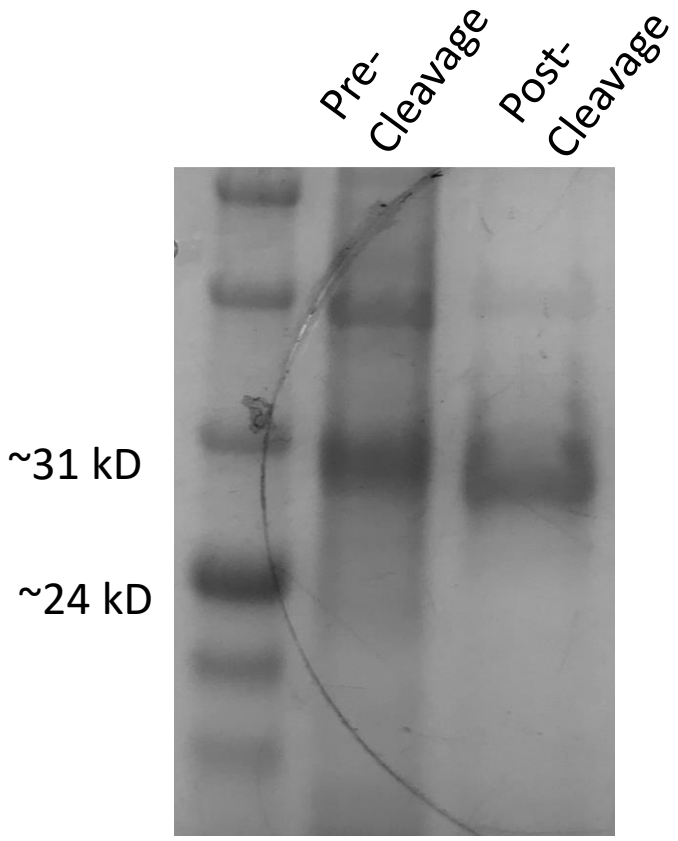

Figure 34. Confirming Cleavage from GFP tag using TEV enzyme
Purified lysate containing the GFP-tagged delta peptide was subjected to TEV cleavage overnight at 4°C. After incubating the sample in the presence of TEV enzyme, aliquots were subjected to Coomassie staining on a denaturing gel to assess a difference in the height of the bands. We also attempted to detect the delta-peptide however no signal was seen on the gel at 3kD.

In order to purify untagged delta peptide, the GFP tag needed to be removed, this could be performed though TEV cleavage at a site separating the GFP tag from the delta peptide. Therefore, we placed the elution in a 1kDa cutoff dialysis tubing containing lysis buffer containing 1mM EDTA, TEV enzyme and 1M DTT, at pH8.

Dialysis was performed at 4°C overnight. The pH was chosen to be specifically high because when resuspending the synthetic delta-peptide we noticed that it was insoluble in water, and by adding 30% acetic acid, we successfully solubilised the peptide. We noticed that post dialysis there was a substantial amount of precipitate. We removed the green lysate solution, spun down the samples at 17,000G on a tabletop centrifuge for 15 minutes and resuspended the precipitate in 30% acetic acid at pH5 which caused the pellet to solubilise. In order to detected whether the delta-peptide was present at this point we subjected 0.5µL of resuspension to MALDI-TOF mass spectrometry analysis, against the solution remaining the dialysis tubing. We found that the peptide was indeed present in the solubilised pellet, and that none was present in the solution that was remaining in the dialysis tubing. As we have now confirmed the presence of the GFP cleaved delta peptide, the solubilised sample was run through a HPLC column.

6.3.5 HPLC purification

The last step to purify the peptide to a high purity, reverse phase HPLC using a was used whereby a gradient of solvent A (10% TFA in ddH_2O) and B (1% TFA in acetonitrile) was subjected to the column containing the sample at a flow rate of 4.5mL per second. Elutions were collected when the UV graph recorded a peak signal intensity, at 35 minutes. Elutions were also collected at minutes 36, 37 and 38, as according to the elution profile, there was still presence of peptide [Figure 35]. Elutions were mixed into one tube and were lyophilised and resuspended in 30% acetic acid. The next step would be to verify that the fully cleaved 23aa peptide was present. This was done by MALDI-TOF mass spectrometry.

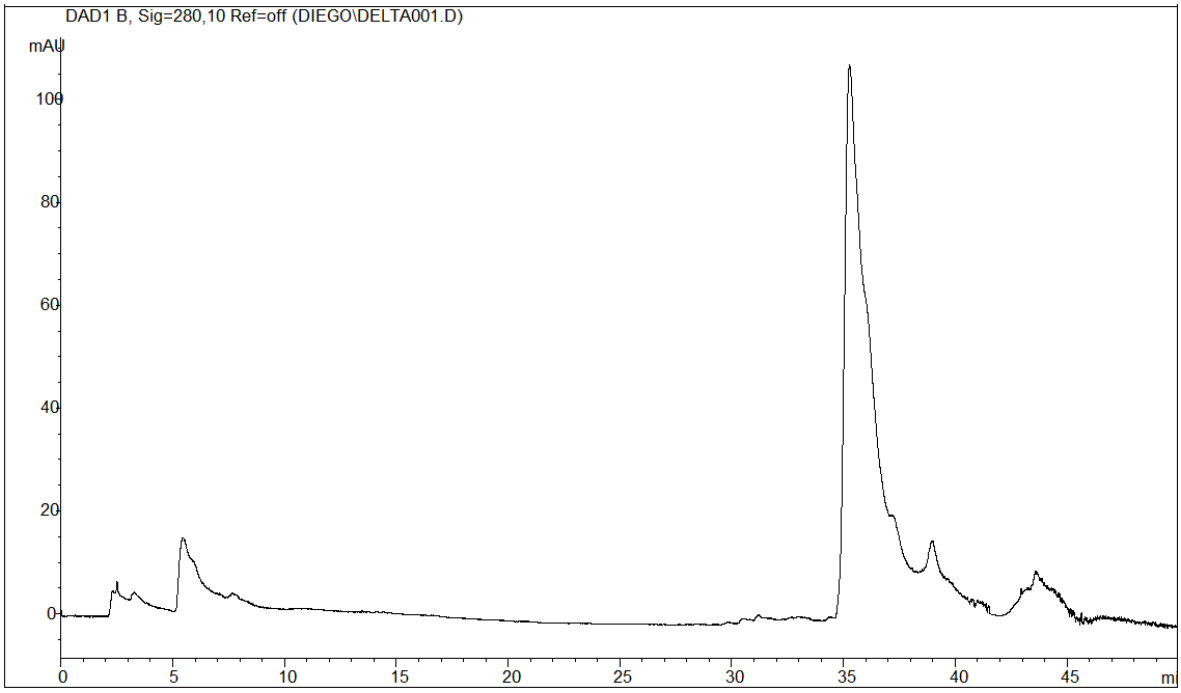

Figure 35. HPLC Elution graph of EBOV Delta Peptide
Reverse phase HPLC was carried out to purify EBOV delta peptide. The elution profile taken at 280nm wavelength reveals peak elution of peptide at 35 minutes. The wavelength of 280nm detects aromatic compounds. The 23aa Zaire EBOV Peptide contains 3 amino acids with aromatic rings; 1 phenylalanine, 2 tryptophans and 1 histidine.

6.3.6 MALDI-TOF

After HPLC purification we verified that the peptide was present. The HPLC purified peptide sample was diluted 100x by using 1µL sample in 99µL TA solution, and 0.5µL spotted onto the sample grid. Once the sample has dried on the anchorplate we added 0.5µL of matrix solution onto the dried spot containing the peptide. Then a calibration mix was added to an adjacent spot to calibrate the MALDI-TOF experiments for peptide detection around 300-3500MW. Using a 10% laser power, the MALDI-TOF was calibrated to detect peptides by firing the laser at the calibration spot, followed by firing the laser at our peptide samples that were eluted from the HPLC and in the supernatant after TEV cleavage [Figure 36]. The spectra obtained

from the supernatant after TEV cleavage showed no peptide was present, whereas the pellet from TEV cleavage that was resolubilised in 30% acetic acid and HPLC purified showed a small peak at molecular weight 3030.610, which corresponds to our peptide. The peptide peak was small, which could indicate that not much peptide was generated using our current experimental methods for recombinant peptide expression.

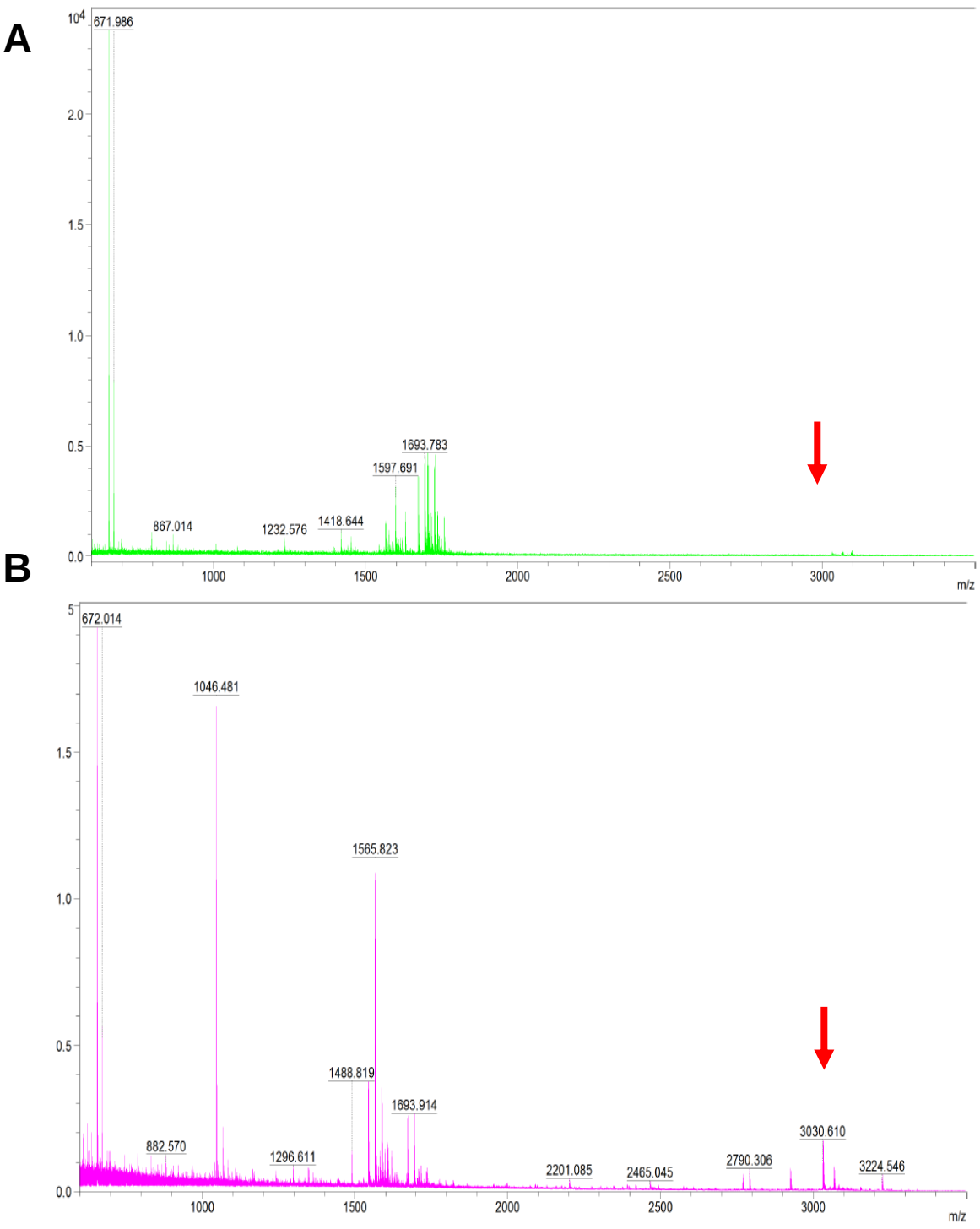

Figure 36. MALDI-TOF analysis of peptide expression.
The final step to verify production of the EBOV delta peptide was by using MALDI-TOF mass spectrometry. Post-TEV cleavage supernatant does not show the peak corresponding to the delta-peptide (A). However, the pellet that was resuspended in acetic acid and purified by HPLC showed a peak at molecular mass 3030.214 Daltons. This mass corresponds to the delta-peptide including 3 amino acids in the N-terminus that linked the peptide to the TEV cleavage site (B).

6.4 Discussion

We had initially planned to carry out in-solution NMR to determine the structure of the delta-peptide. The type of experiments for this would have been proton-proton experiments such as total correlation spectroscopy (TOCSY) and nuclear overhauser effect spectroscopy (NOESY). These experiments are based on the principle of determining signal from protons that are in close proximity to each other. However, proton signals stemming from the lipid membranes would mask signals generated from the protons in the synthetic peptide. prior to NMR structural studies we deemed it was important to determine whether the peptide interacts with the surface or fully inserts into the lipid bilayer. It was for this reason that we initially screened for insertion using GUVs and FITC-tagged delta-peptide. Due to the results of the GUV peptide assay, it was clear that to be able to carry out structural studies of the delta peptide, it would have to be made recombinantly. We chose to use the pCold vector expressing a GFP fusion tag because having the peptide alone, which was proposed to be lytic, may become toxic to the BL21 cells when protein expression was induced, as this had been observed before with other lytic peptides during recombinant peptide production (Li, 2011). It is also of benefit to have used a GFP tag as during cell lysis by sonication, we could see a strong green coloured lysate, indicating successful protein expression. Furthermore, the pCold vector was chosen as induction of protein production occurs at low temperatures of 15°C, where host protease activity remains low, therefore greatly reducing the likelihood of proteolytic degradation. The version of the pCold vector obtained for these experiments also contained a x6 histidine tag and twin-strep tag. This allows for two rounds of different affinity chromatography techniques. Using a nickel bead purification column, we were able to greatly reduce the amount of background protein content in our lysates as nickel has affinity towards polyhistidine tags, reported to enrich samples up to100 fold in a single step (Bornhorst and Falke, 2000). Subsequently, using a strep-tactin immobilisation column that binds with high affinity to strep tags, we were able to purify our sample to only contain our GFP fused peptide to high purity. The reason for two rounds of purification was largely due to

the next step in peptide production which was using the TEV enzyme to cleave the GFP-fusion tag off the peptide. It was at this stage where we encountered difficulty. We had noticed that after cleavage, a substantial insoluble precipitate was present in the solution. We had originally thought this was due to trace impurities precipitating after cleavage. Our initial rounds of purification did not yield any peptide that was detectable by MALDI-TOF. However, after repeating the experiment, we subjected the TEV cleaved sample to centrifugation at >17,000 G to pellet all the precipitate, which was resolubilised by using 30% acetic acid at pH 5. It was this step that ultimately led to detectable levels of peptide by MALDI-TOF. We believe the precipitation occurred due to the basic pH of the buffer at which TEV cleavage was carried out, as we had noticed during resuspension of the synthetic peptide for our GUV experiments that without maintaining a pH lower that 6, the peptide would not dissolve in solution. This highlighted the importance of buffer composition for peptide production, as the conditions can greatly affect solubility. However, after we purified the resuspended pellet by HPLC, the samples were analysed by tris-glycine SDS-PAGE to verify the presence of delta-peptide at roughly 3kD. Unfortunately we were not able to detect a band by Coomassie staining. Therefore, we quantified the concentration of peptide by spectophotometry, which was reported to be 65µM in a volume of 500µL. This meant that the production of this peptide requires large amounts of optimisation, such as pH ranges of buffers, different strains of bacterial cells, to produce 1mg/mL of peptide required for NMR studies, which was not possible due to time constraints of the PhD program. If there was more time to complete this project, we would start by optimising buffer pH's, in particular during the TEV cleavage as the peptide crashed out when the pH was high. Otherwise, using a different expression vector containing fusion tags that enhance solubility such as glutathione-S-transferase (GST) or maltose-binding protein (MBP).

6.5 Lipidic Cubic Phase Crystallography

6.5.1 Introduction

Lipidic cubic phase (LCP) crystallography is a technique that was developed to generate crystal structures of membrane proteins. Since membrane bound proteins possess both hydrophobic transmembrane domains and hydrophilic surfaces protruding from membranes, crystallisation in aqueous solutions has found to be very challenging since the hydrophobic domains rapidly aggregate to amorphous structures (Rummel *et al.*, 1998). Whereas LCP provides a microenvironment that membrane bound proteins are more accustomed to, due to the presence of detergents, aqueous solutions and lipids. There are several lipid polymorphisms, as they may aggregate into membranes, liposomes, micelles for example (Luzzati and Tardieu, 1974). These different structures are referred to as phases, and the phase used for this particular type of crystallography is the cubic phase. This is because this phase possess properties that are favourable for protein crystallisation; they are macroscopically stable, solid and fully transparent materials (Landau *et al.*, 1996). Owing to these properties, membrane proteins can be incorporated to these matrices. We decided that due to these properties, we could attempt to crystallise our delta-peptides using LCP crystallography.

6.5.2 Results

Due to reagent limitations, we decided to initially screen for the 25 amino acid RESTV delta-peptide in reduced form. Using commercially bought screens with 96 different conditions, we screen two 96-well plates by mixing 30µL monoolein lipid with 10µL of peptide dissolved in 15% acetic acid to 20mg/ml. A Mosquito® Robot was used to pipette the lipid:peptide mixtures onto plates containing the commercially bought screens. After two weeks of incubation at 18°C, we detected four conditions that favoured crystal formation on one plate (MemGoldMeso™) [Figure 37] and three conditions on the other plate (MemGold2™)[Figure 38].

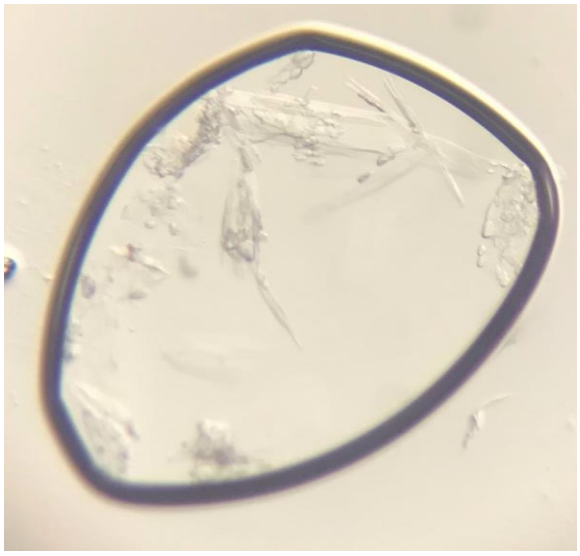

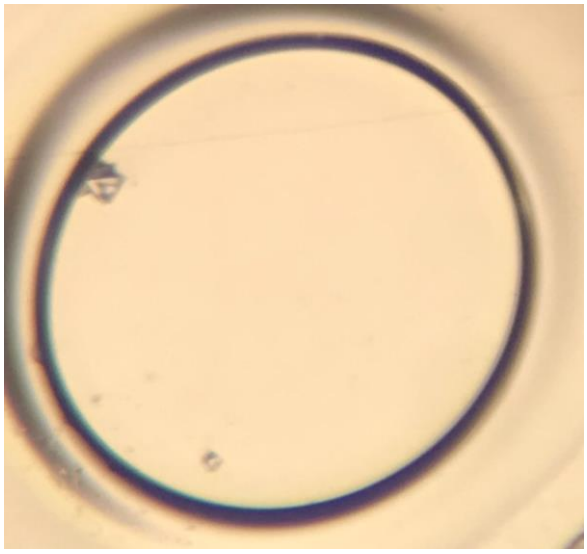

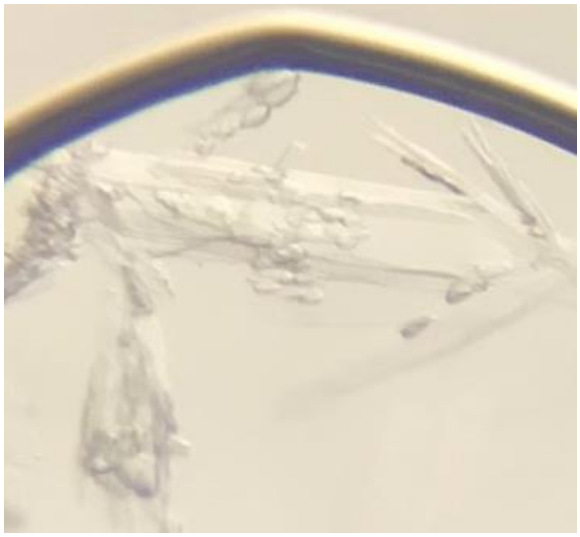

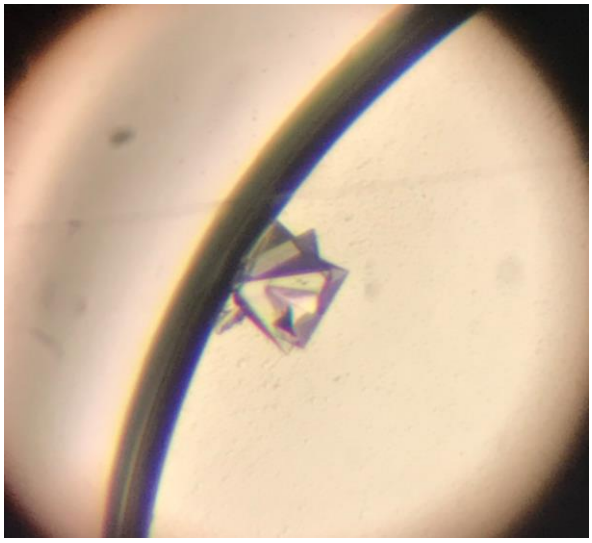

0.2M Lithitum sulfate
0.1M Phosphate/Citrate pH4.2
10% w/v PEG 1000

0.1M Sodium acetate Trihydrate
0.1M Ammonium Fluoride
0.1M MES Monohydrate pH 6
30% v/v PEG 500 DME

Figure continues on next page

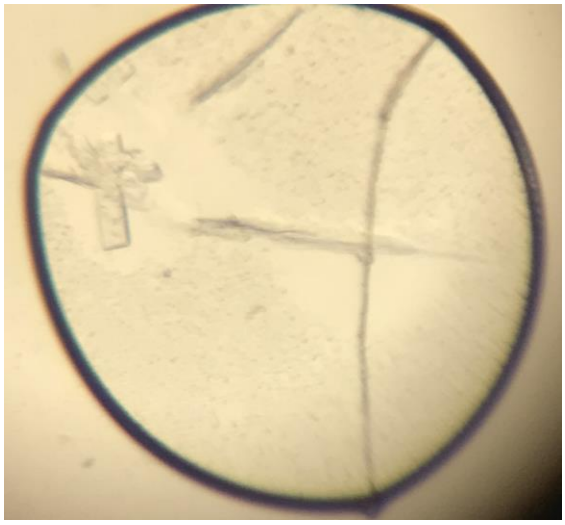

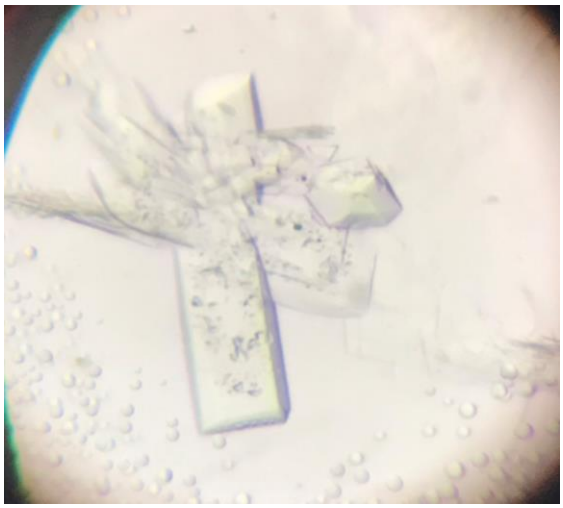

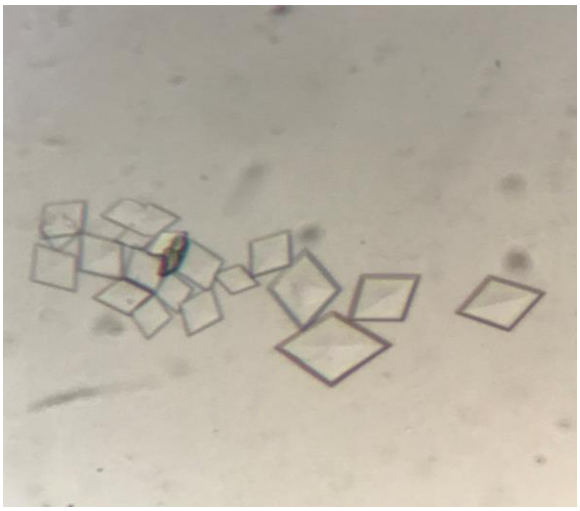

0.35M Magnesium Chloride Hexahydrate

0.15M Sodium Malonate Dibasic Monohydrate

0.1M HEPES pH 7.5

33% v/v PEG 400

0.3M Lithium Sulfate

0.1M HEPES pH 7

35% v/v PEG 400

Figure 37. LCP crystallisation for $R25_{red}$ Delta Peptide with MemGoldMeso™ Screen

30µl monoolein lipid was mixed with 10µL of peptide dissolved in 15% acetic acid and mixed with 96 different conditions from a MemGoldMeso™ screen plate for peptide crystallisation. Plates were monitored once a week for crystal formation under a light microscope. We found four conditions that favoured crystal formation from the MemGoldMeso™ screen. Crystals formed inside the bolus, increasing the likelihood that crystals are not salt precipitates

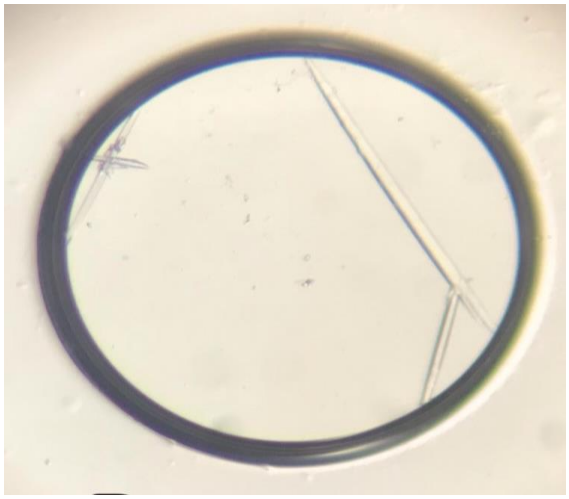

0.1M Sodium Chloride

0.1M BICINE pH 9

45% v/v PEG 500 MME

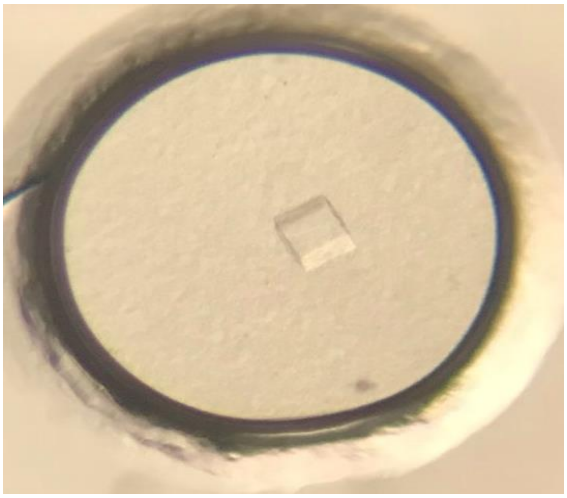

0.4M Potassium Chloride

0.05M HEPES pH 7.5

12% v/v PEG 400

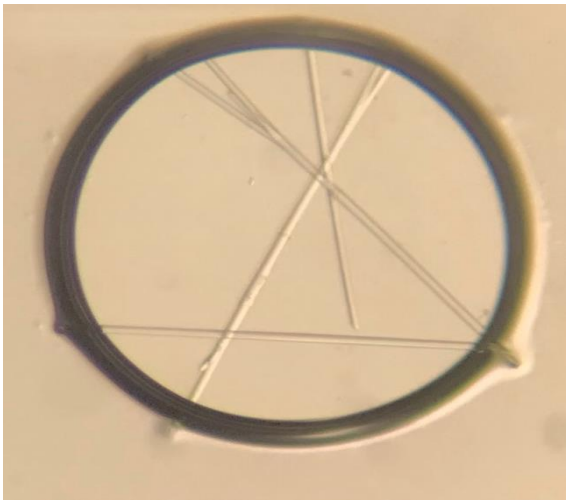

0.1M BICINE pH 9

30% v/v PEG 400

Figure 38. LCP crystallisation for $R25_{red}$ Delta Peptide with MemGold2™ Screen

30µL monoolein lipid was mixed with 10µL of peptide dissolved in 15% acetic acid and mixed with 96 different conditions from a MemGold2™ screen plate for peptide crystallisation. Plates were monitored once a week for crystal formation under a light microscope. We found four conditions that favoured crystal formation from the MemGoldMeso™ screen. Crystals formed inside the bolus, increasing the likelihood that crystals are not salt precipitates.

6.5.3 Discussion

Due to success of crystal formation, the next stage would be to extract a structure of the peptide using X-ray diffraction. However, during crystallography, formation of salt crystals may occur. To differentiate the crystals between peptide or salts, we could employ several techniques. For example, polarisation lenses on microscopes can be used to check the birefringent properties of the crystals. Salts exhibit more birefringence than that of macromolecular crystals. However, our microscope does not possess a set of polarising planes. Therefore, our current plan would be to carry out X-ray diffraction on all of the crystals at Diamond Light Source, located at Harwell Science and Innovation Campus in Oxfordshire. Hopefully, these crystals will lead to the successful LCP crystallisation of the delta-peptide.

6.6 Future Work

Within the final 6 months of the project, our attempt to produce the 23aa C-terminal domain of the EBOV delta peptide was not completely successful. This is because recombinant peptide production has been reported to be fairly challenging. Despite this, we have attempted to crystallise our synthetic peptide using LCP crystallography. Due to detection of crystals, we hope to carry out x-ray diffraction experiments within a few months of submitting this thesis. If the crystals are indeed the delta-peptide, we will be able to generate a structure. Having the structure of the EBOV delta-peptide would allow us to understand how it inserts into membranes, which residues make contact to allow anchorage through the transmembrane, whether the shape of the peptide allows for ion channel activity. Furthermore, repeating the experiment with RESTV oxidised delta peptide as well as EBOV delta peptide, both in reduced and oxidised form, would allow us to compare between the non-human pathogenic species of *Ebolavirus* against the highly pathogenic Zaire Ebola virus species, which may give us insight towards the pathogenic determinants between the two species.

7 Concluding Remarks

Ebolaviruses in Africa have repeatedly demonstrated their lethality through multiple recorded outbreaks, in contrast to the species found out of Africa which have never shown human pathogenicity. The race to understand the mechanisms behind infection, replication and pathogenicity has yielded a promising vaccine candidate. However, a vast expanse of knowledge is yet to be uncovered, as more filoviruses are being discovered around the world, ever increasing the members of the filoviridae, of which several members such as Reston virus and the newly discovered Bombali virus are non-pathogenic in humans. The thought that there are non-human pathogenic filoviruses, that often come into contact with humans due to the proximity of wildlife and local populations, is of increased interest. To date, nobody knows whether there is a simple mechanism that underpins the non-human pathogenic phenotype or whether it is due to a multitude of small differences between the strains that would make it so. Furthermore, the thought of non-pathogenic members of *Ebolavirus* genus becoming pathogenic due to mutations is terrifying, as the countries that they have been isolated in such as Philippines, has a very high density of human population. Throughout the course of this PhD we often compared and contrasted VP24 and delta-peptide between the human pathogenic Ebola virus and Reston virus, with the hopes to identify any difference within their interactions with the host cells or at a structural level. It would appear that for now, we can conclude that our experiments so far have not revealed any differences. To conclude, we are pleased to have revealed signs of a new mechanism of VP24 within host cells; modulation of cell cycle components. We also hope to solve the structures of all forms of the catalytically active C-termini of the delta-peptides, to shed light on structure function properties of these viroporins.

8 References

Adegbola, O. and Pasternack, G. R. (2005) ‘Phosphorylated retinoblastoma protein complexes with pp32 and inhibits pp32-mediated apoptosis.’, *The Journal of biological chemistry*. American Society for Biochemistry and Molecular Biology, 280(16), pp. 15497–502. doi: 10.1074/jbc.M411382200.

Alazard-Dany, N. *et al.* (2006) ‘Ebola virus glycoprotein GP is not cytotoxic when expressed constitutively at a moderate level’, *Journal of General Virology*, 87(5), pp. 1247–1257. doi: 10.1099/vir.0.81361-0.

Aleksandrowicz, P. *et al.* (2011) ‘Ebola Virus Enters Host Cells by Macropinocytosis and Clathrin-Mediated Endocytosis’, *The Journal of Infectious Diseases*. Oxford University Press, 204(suppl_3), pp. S957–S967. doi: 10.1093/infdis/jir326.

Alexander, K. A. *et al.* (2015) ‘What factors might have led to the emergence of ebola in West Africa?’, *PLoS Neglected Tropical Diseases*. doi: 10.1371/journal.pntd.0003652.

Alvarez, C. P. *et al.* (2002) ‘C-Type Lectins DC-SIGN and L-SIGN Mediate Cellular Entry by Ebola Virus in cis and in trans’, *Journal of Virology*. doi: 10.1128/JVI.76.13.6841-6844.2002.

Antico Arciuch, V. G. *et al.* (2012) ‘Mitochondrial regulation of cell cycle and proliferation.’, *Antioxidants & redox signaling*. Mary Ann Liebert, Inc., 16(10), pp. 1150–80. doi: 10.1089/ars.2011.4085.

Baer, A. *et al.* (2012) ‘Induction of DNA damage signaling upon Rift Valley fever virus infection results in cell cycle arrest and increased viral replication.’, *The Journal of biological chemistry*. American Society for Biochemistry and Molecular Biology, 287(10), pp. 7399–410. doi: 10.1074/jbc.M111.296608.

Baize, S. *et al.* (2014) ‘Emergence of Zaire Ebola Virus Disease in Guinea’, *New England Journal of Medicine*. Massachusetts Medical Society, 371(15), pp. 1418–1425. doi: 10.1056/NEJMoa1404505.

Banadyga, L. *et al.* (2017) ‘Ebola virus VP24 interacts with NP to facilitate nucleocapsid assembly and genome packaging’, *Scientific Reports*. Springer US, 7(1), pp. 1–14. doi: 10.1038/s41598-017-08167-8.

Barrette, R. W. *et al.* (2009) ‘Discovery of swine as a host for the Reston ebolavirus.’, *Science (New York, N.Y.)*, 325(5937), pp. 204–206. doi: 10.1126/science.1172705.
Baseler, L. *et al.* (2017) ‘The Pathogenesis of Ebola Virus Disease’, *Annual Review of Pathology: Mechanisms of Disease*, 12(1), pp. 387–418. doi: 10.1146/annurev-pathol-052016-100506.
Basler, C. F. *et al.* (2000) ‘The Ebola virus VP35 protein functions as a type I IFN antagonist.’, *Proceedings of the National Academy of Sciences of the United States of America*, 97(22), pp. 12289–12294. doi: 10.1073/pnas.220398297.
Basler, C. F. *et al.* (2003) ‘The Ebola virus VP35 protein inhibits activation of interferon regulatory factor 3.’, *Journal of virology*, 77(14), pp. 7945–56. doi: 10.1128/JVI.77.14.7945.
Batra, J. *et al.* (2018) ‘Protein Interaction Mapping Identifies RBBP6 as a Negative Regulator of Ebola Virus Replication’, *Cell*. Cell Press, 175(7), pp. 1917-1930.e13. doi: 10.1016/J.CELL.2018.08.044.
Beale, R. *et al.* (2014) ‘A LC3-Interacting Motif in the Influenza A Virus M2 Protein Is Required to Subvert Autophagy and Maintain Virion Stability’, *Cell Host & Microbe*. Cell Press, 15(2), pp. 239–247. doi: 10.1016/J.CHOM.2014.01.006.
Beniac, D. R. *et al.* (2012) ‘The organisation of Ebola virus reveals a capacity for extensive, modular polyploidy’, *PLoS ONE*. Edited by M.-S. Park. Lippincott Williams and Wilkins, 7(1), p. e29608. doi: 10.1371/journal.pone.0029608.
Bente, D. *et al.* (2009) ‘Disease modeling for Ebola and Marburg viruses’, *Disease Models & Mechanisms*, 2, pp. 12–17. doi: 10.1242/dmm.000471.
Biedenkopf, N. *et al.* (2013) ‘Phosphorylation of ebola virus VP30 influences the composition of the viral nucleocapsid complex: Impact on viral transcription and replication’, *Journal of Biological Chemistry*. doi: 10.1074/jbc.M113.461285.
Biedenkopf, N. *et al.* (2016) ‘RNA-binding of Ebola virus VP30 is essential for activating viral transcription.’, *Journal of virology*, 90(16), pp. 7481–7496. doi: 10.1128/JVI.00271-16.
Biedenkopf, N. *et al.* (2017) ‘The natural compound silvestrol is a potent inhibitor of Ebola virus replication’, *Antiviral Research*, 137, pp. 76–81. doi: 10.1016/j.antiviral.2016.11.011.

Biedenkopf, N., Lier, C. and Becker, S. (2016) ‘Dynamic Phosphorylation of VP30 is essential for Ebola virus life cycle’, *Journal of Virology*, 90(March), p. JVI.03257-15. doi: 10.1128/JVI.03257-15.

Bleazard, W. *et al.* (1999) ‘The dynamin-related GTPase Dnm1 regulates mitochondrial fission in yeast’, *Nature Cell Biology*. Nature Publishing Group, 1(5), pp. 298–304. doi: 10.1038/13014.

Boehmann, Y. *et al.* (2005) ‘A reconstituted replication and transcription system for Ebola virus Reston and comparison with Ebola virus Zaire’, *Virology*, 332(1), pp. 406–417. doi: 10.1016/j.virol.2004.11.018.

Bornholdt, Z. A. *et al.* (2013) ‘Structural rearrangement of ebola virus vp40 begets multiple functions in the virus life cycle’, *Cell*, 154(4), pp. 763–774. doi: 10.1016/j.cell.2013.07.015.

Bornhorst, J. A. and Falke, J. J. (2000) ‘Purification of proteins using polyhistidine affinity tags.’, *Methods in enzymology*. NIH Public Access, 326, pp. 245–54. doi: 10.1016/s0076-6879(00)26058-8.

Brannan, J. M. *et al.* (2015) ‘Interferon alpha/beta Receptor-Deficient Mice as a Model for Ebola Virus Disease.’, *The Journal of infectious diseases*, 212 Suppl, pp. S282-94. doi: 10.1093/infdis/jiv215.

Brauburger, K. *et al.* (2014) ‘Analysis of the highly diverse gene borders in Ebola virus reveals a distinct mechanism of transcriptional regulation.’, *Journal of virology*, 88(21), pp. 12558–71. doi: 10.1128/JVI.01863-14.

Bray, M. and Geisbert, T. W. (2005) ‘Ebola virus: The role of macrophages and dendritic cells in the pathogenesis of Ebola hemorrhagic fever’, *The International Journal of Biochemistry & Cell Biology*. Pergamon, 37(8), pp. 1560–1566. doi: 10.1016/J.BIOCEL.2005.02.018.

Brinkmann, C. *et al.* (2016) ‘The Tetherin Antagonism of the Ebola Virus Glycoprotein Requires an Intact Receptor-Binding Domain and Can Be Blocked by GP1-Specific Antibodies.’, *Journal of virology*. American Society for Microbiology, 90(24), pp. 11075–11086. doi: 10.1128/JVI.01563-16.

Brookes, P. S. *et al.* (2004) ‘Calcium, ATP, and ROS: a mitochondrial love-hate triangle’, *American Journal of Physiology-Cell Physiology*. American Physiological Society, 287(4), pp. C817–C833. doi: 10.1152/ajpcell.00139.2004.

Brunner, J. E. *et al.* (2005) ‘Functional interaction of heterogeneous nuclear ribonucleoprotein C with poliovirus RNA synthesis initiation complexes.’, *Journal of virology*, 79(6), pp. 3254–66. doi: 10.1128/JVI.79.6.3254-3266.2005.
Bwaka, M. A. *et al.* (1999) ‘Ebola Hemorrhagic Fever in Kikwit, Democratic Republic of the Congo: Clinical Observations in 103 Patients’, *The Journal of Infectious Diseases*, 179(s1), pp. S1–S7. doi: 10.1086/514308.
Cai, Z. *et al.* (2014) ‘Plasma membrane translocation of trimerized MLKL protein is required for TNF-induced necroptosis’, *Nature Cell Biology*, 16(1), pp. 55–65. doi: 10.1038/ncb2883.
Cantoni, D. *et al.* (2016) ‘Risks Posed by Reston, the Forgotten Ebolavirus’, *mSphere*, 1(6), pp. 1–10. doi: 10.1128/mSphere.00322-16.Editor.
Cantoni, D. and Rossman, J. S. (2018) ‘Ebolaviruses: New roles for old proteins’, *PLOS Neglected Tropical Diseases*. Edited by P. V. Aguilar. Public Library of Science, 12(5), p. e0006349. doi: 10.1371/journal.pntd.0006349.
Cárdenas, W. B. *et al.* (2006) ‘Ebola virus VP35 protein binds double-stranded RNA and inhibits alpha/beta interferon production induced by RIG-I signaling.’, *Journal of virology*, 80(11), pp. 5168–5178. doi: 10.1128/JVI.02199-05.
Carette, J. E. *et al.* (2011) ‘Ebola virus entry requires the cholesterol transporter Niemann-Pick C1’, *Nature*. doi: 10.1038/nature10348.
Carroll, S. a *et al.* (2013) ‘Molecular evolution of viruses of the family Filoviridae based on 97 whole-genome sequences.’, *Journal of virology*, 87(5), pp. 2608–16. doi: 10.1128/JVI.03118-12.
Casari, G., Sander, C. and Valencia, a (1995) ‘A method to predict functional residues in proteins.’, *Nature structural biology*, 2(2), pp. 171–178. doi: 10.1038/nsb0295-171.
CDC (1990) ‘Update: filovirus infection in animal handlers.’, 39(16), pp. 266–7, 273.
CDC (2016) *2014 Ebola Outbreak in West Africa - Case Counts*. Available at: http://www.cdc.gov/vhf/ebola/outbreaks/2014-west-africa/case-counts.htmL (Accessed: 20 April 2016).
Chaitanya, G., Alexander, J. S. and Babu, P. (2010) ‘PARP-1 cleavage fragments: signatures of cell-death proteases in neurodegeneration’, *Cell Communication and*

Signaling. BioMed Central, 8(1), p. 31. doi: 10.1186/1478-811X-8-31.
Chan, S. Y., Ma, M. C. and Goldsmith, M. a. (2000) 'Differential induction of cellular detachment by envelope glycoproteins of Marburg and Ebola (Zaire) viruses', *Journal of General Virology*, 81(9), pp. 2155–2159. doi: 10.1128/JVI.74.10.4933-4937.2000.
Chandran, K. *et al.* (2005) 'Virology: Endosomal proteolysis of the ebola virus glycoprotein is necessary for infection', *Science*. doi: 10.1126/science.1110656.
Chang, T. H. *et al.* (2009) 'Ebola Zaire virus blocks type I interferon production by exploiting the host SUMO modification machinery', *PLoS Pathogens*, 5(6). doi: 10.1371/journal.ppat.1000493.
Chertow, D. S. *et al.* (2016) 'Severe Meningoencephalitis in a Case of Ebola Virus Disease: A Case Report', *Annals of Internal Medicine*, 165(4), p. 301. doi: 10.7326/M15-3066.
Chowdhury, I. H. *et al.* (2003) 'HIV-1 Vpr Activates Cell Cycle Inhibitor p21/Waf1/Cip1: A Potential Mechanism of G2/M Cell Cycle Arrest', *Virology*. Academic Press, 305(2), pp. 371–377. doi: 10.1006/VIRO.2002.1777.
Christofferson, D. E. and Yuan, J. (2010) 'Necroptosis as an alternative form of programmed cell death', *Current Opinion in Cell Biology*. Elsevier Current Trends, 22(2), pp. 263–268. doi: 10.1016/J.CEB.2009.12.003.
Codogno, P. and Meijer, A. J. (2005) 'Autophagy and signaling: Their role in cell survival and cell death', *Cell Death and Differentiation*. doi: 10.1038/sj.cdd.4401751.
Commission, R. of an I. (1978) 'Ebola haemorrhagic fever in Zaire, 1976.', *Bulletin of the World Health Organization*. World Health Organization, 56(2), pp. 271–93.
Cory, A. H. *et al.* (1991) 'Use of an Aqueous Soluble Tetrazolium/Formazan Assay for Cell Growth Assays in Culture', *Cancer Communications*, 3(7), pp. 207–212. doi: 10.3727/095535491820873191.
Dalgard, D. W. *et al.* (1992) 'Combined simian hemorrhagic fever and Ebola virus infection in cynomolgus monkeys.', *Laboratory animal science*, 42(2), pp. 152–157.
Davey, R. A. *et al.* (2017) 'Mechanisms of Filovirus Entry', in. Springer, Cham, pp. 323–352. doi: 10.1007/82_2017_14.
Debnath, J., Baehrecke, E. H. and Kroemer, G. (2005) *Does Autophagy Contribute*

to Cell Death?, *Autophagy*.
Decker, T. *et al.* (2003) 'Rapamycin-induced G 1 arrest in cycling B-CLL cells is associated with reduced expression of cyclin D3, cyclin E, cyclin A, and survivin'. doi: 10.1182/blood-2002-01-0189.
Deen, G. F. *et al.* (2015) 'Ebola RNA Persistence in Semen of Ebola Virus Disease Survivors — Preliminary Report', *New England Journal of Medicine*, p. 151014140118009. doi: 10.1056/NEJMoa1511410.
Dhuriya, Y. K. and Sharma, D. (2018) 'Necroptosis: a regulated inflammatory mode of cell death', *Journal of Neuroinflammation*. BioMed Central, 15(1), p. 199. doi: 10.1186/s12974-018-1235-0.
Diehl, W. E. *et al.* (2016) 'Ebola Virus Glycoprotein with Increased Infectivity Dominated the 2013???2016 Epidemic', *Cell*, 167(4), pp. 1088-1098.e6. doi: 10.1016/j.cell.2016.10.014.
Dietzel, E. *et al.* (2017) 'Functional Characterization of Adaptive Mutations during the West African Ebola Virus Outbreak.', *Journal of virology*. American Society for Microbiology, 91(2), pp. e01913-16. doi: 10.1128/JVI.01913-16.
Dolnik, O. *et al.* (2004) 'Ectodomain shedding of the glycoprotein GP of Ebola virus.', *The EMBO journal*, 23(10), pp. 2175–2184. doi: 10.1038/sj.emboj.7600219.
Emanuel, J., Marzi, A. and Feldmann, H. (2018) 'Filoviruses: Ecology, Molecular Biology, and Evolution', in, pp. 189–221. doi: 10.1016/bs.aivir.2017.12.002.
Escudero-Pérez, B. *et al.* (2014) 'Shed GP of Ebola Virus Triggers Immune Activation and Increased Vascular Permeability', *PLoS Pathogens*, 10(11). doi: 10.1371/journal.ppat.1004509.
Fabozzi, G. *et al.* (2011) 'Ebolavirus proteins suppress the effects of small interfering RNA by direct interaction with the mammalian RNA interference pathway.', *Journal of virology*, 85(6), pp. 2512–2523. doi: 10.1128/JVI.01160-10.
Falzarano, D. *et al.* (2006) 'Structure-function analysis of the soluble glycoprotein, sGP, of ebola virus', *ChemBioChem*, 7(10), pp. 1605–1611. doi: 10.1002/cbic.200600223.
Feldmann, H. Kiley, M. (1999) 'Classification, structure, and replication of filoviruses', *Current Opinion in Immunology*, (235), pp. 1–21.
Feldmann, H. and Geisbert, T. W. (2011) 'Ebola haemorrhagic fever', *The Lancet*,

377(9768), pp. 849–862. doi: 10.1016/S0140-6736(10)60667-8.
Fisher-Hoch, S. P. *et al.* (1992) 'Pathogenic Potential of Filoviruses: Role of Geographic Origin of Primate Host and Virus Strain', *Journal of Infectious Diseases*, 166(4), pp. 753–763. doi: 10.1093/infdis/166.4.753.
Fitzpatrick, G. *et al.* (2015) 'The Contribution of Ebola Viral Load at Admission and Other Patient Characteristics to Mortality in a Médecins Sans Frontières Ebola Case Management Centre, Kailahun, Sierra Leone, June–October 2014', *Journal of Infectious Diseases*, 212(11), pp. 1752–1758. doi: 10.1093/infdis/jiv304.
Furuyama, W. *et al.* (2016) 'Discovery of an antibody for pan-ebolavirus therapy', *Scientific Reports*. Nature Publishing Group, 6, p. 20514. doi: 10.1038/srep20514.
Gallaher, Iliam and Garry, R. (2015) 'Modeling of the Ebola Virus Delta Peptide Reveals a Potential Lytic Sequence Motif', *Viruses*, 7(1), pp. 285–305. doi: 10.3390/v7010285.
García-Dorival, I. *et al.* (2014) 'Elucidation of the Ebola Virus VP24 Cellular Interactome and Disruption of Virus Biology through Targeted Inhibition of Host-Cell Protein Function', *Journal of Proteome Research*. American Chemical Society, 13(11), pp. 5120–5135. doi: 10.1021/pr500556d.
García, M. *et al.* (2012) 'Productive replication of Ebola virus is regulated by the c-Abl1 tyrosine kinase.', *Science translational medicine*, 4(123), p. 123ra24. doi: 10.1126/scitranslmed.3003500.
Geisbert, T. W. *et al.* (2003) 'Pathogenesis of Ebola Hemorrhagic Fever in Cynomolgus Macaques', *The American Journal of Pathology*, 163(6), pp. 2347–2370. doi: 10.1016/S0002-9440(10)63591-2.
Geisbert, T. W. and Hensley, L. E. (2004) 'Ebola virus: new insights into disease aetiopathology and possible therapeutic interventions.', *Expert reviews in molecular medicine*, 6(20), pp. 1–24. doi: 10.1017/S1462399404008300.
Geisbert, T. W. and Jahrling, P. B. (1990) 'Use of immunoelectron microscopy to show Ebola virus during the 1989 United States epizootic.', *Journal of clinical pathology*, 43(10), pp. 813–6. doi: 10.1136/jcp.43.10.813.
Georges, A. J. *et al.* (1999) 'Ebola hemorrhagic fever outbreaks in Gabon, 1994-1997: epidemiologic and health control issues.', *J Infect Dis*, 179 Suppl, pp. S65-75. doi: 10.1086/514290.

Goldstein, T. *et al.* (2018) ‘The discovery of Bombali virus adds further support for bats as hosts of ebolaviruses’, *Nature Microbiology*. Nature Publishing Group, 3(10), pp. 1084–1089. doi: 10.1038/s41564-018-0227-2.
Gong, Y.-N. *et al.* (2017) ‘ESCRT-III Acts Downstream of MLKL to Regulate Necroptotic Cell Death and Its Consequences’, *Cell*, 169(2), pp. 286-300.e16. doi: 10.1016/j.cell.2017.03.020.
Gontarek, R. R. *et al.* (1999) ‘hnRNP C and polypyrimidine tract-binding protein specifically interact with the pyrimidine-rich region within the 3’NTR of the HCV RNA genome’, *Nucleic Acids Research*, 27(6), pp. 1457–1463. doi: 10.1093/nar/27.6.1457.
Gramberg, T. *et al.* (2005) ‘LSECtin interacts with filovirus glycoproteins and the spike protein of SARS coronavirus’, *Virology*. doi: 10.1016/j.virol.2005.06.026.
Gregory, S. M. *et al.* (2011) ‘Structure and function of the complete internal fusion loop from Ebolavirus glycoprotein 2.’, *Proceedings of the National Academy of Sciences of the United States of America*. National Academy of Sciences, 108(27), pp. 11211–6. doi: 10.1073/pnas.1104760108.
Groseth, A. *et al.* (2002) ‘Molecular characterization of an isolate from the 1989/90 epizootic of Ebola virus Reston among macaques imported into the United States’, *Virus Research*, 87(2), pp. 155–163. doi: 10.1016/S0168-1702(02)00087-4.
Groseth, A. *et al.* (2009) ‘The Ebola virus ribonucleoprotein complex: A novel VP30-L interaction identified’, *Virus Research*, 140(1–2), pp. 8–14. doi: 10.1016/j.virusres.2008.10.017.
Groseth, A. *et al.* (2012) ‘The Ebola virus glycoprotein contributes to but is not sufficient for virulence in vivo.’, *PLoS pathogens*, 8(8), p. e1002847. doi: 10.1371/journal.ppat.1002847.
Groseth, A., Feldmann, H. and Strong, J. E. (2007) ‘The ecology of Ebola virus’, *Trends in Microbiology*. Elsevier Current Trends, 15(9), pp. 408–416. doi: 10.1016/J.TIM.2007.08.001.
Guito, J. C. *et al.* (2017) ‘Novel activities by ebolavirus and marburgvirus interferon antagonists revealed using a standardized in vitro reporter system’, *Virology*. Academic Press, 501, pp. 147–165. doi: 10.1016/J.VIROL.2016.11.015.
Gustin, J. K. *et al.* (2015) ‘Ebola Virus Glycoprotein Promotes Enhanced Viral

Egress by Preventing Ebola VP40 From Associating With the Host Restriction Factor BST2/Tetherin.', *The Journal of infectious diseases*. Oxford University Press, (Suppl 2), pp. S181-90. doi: 10.1093/infdis/jiv125.
Haasnoot, J. *et al.* (2007) 'The ebola virus VP35 protein is a suppressor of RNA silencing', *PLoS Pathogens*, 3(6), pp. 0794–0803. doi: 10.1371/journal.ppat.0030086.
Han, Y. *et al.* (2013) 'Inducing cell proliferation inhibition and apoptosis via silencing Dicer, Drosha, and Exportin 5 in urothelial carcinoma of the bladder', *Journal of Surgical Oncology*, 107(2), pp. 201–205. doi: 10.1002/jso.23214.
Han, Z. *et al.* (2003) 'Biochemical and Functional Characterization of the Ebola Virus VP24 Protein: Implications for a Role in Virus Assembly and Budding', *Journal of Virology*, 77(3), p. 1793. doi: 10.1128/JVI.77.3.1793.
Han, Z. *et al.* (2015) 'ALIX Rescues Budding of a Double PTAP/PPEY L-Domain Deletion Mutant of Ebola VP40: A Role for ALIX in Ebola Virus Egress', *Journal of Infectious Diseases*, 212, pp. S138–S145. doi: 10.1093/infdis/jiu838.
Harty, R. N. *et al.* (2000) 'A PPxY motif within the VP40 protein of Ebola virus interacts physically and functionally with a ubiquitin ligase: Implications for filovirus budding', *Proceedings of the National Academy of Sciences of the United States of America*, 97(25), pp. 13871–13876. doi: 10.1073/pnas.1006098107.
Hayes, C. G. *et al.* (1992) 'Outbreak of fatal illness among captive macaques in the Philippines caused by an ebola-related filovirus', *American Journal of Tropical Medicine and Hygiene*, 46(6), pp. 664–671.
Hayman, D. T. S. (2016) 'Bats as Viral Reservoirs', *Annual Review of Virology*. Annual Reviews , 3(1), pp. 77–99. doi: 10.1146/annurev-virology-110615-042203.
He, F. *et al.* (2017) 'Ebolavirus protein VP24 interferes with innate immune responses by inhibiting interferon-λ1 gene expression', *Virology*. Elsevier Inc., 509(February), pp. 23–34. doi: 10.1016/j.virol.2017.06.002.
He, J. *et al.* (1995) 'Human immunodeficiency virus type 1 viral protein R (Vpr) arrests cells in the G2 phase of the cell cycle by inhibiting p34cdc2 activity.', *Journal of virology*. American Society for Microbiology Journals, 69(11), pp. 6705–11.
He, J. *et al.* (2017) 'Ebola Virus Delta Peptide is a Viroporin.', *Journal of virology*.

American Society for Microbiology, 91(16), pp. e00438-17. doi: 10.1128/JVI.00438-17.

Henao-Restrepo, A. M. *et al.* (2016) ‘Efficacy and effectiveness of an rVSV-vectored vaccine in preventing Ebola virus disease: final results from the Guinea ring vaccination, open-label, cluster-randomised trial (Ebola {Ç}a Suffit!)’, *The Lancet*. Elsevier.

Hoenen, T. *et al.* (2012) ‘Inclusion bodies are a site of ebolavirus replication.’, *Journal of virology*. doi: 10.1128/JVI.01525-12.

Hoffmann, M. *et al.* (2017) ‘A Polymorphism within the Internal Fusion Loop of the Ebola Virus Glycoprotein Modulates Host Cell Entry’, *Journal of Virology*. Edited by T. S. Dermody, 91(9), pp. e00177-17. doi: 10.1128/JVI.00177-17.

Holtsberg, F. W. *et al.* (2015) ‘Pan-ebolavirus and pan-filovirus mouse monoclonal antibodies: protection against Ebola and Sudan viruses’, *Journal of Virology*, (October), p. JVI.02171-15. doi: 10.1128/JVI.02171-15.

Honda, M. *et al.* (2000) ‘Hepatitis C virus core protein induces apoptosis and impairs cell-cycle regulation in stably transformed chinese hamster ovary cells’, *Hepatology*. John Wiley & Sons, Ltd, 31(6), pp. 1351–1359. doi: 10.1053/jhep.2000.7985.

Hou, W. *et al.* (2010) ‘Autophagic degradation of active caspase-8’, *Autophagy*. Taylor & Francis, 6(7), pp. 891–900. doi: 10.4161/auto.6.7.13038.

Huang, Y. *et al.* (2002) ‘The assembly of Ebola virus nucleocapsid requires virion-associated proteins 35 and 24 and posttranslational modification of nucleoprotein’, *Molecular Cell*, 10(2), pp. 307–316. doi: 10.1016/S1097-2765(02)00588-9.

Hurst, L. D. (2002) ‘The Ka/Ks ratio: Diagnosing the form of sequence evolution’, *Trends in Genetics*, pp. 486–487. doi: 10.1016/S0168-9525(02)02722-1.

Iampietro, M. *et al.* (2017) ‘Ebola virus glycoprotein directly triggers T lymphocyte death despite of the lack of infection’, *PLOS Pathogens*. Edited by P. G. Thomas. Public Library of Science, 13(5), p. e1006397. doi: 10.1371/journal.ppat.1006397.

Ikegami, T. *et al.* (2001) ‘Genome structure of Ebola virus subtype Reston: Differences among Ebola subtypes’, *Archives of Virology*, 146(10), pp. 2021–2027. doi: 10.1007/s007050170049.

Ilinykh, P. A. *et al.* (2015) ‘Different Temporal Effects of Ebola Virus VP35 and

VP24 Proteins on Global Gene Expression in Human Dendritic Cells.', *Journal of virology*. American Society for Microbiology, 89(15), pp. 7567–83. doi: 10.1128/JVI.00924-15.

Jahrling, P. B. *et al.* (1990) 'Preliminary report: isolation of Ebola virus from monkeys imported to USA', *The Lancet*, 335(8688), pp. 502–505. doi: 10.1016/0140-6736(90)90737-P.

Jin, H. *et al.* (2010) 'The VP35 protein of Ebola virus impairs dendritic cell maturation induced by virus and lipopolysaccharide', *Journal of General Virology*, 91(2), pp. 352–361. doi: 10.1099/vir.0.017343-0.

John, S. P. *et al.* (2007) 'Ebola virus VP30 is an RNA binding protein.', *Journal of virology*, 81(17), pp. 8967–8976. doi: 10.1128/JVI.02523-06.

Kafil, V. and Omidi, Y. (2011) 'Cytotoxic Impacts of Linear and Branched Polyethylenimine Nanostructures in A431 Cells', *BioImpacts : BI*. Tabriz University of Medical Sciences, 1(1), p. 23. doi: 10.5681/BI.2011.004.

Kaletsky, R. L. *et al.* (2009) 'Tetherin-mediated restriction of filovirus budding is antagonized by the Ebola glycoprotein.', *Proceedings of the National Academy of Sciences of the United States of America*. National Academy of Sciences, 106(8), pp. 2886–91. doi: 10.1073/pnas.0811014106.

Kaletsky, R. L., Simmons, G. and Bates, P. (2007) 'Proteolysis of the Ebola Virus Glycoproteins Enhances Virus Binding and Infectivity', *Journal of Virology*. doi: 10.1128/jvi.01170-07.

Kalvari, I. *et al.* (2014) 'iLIR', *Autophagy*. Taylor & Francis, 10(5), pp. 913–925. doi: 10.4161/auto.28260.

Kaner, J. and Schaack, S. (2016) 'Understanding Ebola: the 2014 epidemic'. doi: 10.1186/s12992-016-0194-4.

Karimian, A., Ahmadi, Y. and Yousefi, B. (2016) 'Multiple functions of p21 in cell cycle, apoptosis and transcriptional regulation after DNA damage', *DNA Repair*, 42, pp. 63–71. doi: 10.1016/j.dnarep.2016.04.008.

Kash, J. C. *et al.* (2006) 'Global suppression of the host antiviral response by Ebola- and Marburgviruses: increased antagonism of the type I interferon response is associated with enhanced virulence.', *Journal of virology*, 80(6), pp. 3009–20. doi: 10.1128/JVI.80.6.3009-3020.2006.

Kerr, J. F. R., Wyllie, A. H. and Currie, A. R. (1972) ‘Apoptosis: A basic biological phenomenon with wide-ranging implications in tissue kinetics’, *British Journal of Cancer*. doi: 10.1038/bjc.1972.33.
Kirchdoerfer, R. N. *et al.* (2015) ‘Assembly of the Ebola Virus Nucleoprotein from a Chaperoned VP35 Complex’, *CellReports*, 12(1), pp. 140–149. doi: 10.1016/j.celrep.2015.06.003.
Kirchdoerfer, R. N. *et al.* (2016) ‘The Ebola Virus VP30-NP Interaction Is a Regulator of Viral RNA Synthesis’, *PLoS Pathogens*, 12(10). doi: 10.1371/journal.ppat.1005937.
Kirkham, J. K. *et al.* (2016) ‘Dynein Light Chain LC8 Is Required for RNA Polymerase I-Mediated Transcription in *Trypanosoma brucei*, Facilitating Assembly and Promoter Binding of Class I Transcription Factor A.’, *Molecular and cellular biology*, 36(1), pp. 95–107. doi: 10.1128/MCB.00705-15.
Koo, G.-B. *et al.* (2015) ‘Methylation-dependent loss of RIP3 expression in cancer represses programmed necrosis in response to chemotherapeutics.’, *Cell research*. Nature Publishing Group, 25(6), pp. 707–25. doi: 10.1038/cr.2015.56.
Kubota, T. *et al.* (2009) ‘Ebolavirus VP35 Interacts with the Cytoplasmic Dynein Light Chain 8’, *JOURNAL OF VIROLOGY*, 83(13), pp. 6952–6956. doi: 10.1128/JVI.00480-09.
Kudchodkar, S. B. and Levine, B. (2009) ‘Viruses and autophagy’, *Reviews in Medical Virology*. doi: 10.1002/rmv.630.
Kuhn, J. H. *et al.* (2010) ‘Proposal for a revised taxonomy of the family Filoviridae: Classification, names of taxa and viruses, and virus abbreviations’, *Archives of Virology*, 155(12), pp. 2083–2103. doi: 10.1007/s00705-010-0814-x.
Kuo, L. J. and Yang, L.-X. (2008) ‘Gamma-H2AX - a novel biomarker for DNA double-strand breaks.’, *In vivo (Athens, Greece)*, 22(3), pp. 305–9.
de La Vega, M.-A. *et al.* (2015) ‘The multiple roles of sGP in Ebola pathogenesis.’, *Viral immunology*, 28(1), pp. 3–9. doi: 10.1089/vim.2014.0068.
Landau, E. M. *et al.* (1996) *Lipidic cubic phases: A novel concept for the crystallization of membrane proteins (bacteriorhodopsin structurebicontinuous phaseslipidic matricesx-ray crystallography)*, *Biophysics*.
Lee, J. E. and Saphire, E. O. (2009) ‘Ebolavirus glycoprotein structure and

mechanism of entry.', *Future virology*, 4(6), pp. 621–635. doi: 10.2217/fvl.09.56.
Leroy, E. M. *et al.* (2005) 'Fruit bats as reservoirs of Ebola virus.', *Nature*, 438(7068), pp. 575–576. doi: 10.1038/438575a.
Leung, D. W. *et al.* (2015) 'An intrinsically disordered peptide from ebola virus VP35 controls viral RNA synthesis by modulating nucleoprotein-RNA interactions', *Cell Reports*, 11(3), pp. 376–389. doi: 10.1016/j.celrep.2015.03.034.
Li, J. *et al.* (2008) 'A conserved motif in region v of the large polymerase proteins of nonsegmented negative-sense RNA viruses that is essential for mRNA capping.', *Journal of virology*, 82(2), pp. 775–784. doi: 10.1128/JVI.02107-07.
Li, Y. (2011) 'Recombinant production of antimicrobial peptides in Escherichia coli: A review', *Protein Expression and Purification*. Academic Press, 80(2), pp. 260–267. doi: 10.1016/J.PEP.2011.08.001.
Li, Y. *et al.* (2013) 'RNA interference functions as an antiviral immunity mechanism in mammals', *Science*, 342(6155), pp. 231–234. doi: 10.1126/science.1241911.
Li, Y. H. and Chen, S. P. (2014) 'Evolutionary history of Ebola virus.', *Epidemiology and infection*, 142(6), pp. 1138–45. doi: 10.1017/S0950268813002215.
Licata, J. M. *et al.* (2003) 'Overlapping motifs (PTAP and PPEY) within the Ebola virus VP40 protein function independently as late budding domains: involvement of host proteins TSG101 and VPS-4.', *Journal of virology*, 77(3), pp. 1812–1819. doi: 10.1128/JVI.77.3.1812-1819.2003.
Licata, J. M. *et al.* (2004) 'Contribution of Ebola Virus Glycoprotein, Nucleoprotein, and VP24 to Budding of VP40 Virus-Like Particles', *Journal of Virology*, 78(14), pp. 7344–7351. doi: 10.1128/JVI.78.14.7344-7351.2004.
Liu, G. *et al.* (2017) 'A Sensitive In Vitro High-Throughput Screen to Identify Pan-Filoviral Replication Inhibitors Targeting the VP35-NP Interface', *ACS Infectious Diseases*. ACS Publications.
Liu, X. *et al.* (2017) 'Transcriptomic signatures differentiate survival from fatal outcomes in humans infected with Ebola virus', *Genome Biology*. BioMed Central, 18(1), p. 4. doi: 10.1186/s13059-016-1137-3.
Liu, Y. and Levine, B. (2015) 'Autosis and autophagic cell death: The dark side of autophagy', *Cell Death and Differentiation*. doi: 10.1038/cdd.2014.143.
Lopez, L. A. *et al.* (2010) 'Ebola virus glycoprotein counteracts BST-2/Tetherin

restriction in a sequence-independent manner that does not require tetherin surface removal.', *Journal of virology*. American Society for Microbiology, 84(14), pp. 7243–55. doi: 10.1128/JVI.02636-09.
Lubaki, N. M. *et al.* (2013) 'The lack of maturation of Ebola virus-infected dendritic cells results from the cooperative effect of at least two viral domains.', *Journal of virology*. American Society for Microbiology, 87(13), pp. 7471–85. doi: 10.1128/JVI.03316-12.
Luthra, P. *et al.* (2013) 'Mutual antagonism between the Ebola virus VP35 protein and the RIG-I activator PACT determines infection outcome.', *Cell host & microbe*, 14(1), pp. 74–84. doi: 10.1016/j.chom.2013.06.010.
Luthra, P. *et al.* (2015) 'Ebola virus VP35 interaction with dynein LC8 regulates viral RNA synthesis.', *Journal of virology*, 89(9), pp. 5148–53. doi: 10.1128/JVI.03652-14.
Luzzati, V. and Tardieu, A. (1974) *LIPID PHASES: STRUCTURE AND STRUCTURAL TRANSITIONS*.
Maes, P. *et al.* (2019) 'Taxonomy of the order Mononegavirales: second update 2018', *Archives of Virology*. Springer Vienna, pp. 1–12. doi: 10.1007/s00705-018-04126-4.
Mahale, K. N. and Patole, M. S. (2015) 'The crux and crust of ebolavirus: Analysis of genome sequences and glycoprotein gene', *Biochemical and Biophysical Research Communications*, 463(4), pp. 756–761. doi: 10.1016/j.bbrc.2015.06.008.
Mahanty, S. *et al.* (2003) 'Cutting edge: impairment of dendritic cells and adaptive immunity by Ebola and Lassa viruses.', *Journal of immunology (Baltimore, Md. : 1950)*. American Association of Immunologists, 170(6), pp. 2797–801. doi: 10.4049/jimmunol.170.6.2797.
Malashkevich, V. N. *et al.* (1999) 'Core structure of the envelope glycoprotein GP2 from Ebola virus at 1.9-Å resolution', *Proceedings of the National Academy of Sciences*. doi: 10.1073/pnas.96.6.2662.
Markosyan, R. M. *et al.* (2016) 'Induction of Cell-Cell Fusion by Ebola Virus Glycoprotein: Low pH Is Not a Trigger', *PLoS Pathogens*. doi: 10.1371/journal.ppat.1005373.
Marsh, G. a *et al.* (2011) 'Ebola Reston virus infection of pigs: clinical significance

and transmission potential.', *The Journal of infectious diseases*, 204 Suppl(Suppl 3), pp. S804-9. doi: 10.1093/infdis/jir300.
Mateo, M. *et al.* (2011) 'Knockdown of Ebola virus VP24 impairs viral nucleocapsid assembly and prevents virus replication', *Journal of Infectious Diseases*, 204(SUPPL. 3). doi: 10.1093/infdis/jir311.
McElroy, A. K. *et al.* (2014) 'Ebola Hemorrhagic Fever: Novel Biomarker Correlates of Clinical Outcome', *Journal of Infectious Diseases*. Oxford University Press, 210(4), pp. 558–566. doi: 10.1093/infdis/jiu088.
Meeusen, S. *et al.* (2006) 'Mitochondrial Inner-Membrane Fusion and Crista Maintenance Requires the Dynamin-Related GTPase Mgm1', *Cell*. Cell Press, 127(2), pp. 383–395. doi: 10.1016/J.CELL.2006.09.021.
Mehedi, M. *et al.* (2011) 'A new Ebola virus nonstructural glycoprotein expressed through RNA editing.', *Journal of virology*, 85(11), pp. 5406–14. doi: 10.1128/JVI.02190-10.
Mingo, R. M. *et al.* (2015) 'Ebola virus and severe acute respiratory syndrome coronavirus display late cell entry kinetics: evidence that transport to NPC1+ endolysosomes is a rate-defining step.', *Journal of virology*. American Society for Microbiology, 89(5), pp. 2931–43. doi: 10.1128/JVI.03398-14.
Modrof, J. *et al.* (2002) 'Phosphorylation of VP30 impairs Ebola virus transcription', *Journal of Biological Chemistry*, 277(36), pp. 33099–33104. doi: 10.1074/jbc.M203775200.
Modrof, J., Becker, S. and Mühlberger, E. (2003) 'Ebola Virus Transcription Activator VP30 Is a Zinc-Binding Protein', *Journal of Virology*, 77(5), pp. 3334–3338. doi: 10.1128/JVI.77.5.3334–3338.2003.
Mohan, G. S. *et al.* (2012) 'Antigenic Subversion: A Novel Mechanism of Host Immune Evasion by Ebola Virus', *PLoS Pathogens*. Edited by C. F. Basler. Public Library of Science, 8(12), p. e1003065. doi: 10.1371/journal.ppat.1003065.
Mohan, G. S. *et al.* (2015) 'Less is more: Ebola virus surface glycoprotein expression levels regulate virus production and infectivity.', *Journal of virology*, 89(2), pp. 1205–17. doi: 10.1128/JVI.01810-14.
Moller-Tank, S. *et al.* (2013) 'Role of the Phosphatidylserine Receptor TIM-1 in Enveloped-Virus Entry', *Journal of Virology*. doi: 10.1128/JVI.01025-13.

Moller-Tank, S. *et al.* (2015) ‘Ebola Virus Entry: A Curious and Complex Series of Events’, *PLOS Pathogens*. Edited by R. E. Dutch. Public Library of Science, 11(4), p. e1004731. doi: 10.1371/journal.ppat.1004731.
Mosmann, T. (1983) ‘Rapid colorimetric assay for cellular growth and survival: application to proliferation and cytotoxicity assays.’, *Journal of immunological methods*, 65(1–2), pp. 55–63.
Mühlberger, E. (2007) ‘Filovirus replication and transcription’, *Future Virology*. doi: 10.2217/17460794.2.2.205.
Nanbo, A. *et al.* (2010) ‘Ebolavirus is internalized into host cells via macropinocytosis in a viral glycoprotein-dependent manner’, *PLoS Pathogens*, 6(9). doi: 10.1371/journal.ppat.1001121.
Negredo, A. *et al.* (2011) ‘Discovery of an ebolavirus-like filovirus in Europe’, *PLoS Pathogens*, 7(10), pp. 1–8. doi: 10.1371/journal.ppat.1002304.
Neumann, G., Watanabe, S. and Kawaoka, Y. (2009) ‘Characterization of Ebolavirus regulatory genomic regions’, *Virus Research*, 144(1–2), pp. 1–7. doi: 10.1016/j.virusres.2009.02.005.
Nieva, J. L., Madan, V. and Carrasco, L. (2012) ‘Viroporins: structure and biological functions’, *Nature Reviews Microbiology*. Nature Publishing Group, 10(8), pp. 563–574. doi: 10.1038/nrmicro2820.
Noda, T. *et al.* (2005) ‘Nucleocapsid-like structures of Ebola virus reconstructed using electron tomography.’, *The Journal of veterinary medical science / the Japanese Society of Veterinary Science*, 67(3), pp. 325–8. doi: 10.1292/jvms.67.325.
Noda, T. *et al.* (2006) ‘Assembly and Budding of Ebolavirus’, *PLoS Pathogens*. Public Library of Science, 2(9), p. e99. doi: 10.1371/journal.ppat.0020099.
O’Hearn, A. *et al.* (2015) ‘Role of EXT1 and Glycosaminoglycans in the Early Stage of Filovirus Entry’, *Journal of Virology*. doi: 10.1128/JVI.03689-14.
Olejnik, J. *et al.* (2013) ‘Ebola virus does not block apoptotic signaling pathways.’, *Journal of virology*, 87(10), pp. 5384–96. doi: 10.1128/JVI.01461-12.
Olejnik, J. *et al.* (2017) ‘Ebolaviruses associated with differential pathogenicity induce distinct host responses in human macrophages’, *Journal of Virology*, 91(11), pp. e00179-17. doi: 10.1128/JVI.00179-17.

Olival, K. J. *et al.* (2013) ‘Ebola virus antibodies in fruit bats, bangladesh.’, *Emerging infectious diseases*, 19(2), pp. 270–273. doi: 10.3201/eid1902.120524.
Pallesen, J. *et al.* (2016) ‘Structures of Ebola virus GP and sGP in complex with therapeutic antibodies’, *Nature Microbiology*. Macmillan Publishers Limited, 1, p. 16128.
Pan, Y. *et al.* (2014) ‘Reston virus in domestic pigs in China’, *Archives of Virology*, 159(5), pp. 1129–1132. doi: 10.1007/s00705-012-1477-6.
Pappalardo, M. *et al.* (2016) ‘Conserved differences in protein sequence determine the human pathogenicity of Ebolaviruses’, *Scientific Reports*. Nature Publishing Group, 6, p. 23743. doi: 10.1038/srep23743.
Pattyn, S. *et al.* (1977) ‘Isolation of Marburg-like virus from a case of haemorrhagic fever in Zaire.’, *Lancet*, pp. 573–574.
Pleet, M. L. *et al.* (2016) ‘Ebola VP40 in Exosomes Can Cause Immune Cell Dysfunction.’, *Frontiers in microbiology*, 7, p. 1765. doi: 10.3389/fmicb.2016.01765.
Pleet, M. L. *et al.* (2017) ‘The Role of Exosomal VP40 in Ebola Virus Disease’, *DNA and Cell Biology*, 36(4), p. dna.2017.3639. doi: 10.1089/dna.2017.3639.
Prins, K. C. *et al.* (2010) ‘Basic Residues within the Ebolavirus VP35 Protein Are Required for Its Viral Polymerase Cofactor Function’, *Journal of Virology*, 84(20), pp. 10581–10591. doi: 10.1128/JVI.00925-10.
Prins, K. C., Cárdenas, W. B. and Basler, C. F. (2009) ‘Ebola virus protein VP35 impairs the function of interferon regulatory factor-activating kinases IKKepsilon and TBK-1.’, *Journal of virology*, 83, pp. 3069–3077. doi: 10.1128/JVI.01875-08.
Rausell, A. *et al.* (2010) ‘Protein interactions and ligand binding: From protein subfamilies to functional specificity’, *Proceedings of the National Academy of Sciences*, pp. 1995–2000. doi: http://dx.doi.org/10.1073/pnas.0908044107.
Ray, R. B. *et al.* (2004) ‘Ebola virus glycoprotein-mediated anoikis of primary human cardiac microvascular endothelial cells’, *Virology*, 321(2), pp. 181–188. doi: 10.1016/j.virol.2003.12.014.
Raymond, J., Bradfute, S. and Bray, M. (2011) ‘Filovirus infection of STAT-1 knockout mice’, *Journal of Infectious Diseases*, 204(SUPPL. 3). doi: 10.1093/infdis/jir335.
Reddy, E. P. (2014) *Cell cycle control in mammalian cells: Role of cyclins, cyclin*

dependent kinases (CDKs), growth suppressor genes and cyclin-dependent kinase inhibitors (CKIs).
Reid, S. P. *et al.* (2006) 'Ebola virus VP24 binds karyopherin alpha1 and blocks STAT1 nuclear accumulation.', *Journal of virology*, 80(11), pp. 5156–67. doi: 10.1128/JVI.02349-05.
Reid, S. P. *et al.* (2007) 'Ebola virus VP24 proteins inhibit the interaction of NPI-1 subfamily karyopherin alpha proteins with activated STAT1.', *Journal of virology*, 81(24), pp. 13469–77. doi: 10.1128/JVI.01097-07.
Ren, J. X. *et al.* (2016) 'Identification of novel VP35 inhibitors: Virtual screening driven new scaffolds', *Biomedicine and Pharmacotherapy*, 84, pp. 199–207. doi: 10.1016/j.biopha.2016.09.034.
Richman, DD. Cleveland, PH. McCormick, PB. Johnson, K. (1983) 'Antigenic analysis of strains of Ebola virus: identification of two Ebola virus serotypes', *Journal of Infectious Diseases*, 2(147), pp. 268–71.
Rollin, P. E. *et al.* (1999) 'Ebola (subtype Reston) virus among quarantined nonhuman primates recently imported from the Philippines to the United States.', *The Journal of infectious diseases*, 179 Suppl, pp. S108-14. doi: 10.1086/514303.
Rossman, J. S. and Lamb, R. A. (2011) 'Influenza virus assembly and budding', *Virology*. Academic Press, 411(2), pp. 229–236. doi: 10.1016/J.VIROL.2010.12.003.
Ruedas, J. B. *et al.* (2017) 'Spontaneous mutation at amino acid 544 of the Ebola glycoprotein potentiates virus entry and selection in tissue culture.', *Journal of virology*. American Society for Microbiology, p. JVI.00392-17. doi: 10.1128/JVI.00392-17.
Ruigrok, R. W. *et al.* (2000) 'Structural characterization and membrane binding properties of the matrix protein VP40 of Ebola virus.', *Journal of molecular biology*, 300, pp. 103–112. doi: 10.1006/jmbi.2000.3822.
Rummel, G. *et al.* (1998) 'Lipidic Cubic Phases: New Matrices for the Three-Dimensional Crystallization of Membrane Proteins', *Journal of Structural Biology*, 121(2), pp. 82–91. doi: 10.1006/jsbi.1997.3952.
Ryan, E. *et al.* (2016) 'Activation of the DNA Damage Response by RNA Viruses', *Biomolecules*. Multidisciplinary Digital Publishing Institute, 6(1), p. 2. doi:

10.3390/biom6010002.
Saeed, M. F. *et al.* (2008) 'Phosphoinositide-3 Kinase-Akt Pathway Controls Cellular Entry of Ebola Virus', *PLoS Pathogens*. Edited by M. Farzan. Public Library of Science, 4(8), p. e1000141. doi: 10.1371/journal.ppat.1000141.
Saeed, M. F. *et al.* (2010) 'Cellular entry of ebola virus involves uptake by a macropinocytosis-like mechanism and subsequent trafficking through early and late endosomes', *PLoS Pathogens*. doi: 10.1371/journal.ppat.1001110.
Sanchez, A. *et al.* (1996) 'The virion glycoproteins of Ebola viruses are encoded in two reading frames and are expressed through transcriptional editing.', *Proceedings of the National Academy of Sciences of the United States of America*, 93(8), pp. 3602–7. doi: 10.1073/pnas.93.8.3602.
Sanchez, A. (2001) 'Ebola Viruses', *Encyclopedia of Life Sciences*, pp. 1–4. doi: 10.1038/npg.els.0001019.
Sandeep Chakraborty, Basuthkar J. Rao, Bjarni Asgeirsson, A. M. D. (2014) 'Correlating the ability of VP24 protein from Ebola and Marburg viruses to bind human karyopherin to their immune suppression mechanism and pathogenicity using computational methods. [version 2; referees: 2 approved with reservations]', *F1000Research*, 3(265). doi: 10.12688/f1000research.5666.2.
Sandor, V. *et al.* (2000) 'P21-dependent G1arrest with downregulation of cyclin D1 and upregulation of cyclin E by the histone deacetylase inhibitor FR901228', *British Journal of Cancer*. Nature Publishing Group, 83(6), pp. 817–825. doi: 10.1054/bjoc.2000.1327.
Schindelin, J. *et al.* (2015) 'The ImageJ ecosystem: An open platform for biomedical image analysis.', *Molecular reproduction and development*. NIH Public Access, 82(7–8), pp. 518–29. doi: 10.1002/mrd.22489.
Schlereth, J. *et al.* (2016) 'RNA binding specificity of Ebola virus transcription factor VP30.', *RNA biology*, 13(9), pp. 783–98. doi: 10.1080/15476286.2016.1194160.
Shabman, R. S. *et al.* (2011) 'The Ebola virus VP24 protein prevents hnRNP C1/C2 binding to karyopherin α1 and partially alters its nuclear import.', *The Journal of infectious diseases*, 204 Suppl, pp. S904-10. doi: 10.1093/infdis/jir323.
Shimojima, M. *et al.* (2006) 'Tyro3 family-mediated cell entry of Ebola and Marburg viruses.', *Journal of virology*, 80(20), pp. 10109–16. doi: 10.1128/JVI.01157-06.

Silva, L. P. *et al.* (2012) ‘Assembly of Ebola virus matrix protein VP40 is regulated by latch-like properties of N and C terminal tails.’, *PloS one*, 7(7), p. e39978. doi: 10.1371/journal.pone.0039978.

Simmons, G. *et al.* (2002) ‘Ebola virus glycoproteins induce global surface protein down-modulation and loss of cell adherence.’, *Journal of virology*, 76(5), pp. 2518–28. doi: 10.1128/JVI.76.5.2518.

Simmons, J. A. *et al.* (2016) ‘Ebolavirus Glycoprotein Directs Fusion through NPC1+ Endolysosomes.’, *Journal of virology*, 90(1), pp. 605–610. doi: 10.1128/JVI.01828-15.

Spence, J. S. *et al.* (2016) ‘Direct Visualization of Ebola Virus Fusion Triggering in the Endocytic Pathway.’, *mBio*. American Society for Microbiology, 7(1), pp. e01857-15. doi: 10.1128/mBio.01857-15.

Stahelin, R. V. (2014) ‘Membrane binding and bending in Ebola VP40 assembly and egress’, *Frontiers in Microbiology*. Frontiers, 5, p. 300. doi: 10.3389/fmicb.2014.00300.

Stahelin, R. V (2014) ‘Could the Ebola virus matrix protein VP40 be a drug target?’, *Expert opinion on therapeutic targets*, 18(2), pp. 115–20. doi: 10.1517/14728222.2014.863877.

Strasser, A., O’Connor, L. and Dixit, V. M. (2002) ‘Apoptosis Signaling’, *Annual Review of Biochemistry*. doi: 10.1146/annurev.biochem.69.1.217.

Sullivan, N. J. *et al.* (2005) ‘Ebola virus glycoprotein toxicity is mediated by a dynamin-dependent protein-trafficking pathway.’, *Journal of virology*, 79(1), pp. 547–53. doi: 10.1128/JVI.79.1.547-553.2005.

Swanepoel, R. *et al.* (1996) ‘Experimental Inoculation of Plants and Animals with Ebola Virus’, *Emerging Infectious Diseases*. doi: 10.3201/eid0204.960407.

Takada, A. *et al.* (2004) ‘Human Macrophage C-Type Lectin Specific for Galactose and N-Acetylgalactosamine Promotes Filovirus Entry’, *Journal of Virology*. doi: 10.1128/JVI.78.6.2943-2947.2004.

Takase, S. *et al.* (2017) ‘A quantitative shRNA screen identifies ATP1A1 as a gene that regulates cytotoxicity by aurilide B.’, *Scientific reports*. Nature Publishing Group, 7(1), p. 2002. doi: 10.1038/s41598-017-02016-4.

Tan, G. S. *et al.* (2007) ‘The dynein light chain 8 binding motif of rabies virus

phosphoprotein promotes efficient viral transcription.', *Proceedings of the National Academy of Sciences of the United States of America*, 104(17), pp. 7229–34. doi: 10.1073/pnas.0701397104.
Tanida, I., Ueno, T. and Kominami, E. (2008) 'LC3 and Autophagy', in. Humana Press, pp. 77–88. doi: 10.1007/978-1-59745-157-4_4.
Taniguchi S, Watanabe S, Masangkay JS, Omatsu T, Ikegami T, Alviola P, et al. (no date) 'Reston Ebolavirus antibodies in bats, the Philippines [letter]', *CDC*, 17(8). doi: 10.3201/eid1708.101693.
Taniguchi, S. *et al.* (2011) 'Reston ebolavirus antibodies in bats, the Philippines', *Emerging Infectious Diseases*, pp. 1559–1560. doi: 10.3201/eid1708.101693.
Team, R. of a W. S. (1978) 'Ebola haemorrhagic fever in Sudan, 1976. Report of a WHO/International Study Team.', *Bulletin of the World Health Organization*. World Health Organization, 56(2), pp. 247–70.
Timmins, J., Schoehn, G., Ricard-Blum, S., *et al.* (2003) 'Ebola virus matrix protein VP40 interaction with human cellular factors Tsg101 and Nedd4', *Journal of Molecular Biology*, 326(2), pp. 493–502. doi: 10.1016/S0022-2836(02)01406-7.
Timmins, J., Schoehn, G., Kohlhaas, C., *et al.* (2003) 'Oligomerization and polymerization of the filovirus matrix protein VP40', *Virology*, 312(2), pp. 359–368. doi: 10.1016/S0042-6822(03)00260-5.
Timothy, J. W. S. *et al.* (2019) 'Early transmission and case fatality of Ebola virus at the index site of the 2013-16 west African Ebola outbreak: a cross-sectional seroprevalence survey.', *The Lancet. Infectious diseases*. Elsevier, 19(4), pp. 429–438. doi: 10.1016/S1473-3099(18)30791-6.
Towner, J. S. *et al.* (2007) 'Marburg virus infection detected in a common African bat', *PLoS One*, 2(8), p. e764. doi: 10.1371/journal.pone.0000764.
Trunschke, M. *et al.* (2013) 'The L-VP35 and L-L interaction domains reside in the amino terminus of the Ebola virus L protein and are potential targets for antivirals', *Virology*, 441(2), pp. 135–145. doi: 10.1016/j.virol.2013.03.013.
Urbanowicz, R. A. *et al.* (2016) 'Human Adaptation of Ebola Virus during the West African Outbreak', *Cell*, 167(4), pp. 1079-1087.e5. doi: 10.1016/j.cell.2016.10.013.
V.A., V., H.-D., K. and V.E., V. (1999) 'Delta-peptide is the carboxy-terminal cleavage fragment of the nonstructural small glycoprotein sGP of Ebola virus',

Virology, pp. 164–171.

Varkey, J. B. *et al.* (2015) 'Persistence of Ebola Virus in Ocular Fluid during Convalescence', *New England Journal of Medicine*, 372(25), pp. 2423–2427. doi: 10.1056/NEJMoa1500306.

Volchkov, viktor e. *et al.* (1995) 'GP mRNA of Ebola Virus Is Edited by the Ebola Virus Polymerase and by T7 and Vaccinia Virus Polymerases1', *Virology*, 214(2), pp. 421–430. doi: 10.1006/viro.1995.0052.

Volchkov, V. E. *et al.* (1998) 'Processing of the Ebola virus glycoprotein by the proprotein convertase furin.', *Proceedings of the National Academy of Sciences of the United States of America*, 95(10), pp. 5762–5767. doi: 10.1073/pnas.95.10.5762.

Volchkova, V. A. *et al.* (2011) 'Genomic RNA Editing and Its Impact on Ebola Virus Adaptation During Serial Passages in Cell Culture and Infection of Guinea Pigs', *The Journal of Infectious Diseases*. Oxford University Press, 204(suppl_3), pp. S941–S946. doi: 10.1093/infdis/jir321.

Volchkova, V. A., Klenk, H.-D. and Volchkov, V. E. (1999) 'Delta-Peptide Is the Carboxy-Terminal Cleavage Fragment of the Nonstructural Small Glycoprotein sGP of Ebola Virus', *Virology*, 265(1), pp. 164–171. doi: 10.1006/viro.1999.0034.

Volchkova, V. a *et al.* (1998) 'The nonstructural small glycoprotein sGP of Ebola virus is secreted as an antiparallel-orientated homodimer.', *Virology*, 250, pp. 408–414. doi: 10.1006/viro.1998.9389.

Wahl-Jensen, V. M. *et al.* (2005) 'Effects of Ebola virus glycoproteins on endothelial cell activation and barrier function.', *Journal of virology*, 79(16), pp. 10442–50. doi: 10.1128/JVI.79.16.10442-10450.2005.

Wang, F. *et al.* (2013) 'APRIL depletion induces cell cycle arrest and apoptosis through blocking TGF-β1/ERK signaling pathway in human colorectal cancer cells', *Molecular and Cellular Biochemistry*. Springer US, 383(1–2), pp. 179–189. doi: 10.1007/s11010-013-1766-8.

Wang, M. K. *et al.* (2017) 'Biochemical Basis for Increased Activity of Ebola Glycoprotein in the 2013???16 Epidemic', *Cell Host and Microbe*, 21(3), pp. 367–375. doi: 10.1016/j.chom.2017.02.002.

Watanabe, S. *et al.* (2007) 'Ebola virus (EBOV) VP24 inhibits transcription and

replication of the EBOV genome.', *The Journal of infectious diseases*, 196 Suppl(Suppl 2), pp. S284–S290. doi: 10.1086/520582.
Watanabe, S., Noda, T. and Kawaoka, Y. (2006) 'Functional mapping of the nucleoprotein of Ebola virus.', *Journal of virology*, 80(8), pp. 3743–51. doi: 10.1128/JVI.80.8.3743-3751.2006.
Watt, A. *et al.* (2014) 'A novel life cycle modeling system for Ebola virus shows a genome length-dependent role of VP24 in virus infectivity.', *Journal of virology*, 88(18), pp. 10511–24. doi: 10.1128/JVI.01272-14.
Wauquier, N. *et al.* (2010) 'Human fatal zaire ebola virus infection is associated with an aberrant innate immunity and with massive lymphocyte apoptosis', *PLoS Neglected Tropical Diseases*, 4(10). doi: 10.1371/journal.pntd.0000837.
Weik, M. *et al.* (2002) 'Ebola Virus VP30-Mediated Transcription Is Regulated by RNA Secondary Structure Formation', *JOURNAL OF VIROLOGY*, 76(17), pp. 8532–8539. doi: 10.1128/JVI.76.17.8532–8539.2002.
Whelan, S. P., Barr, J. N. and Wertz, G. W. (2004) 'Transcription and replication of nonsegmented negative-strand RNA viruses', *Current Topics in Microbiology and Immunology*.
de Wit, E. *et al.* (2011) 'Assessment of rodents as animal models for Reston ebolavirus.', *The Journal of infectious diseases*, 204 Suppl(Suppl 3), pp. S968-72. doi: 10.1093/infdis/jir330.
Xu, W. *et al.* (2014) 'Ebola virus VP24 targets a unique NLS binding site on karyopherin alpha 5 to selectively compete with nuclear import of phosphorylated STAT1', *Cell Host and Microbe*, 16(2), pp. 187–200. doi: 10.1016/j.chom.2014.07.008.
Yang, X. *et al.* (2016) 'ANP32A Regulates Histone 3 Acetylation and Promotes Leukemogenesis in AML', *Blood*, 128(22).
Yang, Z. Y. *et al.* (2000) 'Identification of the Ebola virus glycoprotein as the main viral determinant of vascular cell cytotoxicity and injury.', *Nature medicine*, 6(8), pp. 886–889. doi: 10.1038/78645.
Youle, R. J. and van der Bliek, A. M. (2012) 'Mitochondrial Fission, Fusion, and Stress', *Science*, 337(6098), pp. 1062–1065. doi: 10.1126/science.1219855.
Yuan, J. *et al.* (2012) 'Serological evidence of ebolavirus infection in bats, China',

Virol J, 9, p. 236. doi: 10.1186/1743-422x-9-236.
Zampieri, C. A. *et al.* (2007) 'The ERK mitogen-activated protein kinase pathway contributes to Ebola virus glycoprotein-induced cytotoxicity.', *Journal of virology*. American Society for Microbiology, 81(3), pp. 1230–40. doi: 10.1128/JVI.01586-06.
Zampieri, C. a, Sullivan, N. J. and Nabel, G. J. (2007) 'Immunopathology of highly virulent pathogens: insights from Ebola virus.', *Nature immunology*, 8(11), pp. 1159–1164. doi: 10.1038/ni1519.
Zhang, A. P. P., Bornholdt, Z. A., *et al.* (2012) 'The ebola virus interferon antagonist VP24 directly binds STAT1 and has a novel, pyramidal fold.', *PLoS pathogens*, 8(2), p. e1002550. doi: 10.1371/journal.ppat.1002550.
Zhang, A. P. P., Abelson, D. M., *et al.* (2012) 'The ebolavirus VP24 interferon antagonist: know your enemy.', *Virulence*, 3(5), pp. 440–5. doi: 10.4161/viru.21302.
Zhang, G. *et al.* (2018) 'Induction of a Na^+/K^+-ATPase-dependent form of autophagy triggers preferential cell death of human immunodeficiency virus type-1-infected macrophages', *Autophagy*. Taylor & Francis, 14(8), pp. 1359–1375. doi: 10.1080/15548627.2018.1476014.
Zhao, D. *et al.* (2016) 'The Myeloid LSECtin Is a DAP12-Coupled Receptor That Is Crucial for Inflammatory Response Induced by Ebola Virus Glycoprotein', *PLoS Pathogens*, 12(3). doi: 10.1371/journal.ppat.1005487.